

Characterization of *Leishmania infantum* infection in hepatocyte organoid immune cell co-cultures

Dissertation

For the award of the degree
“Doctor rerum naturalium”
(Dr. rer. nat.)

at the faculty of
Mathematics, Informatics and Natural Science
- Department of Biology -
University of Hamburg

Submitted by
Melanie Katja Lütkemeyer

Hamburg, April 2024

This work has been conducted in the research group and under the guidance of Prof. Dr. med. vet. Hannelore Lotter at the Bernhard Nocht Institute for Tropical Medicine

1. Examiner: **Prof. Dr. rer. nat. Tim-Wolf Gilberger**

Deutsches Elektronen-Synchrotron (DESY)
CSSB Centre for Structural Systems Biology
Notkestraße 85, Gebäude 15, 22607 Hamburg

2. Examiner: **Prof. Dr. med. vet. Hannelore Lotter**

Molecular Infection Immunology
Bernhard Nocht Institute for Tropical Medicine (BNITM)
Bernhard-Nocht-Straße 74, 20359 Hamburg

Date of oral defense: **05.07.2024**

Chairman of committee: Prof. Dr. rer. nat. Tim Gilberger

Deputy chairman of committee: Prof. Dr. rer. nat. Iris Bruchhaus

Members of committee: Prof. Dr. med. vet. Hannelore Lotter

Prof. Dr. rer. nat. Julia Kehr

Eidesstattliche Erklärung / Declaration on oath

Hiermit erkläre ich an Eides statt, dass ich die vorliegende Dissertationsschrift selbst verfasst und keine anderen als die angegebenen Quellen und Hilfsmittel genutzt habe.

I hereby declare, under oath, that I have written the present dissertation on my own and have not used other than the acknowledged resources and aids.

Hamburg, 22.04.2024



Melanie Katja Lütkemeyer

Table of content

Summary	IV
Zusammenfassung	V
Abbreviations	VIII
1 Introduction	1
1.1 <i>Leishmaniasis</i>	1
1.1.1 Life cycle and transmission	2
1.1.2 <i>L. infantum</i> infection	3
1.1.3 Diagnosis and treatment of visceral leishmaniasis	3
1.2 <i>The innate immune system</i>	4
1.2.1 Monocytes and macrophages.....	5
1.2.2 Immune response to <i>L. infantum</i> infection	7
1.3 <i>Organoids</i>	9
1.3.1 Liver organoids.....	10
1.3.2 Application of organoids in immunological research	11
1.3.3 Aim of this thesis.....	13
2 Material and Methods	14
2.1 <i>Material</i>	14
2.1.1 Laboratory equipment	14
2.1.2 Consumables	15
2.1.3 Chemicals and reagents	16
2.1.4 Kits	16
2.1.5 Antibodies	17
2.1.6 Culture media and buffers	18
2.1.7 Oligonucleotides	21
2.1.8 Organisms.....	22
2.1.9 Software and Databases	22
2.1.10 List of utilized tools	23
2.2 <i>Cell Biology Methods</i>	23
2.2.1 Isolation of murine hepatocytes	23
2.2.2 Handling of isolated primary human hepatocytes	24
2.2.3 Cultivation of murine and human 3D hepatocyte organoids.....	24
2.2.4 Production of R-Spondin1 conditioned medium.....	25
2.2.5 Cultivation of <i>Leishmania</i> parasites	25
2.2.6 Transfection of <i>Leishmania</i> parasites	25
2.2.7 Isolation of murine bone marrow cells	26
2.2.8 Isolation of monocytes from murine bone marrow cells.....	26
2.2.9 Differentiation of murine bone marrow cells into macrophages (BMDMs)	26
2.2.10 CMFDA staining	27
2.2.11 Determination of cell count.....	27
2.2.12 Staining of murine cells for FACS analysis – Monocyte purity control	27
2.3 <i>Cellular Assays</i>	28

2.3.1	<i>L. infantum</i> infection of murine HepOrgs in suspension	28
2.3.2	Co-culture of murine <i>L. infantum</i> -infected HepOrgs with monocytes.....	29
2.3.3	<i>L. infantum</i> infection of murine macrophages (BMDMs).....	29
2.3.4	Co-cultivation of murine HepOrgs with <i>L. infantum</i> -infected macrophages	30
2.4	Molecular Biology Methods	31
2.4.1	Isolation of gDNA from <i>Leishmania</i> -infected macrophages	31
2.4.2	<i>Leishmania</i> quantification by TaqMan real-time PCR.....	31
2.4.3	RNA isolation	32
2.4.4	RNA integrity control using Bioanalyzer Agilent 2100	32
2.4.5	RNA sequencing	33
2.4.6	Analysis of RNA sequencing results	33
2.4.7	cDNA synthesis	34
2.4.8	Quantitative Real-Time Polymerase Chain Reaction (RT-qPCR).....	34
2.5	Biochemical Methods	35
2.5.1	Enzyme-Linked Immunosorbent Assay (ELISA)	35
2.5.2	Multiplex Immunoassay - LEGENDplex™	37
2.5.3	Whole mount immunostaining of organoids.....	37
2.5.4	Analysis of the infection parameters of <i>L. infantum</i> infected macrophages using High Content Screening (HCS).....	38
2.5.5	Statistics	39
3	Results	40
3.1	Generation of functional 3D organoids	40
3.1.1	Implementation of murine 3D hepatocyte organoid culture	40
3.1.2	Characterization of murine hepatocyte organoids	42
3.1.3	Establishment and characterization of human 3D hepatocyte organoids	43
3.2	Establishment of <i>L. infantum</i> infection in hepatocyte organoid immune cell co-cultures	45
3.3	Implementation of <i>L. infantum</i> infection in hepatocyte organoids	47
3.3.1	Generation of fluorescent <i>L. infantum</i> parasites	48
3.3.2	Evaluation of the infiltration of murine hepatocyte organoids by <i>L. infantum</i> parasites ...	49
3.3.3	The cytokine profile of <i>L. infantum</i> -exposed hepatocyte organoids	51
3.3.4	Application of the established infection protocol to human hepatocyte organoids.....	53
3.3.5	Transcriptome analysis of murine <i>L. infantum</i> -exposed hepatocyte organoids.....	56
3.4	Co-culture of murine monocytes with <i>L. infantum</i>-infected hepatocyte organoids	60
3.4.1	a) Co-culture of monocytes and infected organoids embedded in BME	61
3.4.2	b) Co-culture of monocytes and infected organoids in semi-suspension.....	63
3.4.3	c) Co-culture of monocytes and infected organoids in suspension.....	65
3.5	Co-culture of hepatocyte organoids with <i>L. infantum</i>-infected macrophages	68
3.5.1	Co-culture of dissociated hepatocyte organoids and <i>L. infantum</i> -infected macrophages	70
3.5.2	Co-culture of intact hepatocyte organoids with <i>L. infantum</i> -infected macrophages	74
3.6	Summary of the cytokine data obtained from the distinct co-culture approaches	77
4	Discussion	78
4.1	Establishment of murine and human 3D hepatocyte organoids	78
4.2	Infection of hepatocyte organoids with <i>L. infantum</i> parasites	80
4.2.1	<i>L. infantum</i> parasites form direct contacts with HepOrgs following infection in suspension	80

4.2.2	<i>L. infantum</i> parasites infiltrate murine and human HepOrgs.....	81
4.2.3	Cytokine profiles of <i>L. infantum</i> -infected HepOrgs	82
4.2.4	Transcriptome analysis of murine <i>L. infantum</i> infected HepOrgs.....	84
4.3	Co-culture of murine <i>L. infantum</i> -infected HepOrgs and monocytes.....	85
4.4	Co-culture of hepatocyte organoids with <i>L. infantum</i> -infected macrophages.....	88
Supplementary data		91
	<i>Transcriptome analysis</i>	<i>91</i>
	<i>Harmony software setup.....</i>	<i>95</i>
References.....		A
Acknowledgements.....		J

Summary

Visceral leishmaniasis is a neglected tropical disease caused by a systemic infection with protozoan parasites of the genus *Leishmania*. Throughout the course of the disease, tissue-resident macrophages in the liver (Kupffer cells) are infected. This initiates a pivotal immune response essential for parasite elimination. To date, little is known about the degree to which functional liver cells, such as hepatocytes, are directly impacted by the infection and contribute to the development of this immune response. Furthermore, the investigation of underlying immune mechanisms is impeded by the absence of appropriate model systems.

In this study, an *in vitro* co-cultivation system was established, that integrates murine hepatocyte organoids with monocytes or macrophages, to simulate hepatic infection with *Leishmania infantum* parasites.

The initial part of this study demonstrated the successful generation of three-dimensional hepatocyte organoids derived from both human and murine primary hepatocytes. The functionality as well as the proliferative capacity of the cultured organoids was proven. Additionally, it was illustrated that under appropriate culture conditions, *L. infantum* parasites could infiltrate the generated hepatocyte organoids. The resulting immune response of the organoids was comprehensively investigated through cytokine and transcriptome analyses. Overall, both methodologies revealed only minimal responsiveness of the hepatocyte organoids to the infection.

Moreover, a total of five distinct systems for co-cultivating hepatocyte organoids with either monocytes or macrophages were applied, distinguished primarily by the utilization of a hydrogel that mimics the extracellular matrix. Infection with *L. infantum* parasites within these co-cultures was represented either through prior infection of murine organoids, following the established methodology, or by infection of murine macrophages. To assess the efficacy of these systems, the dynamics in cytokine production in comparison to the murine model were analyzed via ELISA and Multiplex Cytokine assay. Co-cultivation of murine monocytes with *L. infantum*-infected hepatocyte organoids in suspension resulted in an infection-specific induction of cytokines, including CCL3, CCL2, TNF, IFN- γ and IL-10, aligning with trends observed in the murine experimental model of VL. Furthermore, it was observed that the induction of specific cytokines, such as CCL3 and TNF, was exclusive to co-cultures including both hepatocyte organoids and monocytes. Additionally, utilizing qPCR, infection-specific differences in the transcript levels of *Nos2* and *Arg1* were discerned, indicating upregulation of *Nos2* and downregulation of *Arg1* following infection, consistent with mechanisms typically associated with the elimination of parasites. These findings provide insights into the role of hepatocytes in modulating liver microenvironment conducive to the eradication of *Leishmania* parasites.

The replication of infection-specific cytokine dynamics observed in the animal model within the *in vitro* co-cultivation system of hepatocyte organoids and monocytes demonstrated in this study, underscores the potential of this methodology to advance the reduction of animal experiments in line with the 3R principle (Reduce, Refine, Replace). Furthermore, these established techniques offer a platform for future investigations utilizing human specimens, thereby enriching the current understanding of immune mechanisms during visceral leishmaniasis in humans.

Zusammenfassung

Viszerale Leishmaniose ist eine vernachlässigte Tropenkrankheit, die durch eine systemische Infektion mit protozoischen Parasiten der Gattung *Leishmania* hervorgerufen wird. Im Verlauf der Erkrankung werden unter anderem gewebeständige Makrophagen in der Leber (Kupffer-Zellen) infiziert. In der Folge wird eine Immunantwort ausgelöst, die entscheidend für die erfolgreiche Eliminierung der Parasiten ist. Bisher ist wenig darüber bekannt, inwieweit funktionale Leberzellen, wie Hepatozyten, direkt von der Infektion betroffen sind und die Bildung dieser Immunantwort beeinflussen. Des Weiteren wird die Erforschung der zugrundeliegenden Immunmechanismen durch einen Mangel an geeigneten Modellsystemen erschwert.

In der vorliegenden Studie wurde ein *in vitro* Co-Kultivierungssystem etabliert, welches murine Hepatozyt-Organoiden mit Monozyten bzw. Makrophagen kombiniert, um die hepatische Infektion mit *Leishmania infantum* Parasiten zu modellieren.

Im ersten Abschnitt wurde die erfolgreiche Generierung dreidimensionaler Hepatozyt-Organoiden auf der Basis humaner und muriner primärer Hepatozyten dargestellt. Dabei wurden sowohl die Funktionalität als auch die Proliferationsfähigkeit der kultivierten Organoiden nachgewiesen. Weiterhin wurde gezeigt, dass unter geeigneten Kultivierungsbedingungen *L. infantum* Parasiten die generierten Hepatozyt-Organoiden infiltrieren können. Die resultierende Immunantwort der Hepatozyten wurde umfassend mittels Zytokin- und Transkriptomanalyse untersucht. Insgesamt zeigte sich in beiden Untersuchungsmethoden lediglich eine sehr geringe Reaktion der Hepatozyt-Organoiden auf die Infektion.

Zudem wurden insgesamt fünf verschiedene Systeme zur Co-Kultivierung von Hepatozyt-Organoiden mit Monozyten bzw. Makrophagen untersucht, die sich insbesondere in der Verwendung eines Hydrogels unterscheiden, das die extrazelluläre Matrix nachahmt. Die Infektion mit *L. infantum* Parasiten innerhalb der Co-Kulturen wurde dabei entweder durch vorherige Infektion muriner Organoiden gemäß der zuvor etablierten Methodik, oder durch Infektion muriner Makrophagen dargestellt. Zur Beurteilung der verschiedenen Systeme wurden die Dynamiken in der Zytokin-Produktion im Vergleich zum murinen Tiermodell mittels ELISA und Multiplex Zytokinassay untersucht. Die Co-Kultivierung von murinen Monozyten mit *L. infantum*-infizierten Hepatozyt-Organoiden in Suspension führte zu einer infektionsspezifischen Induktion der Zytokine CCL3, CCL2, TNF, IFN- γ und IL-10, ähnlich wie im murinen Tiermodell. Darüber hinaus zeigte sich, dass die Induktion einzelner Zytokine, wie CCL3 und TNF, ausschließlich in Co-Kulturen von Hepatozyt-Organoiden und Monozyten auftrat. Mittels qPCR wurden zudem infektionsspezifische Unterschiede in den Transkriptmengen von *Nos2* und *Arg1* nachgewiesen, wobei *Nos2* nach der Infektion hochreguliert und *Arg1* herunterreguliert wurde, was im Allgemeinen mit der Eliminierung von *Leishmania* Parasiten assoziiert ist. Diese Erkenntnisse liefern Einblicke in die Beteiligung von Hepatozyten an der Modulation eines Gewebemilieus, das die Eliminierung von *Leishmania* Parasiten begünstigt.

Die Reproduktion, der im Tiermodell beobachteten, infektionsspezifischen Dynamiken in der Zytokin-Produktion im hier dargestellten *in vitro* Co-Kultivierungssystem von Hepatozyt-Organoiden und Monozyten, verdeutlicht das Potential dieser Methodik zur Reduktion von Tierversuchen im Rahmen des 3R-Prinzips (Reduce, Refine, Replace) beizutragen. Darüber hinaus bieten die etablierten Methoden eine Plattform für weiterführende Untersuchungen mit humanem Material, was dazu beitragen könnte, das bestehende Verständnis der Immunmechanismen während der viszeralen Leishmaniose im Menschen zu vertiefen.

List of figures

Figure 1: The Life cycle of <i>Leishmania</i> spp.....	2
Figure 2: Immune dynamics during VL in the liver.	9
Figure 3: Co-culture systems to study the interaction of epithelial cells and immune cells...	12
Figure 4: Agilent 2100 Bioanalyzer output.....	33
Figure 5: Seeding of primary murine hepatocytes into 3D liver organoids.....	41
Figure 6: Immunofluorescence-based characterization of hepatocyte organoids.....	42
Figure 7: Establishment of human 3D hepatocyte organoids.	44
Figure 8: Scheme for establishing co-cultures of hepatocytes organoids with immune cells.	46
Figure 9: Evaluation of different hepatocyte organoid infection protocols.....	47
Figure 10: Generation of mCherry <i>L. infantum</i> transfectant.	48
Figure 11: Imaging of the infiltration of hepatocyte organoids by <i>L. infantum</i> parasites.....	50
Figure 12: Cytokine profiling of hepatocyte organoids exposed to <i>L. infantum</i> parasites.	52
Figure 13: Microscopic evaluation of <i>L. infantum</i> infection in human hepatocyte organoids.	53
Figure 14: Cytokine profiling of human hepatocyte organoids infected with <i>L. infantum</i> parasites.....	55
Figure 15: Analysis of differentially expressed genes between uninfected and infected hepatocyte organoids derived from male and female mice.....	56
Figure 16: Transcriptome analysis of the defined sample subset.	58
Figure 17: Analysis of relevant gene transcripts using the selected data set from <i>L. infantum</i> -infected organoids.	59
Figure 18: Schematic depiction of the co-cultivation of monocytes with <i>L. infantum</i> -infected hepatocyte organoids.	60
Figure 19: Purity control of monocytes isolated from murine bone marrow.	61
Figure 20: Co-culture of <i>L. infantum</i> -infected hepatocyte organoids with monocytes in BME.	62
Figure 21: Co-culture of <i>L. infantum</i> -infected hepatocyte organoids with monocytes in semi-suspension.	64
Figure 22: Co-culture of <i>L. infantum</i> -infected hepatocyte organoids with monocytes in suspension.	66
Figure 23: qPCR of genes of interest using suspension co-culture RNA samples.	67
Figure 24: Co-culture set up of macrophages and hepatocyte organoids and evaluation of the infection of murine macrophages with <i>L. infantum</i> parasites.	69
Figure 25: Microscopic monitoring of the co-cultivation of dissociated organoids and macrophages.....	71
Figure 26: Immunofluorescence analysis of the co-culture comprising dissociated organoids and macrophages, and <i>Leishmania</i> β -Actin quantification.....	72
Figure 27: Assessment of cytokine levels in the culture supernatants of co-cultures comprising dissociated organoids and macrophages.....	73
Figure 28: Co-culture of adherent macrophages with intact organoids.....	76

List of tables

Table 1: List of utilized instruments	14
Table 2: List of utilized consumables.....	15
Table 3: List of utilized solutions.....	16
Table 4: List of utilized Kits.....	16
Table 5: List of primary antibodies utilized for IFA.....	17
Table 6: List of conjugated antibodies	17
Table 7: List of buffers and media supplements	18
Table 8: Composition of utilized buffers and media.....	19
Table 9: List of utilized primers for RT-qPCR	21
Table 10: List of utilized organisms	22
Table 11: List of utilized softwares.....	22
Table 12: List of utilized Websites	23
Table 13: TaqMan qPCR sample set up	31
Table 14: Cyclor program for RT-qPCR.....	34
Table 15: Summary of co-culture cytokine data.	77

Abbreviations

°C	degree Celsius
<i>Acta1</i>	<i>Actin alpha 1, skeletal muscle</i>
AF	Alexa Fluor
APC	Antigen presenting cell
APC	Allophycocyanin
<i>Arg1</i>	<i>Arginase1</i>
AUC	Area under the curve
BCP	1-bromo-3-chloropropane
BMDM	Bone marrow-derived macrophage
BNITM	Bernhard Nocht Institute for Tropical Medicine
BSA	Bovine serum albumine
CCL	CC-chemokine ligand
CCR	CC-chemokine receptor
CholOrgs	Cholangiocyte organoids
CL	Cutaneous leishmaniasis
CX ₃ CR	CX ₃ C-chemokine receptor
CXCL	CXC motif chemokine ligand
CXCR	CXC motif chemokine receptor
DAPI	4,6-Diamidin-2-phenylindol
DC	Dendritic cell
DCL	Diffuse cutaneous leishmaniasis
DEG	Differentially expressed genes
dH ₂ O	Distilled water
DIC	Different interference contrast
dPBS	Dulbecco's PBS
ECM	Extracellular matrix
ELISA	Enzyme-linked immunosorbent assay
FACS	Fluorescence activated cell sorting
FBS	Fetal bovine serum
FC	Fold change
gDNA	genomic deoxyribonucleic acid
h	hour

HCS	High content screening
HepOrg	Hepatocyte organoid
HIV	Human immunodeficiency virus
HRP	Horseradish peroxidase
HSP90	Heat shock protein 90
HTCR	Human and Tissue Cell Research
IFN	Interferon
IL	Interleukin
<i>Il6ra</i>	<i>interleukin 6 receptor, alpha</i>
iNOS	Inducible nitric oxide synthetase
<i>L.</i>	<i>Leishmania</i>
LBP	Laminin binding protein
LCL	Localized cutaneous leishmaniasis
LHSP90	pan- <i>Leishmania</i> heat shock protein 90
LPG	Lipophosphoglycan
LPS	Lipopolysaccharide
Ly	Lymphocyte (antigen)
MCL	Mucocutaneous leishmaniasis
M-CSF	Macrophage colony-stimulating factor
MFI	Median fluorescence intensity
min	minute(s)
MOI	Multiplicity of infection
n	samples size
NET	Neutrophil extracellular trap
NGS	Next Generation Sequencing
NK	Natural killer cell
NO	Nitric oxide
<i>Nod2</i>	Nucleotide-binding oligomerization domain 2
<i>Nos2</i>	Nitric oxide synthase 2
NTD	Neglected tropical disease
PAMPs	Pathogen-associated molecular pattern
PBS	Phosphate buffer saline
PCA	Principal component analysis
PCR	Polymerase chain reaction

PE	Phycoerythrin
PFA	Paraformaldehyde
PHx	Partial hepatectomy
pg	picogram(s)
<i>Plekhs1</i>	<i>Pleckstrin homology domain containing, family S member 1</i>
POC	Percentage of control
PRR	Pattern recognition receptor
PSC	Pluripotent stem cell
RCM	R-Spondin1 conditioned medium
RIN	RNA integrity number
RNA	Ribonucleic acid
RNase	Ribonuclease
ROS	Reactive oxygen species
<i>Rps9</i>	40S Ribosomal protein S9
RT	Room temperature
RT-qPCR	Real-time quantitative polymerase chain reaction
s	second(s)
<i>Sass6</i>	<i>SAS-6 centriolar assembly protein</i>
spp.	Species
<i>S100a14</i>	<i>S100 calcium binding protein A14</i>
TGF	Transforming growth factor
T _H	T Helper cell
TMB	3,3',5,5'-Tetramethylbenzidine
TNF	Tumor necrosis factor
<i>Tlr2</i>	Toll-like receptor 2
U	Units
VL	Visceral leishmaniasis
WHO	World health organization
vs.	versus
µg	microgram(s)
µl	microliter(s)
µm	micrometer(s)

1 Introduction

1.1 Leishmaniasis

Leishmaniasis is a vector-borne disease caused by protozoan parasites of the *Leishmania* spp.. Estimations suggest that between 0.9 to 1.7 million people are annually infected with the parasites, with 20,000 to 30,000 deaths attributed to leishmaniasis each year. The disease is most widespread in tropical and subtropical areas and has been recognized by the World Health Organization (WHO) as one of the top 10 neglected tropical disease (NTD) [1–3]. The parasite is transmitted to mammalian hosts through infected female phlebotomine sandflies. Consequently, disease distribution is closely correlated to the geographic distribution of these sandflies, which is expanding due to the ongoing climate change. In this context, leishmaniasis might represent an increasing health threat. Additional risk factors that can contribute to the development of severe disease are amongst others malnutrition, poverty, poor hygiene standards, little access to medical care as well as immunosuppression [2].

A variety of approximately 53 different *Leishmania* species have been documented so far, of which 31 species are known to be pathogenic for mammals. The various parasite species can cause distinct forms of the disease. Thus, clinical manifestations of the disease are associated with the global distribution of the causative parasite species as well as the host immune-status [1,4]. In humans, the disease presents in three prominent forms, with a broad spectrum of severity: visceral leishmaniasis (VL) or kala azar, cutaneous leishmaniasis (CL) and mucocutaneous leishmaniasis (MCL).

Cutaneous leishmaniasis is the most prevalent form of leishmaniasis, as it accounts for 600,000 to 1 million cases annually worldwide. It is caused by *L. tropicana*, *L. aethiopica* and *L. major* in the Old World, referring to the eastern hemisphere (Asia, Middle East, Africa and Europe), and by *L. mexicana*, *L. amazonensis* and *L. brasiliensis* in the New World, referring to the western hemisphere (Mexico, Central, South and North America) [5,6]. This form is characterized by the formation of localized skin lesions at the site of parasite inoculation and therefore also referred to as localized CL (LCL). Initially appearing as asymptomatic papules, the infection can progress to form multiple rounded ulcers. The development of secondary infections with bacteria or fungi can additionally worsen lesion progression. The duration of these lesions varies from a few months up to decades, while potentially causing lifelong scarring and social stigmatization [7–9]. In diffuse CL (DCL), an insufficient immune response leads to the formation of lesions on extensive areas of the skin. Mucocutaneous leishmaniasis (MCL), a distinct form of CL, predominantly occurs in Latin America. In this form, the infection extends to the mucous membranes, particularly in the nose, mouth and throat subsequent to the resolution of the initial skin lesion. As a result, the destruction of these membranes can cause profound facial disfiguration [2,3,10,11].

The most severe manifestation is visceral leishmaniasis, also known as kala-azar (black fever), which affects an estimated 0.2 to 0.4 million individuals annually worldwide. This type of infection is caused by *L. donovani* and *L. infantum* in the Old World and *L. chagasi*, *L. amazonensis* and *L. tropica* in the New World. In contrast to CL, where the parasitic infection is confined to the skin, VL manifests as a systemic infection, causing further infiltration of liver, spleen, bone marrow, lymph nodes and intestine. Patients affected by VL typically present with symptoms including irregular fever, weight loss, hepatomegaly, splenomegaly, or even hepatosplenomegaly and anemia. If left untreated, it leads to death in 95 % of cases [2,3].

1.1.1 Life cycle and transmission

Leishmania parasites evidence a complex life cycle that is closely linked to sandflies as their transmission vector (Figure 1). Within this life cycle two distinct morphological forms of the parasite are distinguished: the motile extracellular promastigotes and the intracellular amastigotes. While promastigotes exhibit an elongated cell shape with a flagellum, amastigotes appear round and aflagellated. Both forms are highly adapted to their respective life stage [12,13].

During the blood meal of an infected phlebotomine sandfly, infective metacyclic promastigotes are injected into the mammalian host via the proboscis. In the skin, the parasites are uptaken by mononuclear cells, mainly macrophages around the incision site. Inside the macrophages the promastigotes differentiate into amastigotes due to temperature and pH changes within the phagolysosome. Intracellular amastigotes replicate until the host cell ruptures, allowing the reinvasion of adjacent phagocytic cells. These phagocytes can subsequently be ingested by a sandfly during a blood meal. The life cycle is closed, as amastigotes undergo differentiation initially into procyclic promastigotes and later into infective metacyclic promastigotes within the midgut of the sandfly [9,14].

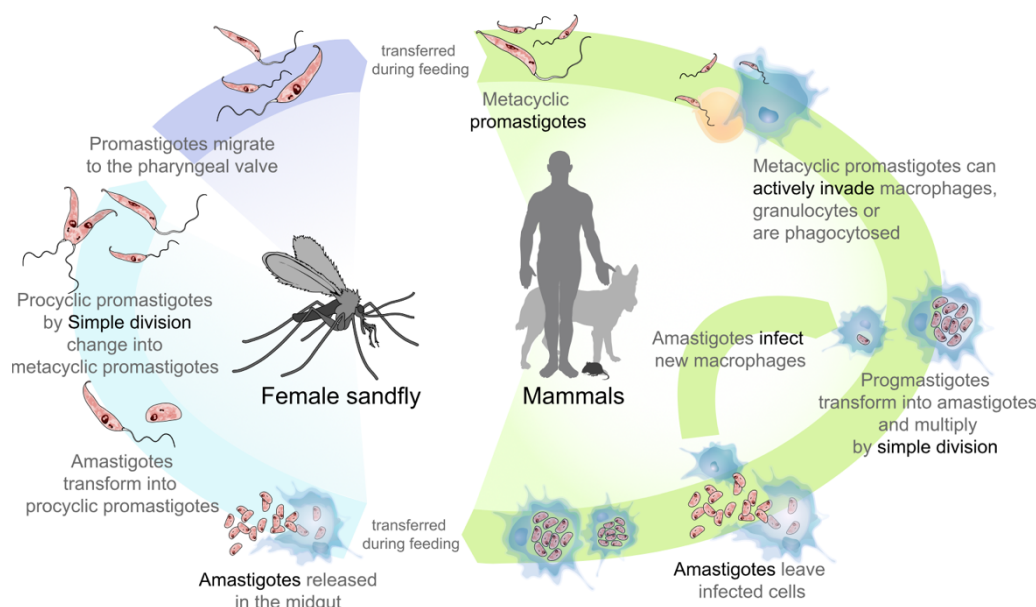


Figure 1: The Life cycle of *Leishmania* spp.

Metacyclic promastigotes are injected into the host's skin during the blood meal of an infected female phlebotomine sandfly. Local phagocytes internalize the parasites and promastigotes undergo transformation into amastigotes within the phagolysosome of the host cell. Amastigotes proliferate until the host cells rupture, releasing amastigotes that subsequently infect new phagocytic cells, primarily macrophages. During the blood meal of another sandfly on an infected host, amastigotes within macrophages are taken up again. Within the midgut of the sandfly, amastigotes are released, transform into procyclic promastigotes, which multiply through simple division and convert into metacyclic promastigotes. These migrate to the pharyngeal valve, from where they can be transmitted to a new host, during subsequent blood meals. Illustration: [15]

The transmission of *Leishmania* spp. by sandflies primarily originates from symptomatic humans, whereas asymptomatic individuals are thought to play a negligible role in infecting phlebotomine vectors [16,17]. Consequently, the life cycle of *Leishmania* is closely linked to human hosts for certain species, such as *L. tropica* in the New World and *L. donovani* in India (anthroponotic cycle). However, *Leishmania* can also sustain their lifecycle through various other mammalian hosts (zoonotic cycle), including dogs, rodents, marsupials, monkeys and

edentates, all of which may show signs of infection. Among these, dogs serve as the primary reservoir host. In rare cases, leishmaniasis can be transmitted directly from human to human through organ donation, blood transfusion or intravenous drug administration [18–20].

1.1.2 *L. infantum* infection

L. infantum parasites are the causative agent of VL across the Mediterranean area, the Middle East, Afghanistan, Iran, Pakistan and Brazil, with Brazil alone representing 90 % of all VL cases in the Americas [21,22]. Belonging to the *L. donovani* complex, *L. infantum* is synonymously referred to as *L. chagasi* in South America. These parasites demonstrate a zoonotic life cycle, with dogs acting as its primary host reservoir. Conversely to *L. donovani*, which infects individuals across all age groups, *L. infantum* infection predominantly affects children and immunocompromised adults [23,24]. Notably, VL has been strongly associated with co-infection with the human immunodeficiency virus (HIV), as HIV-infected individuals are especially prone to develop severe VL. Especially as both conditions synergistically suppress immune responses, thereby limiting therapeutic options and leading to higher rates of disease relapse and ultimately elevated mortality rates. As of now, HIV coinfection is reported in 45 countries where both diseases prevail, specifically affecting Brazil, Ethiopia and Bihar (India) [25].

Interestingly, previous studies have demonstrated a sex difference in the prevalence of VL caused by *L. infantum*. Specifically, while infection rates are comparable between males and females, males exhibited a bias to develop symptomatic VL. This suggests that disease susceptibility may be influenced by factors associated with biological sex [26,27]. Discrepancies in susceptibility between males and females were observed across the age range of 6-60 years, with the most prominent difference observed among individuals aged 21-40 years, indicating a potential correlation with sex steroids. However, the underlying mechanisms of this relationship remain incompletely understood [27,28].

Sex-specific differences in susceptibility to VL, have also been documented in experimental mouse models. Here male mice in both BALB/c and C57BL/6 genetic backgrounds, evidenced significantly higher parasite loads in the liver compared to female mice, following *L. infantum* inoculation [27]. This suggests that mouse models of *L. infantum* infection can partially reproduce human responses. However, these models alongside other experimental animal models including hamsters, domestic dogs and non-human primates fail to reproduce the clinical picture observed in humans in its entirety [29]. To gain deeper insights into the specific interactions between host and parasite, that underlie (sex-specific differences in) susceptibility vs. resistance in humans, as well as to identify potential therapeutic targets, the development of novel and refined models is imperative [30].

1.1.3 Diagnosis and treatment of visceral leishmaniasis

Diagnosing VL can pose significant challenges, especially in resource-limited countries. However, patients in endemic regions presenting with common symptoms such as persistent fevers, fatigue, weight loss, anemia, leucopenia and hepatosplenomegaly should undergo thorough diagnostic evaluation. Ideally, confirmation of *Leishmania* infection is achieved through the detection of parasites in tissue samples or via molecular testing [20,31,32]. The identification of parasites in tissue samples is most reliable in splenic biopsies. Alternative sources such as bone marrow, liver, enlarged lymph nodes and whole blood can be utilized, albeit with lower sensitivity [33,34]. Within appropriate tissue specimens, the presence of potential amastigotes in or around macrophages can be detected through Giemsa staining. Alternatively, infected tissues can be cultured and parasites can be identified via culture

histology [35]. However, further molecular methods are required to identify the specific *Leishmania* species, which is crucial in determining appropriate treatment strategies. Polymerase chain reaction (PCR) represents a common method with high sensitivity, suitable to detect infection albeit low parasite burden and to identify the *Leishmania* species. In addition, serological tests serve as an alternative when direct parasite confirmation is not available. Methods for detecting IgG antibodies, such as direct agglutination, enzyme-linked immunosorbent assay (ELISA), immunofluorescence analysis (IFA) and Western Blot are employed [34]. Among these, antibodies against the *Leishmania*-specific antigen K39 are a preferred target with high sensitivity [36,37].

Previously, the treatment regimen for VL predominantly comprised the systemic administration of pentavalent antimonials, such as meglumine antimoniate and sodium stibogluconate. However, the widespread use of these medications has been associated with the emergence of resistance in various strains of *Leishmania* [31,38]. Consequently, newer treatment strategies include the administration of liposomal Amphotericin B or Miltefosine. Pentavalent antimonials are now reserved as an alternative treatment option for patients who are unable to tolerate Amphotericin B or Miltefosine administration, or in regions where *Leishmania* strains exhibit low levels of drug resistance. Regardless of the treatment modality employed, close monitoring of patients is essential even after successful treatment to promptly address any potential relapses [31].

1.2 The innate immune system

The mammalian immune system serves as a crucial defense apparatus to protect the organism against a wide spectrum of pathogenic agents, such as toxins, microbes, viruses and cancer cells. To achieve optimal protection, structural and chemical barriers, alongside the innate and adaptive components of the immune system operate in close coordination. The innate immune system comprises physical barriers, as well as humoral and cellular components, mounting a rapid but antigen-independent response to invading pathogens. Conversely, the adaptive immune system, encompassing T- and B-lymphocytes, responds antigen-specific, but with a time delay between antigen recognition and maximum response. B-cells primarily generate antibodies upon direct encounter with foreign antigens, while T-cells interact with antigen presenting cells (APCs). Consequently, T-cell differentiation is induced, yielding predominantly cytotoxic T-cells (CD8⁺) or T-helper (T_H) cells (CD4⁺). T_H-cells primarily regulate immune responses and activate other cells, including the APCs that stimulated their activation, whereas cytotoxic T-cells are engaged in eliminating cells that present foreign antigens. Notably, adaptive immunity possesses the remarkable capability to form a memory of previously recognized antigens, facilitating a rapid and efficient immune response upon subsequent exposure. Both parts of the immune system complement each other and any dysregulation in either part can result in compromised immune responses and increased host vulnerability [39–42].

Cells of the innate immune system originate from hematopoietic stem cells, encompassing macrophages, dendritic cells (DCs), mast cells, monocytes, neutrophils, eosinophils, basophils, natural killer (NK) cells and natural killer T cells. Additionally, cells of non-hematopoietic origin, such as epithelial cells lining the gastrointestinal, genitourinary and respiratory tracts, contribute to innate immunity [39]. Operating in an antigen-independent manner, innate immunity recognizes conserved motifs among pathogens, commonly referred to as pathogen associated molecular patterns (PAMPs). Typical examples of PAMPs include

viral double-stranded ribonucleic acid (RNA) and components from bacterial cell walls like lipopolysaccharides (LPS). Pattern recognition receptors (PRRs), such as Toll-like receptors (TLRs), expressed by cells of the innate immune system facilitate the identification of these motifs and subsequent response [42].

A fundamental mechanism of the innate immune system involves the release of cytokines and chemokines, which orchestrate the recruitment of immune cells to the site of infection and induce local inflammation. These processes are crucial for the effective elimination of many pathogens. Notably, cytokines such as tumor necrosis factor (TNF), interleukin (IL-) 1 and IL-6 are known to be released as an initial response to pathogen invasion. Furthermore, specialized phagocytes within the innate immune system, including macrophages and neutrophils engage in the engulfment of parasites, subsequently killing them through bactericidal pathways. Neutrophils additionally eliminate extracellular pathogens via granules and specific enzymes. Macrophages as well as DCs, proficient in phagocytosing microbes, serve as APCs, bridging the innate and adaptive immunity [39,41,42].

Interestingly, numerous immune responses in both innate and adaptive immunity exhibit sexual dimorphism. This disparity can be attributed to epigenetic and genetic differences between male and female individuals, primarily involving sex-chromosomes, as well as specific sex-related steroid hormones that directly influence immune cell function. In particular, androgens have been shown to suppress the expression of inflammatory mediators, such as TNF and nitric oxide (NO) in innate immune cells, whereas estrogens stimulate the expression of inflammatory cytokines. In general, this implies that females typically mount a stronger immune response compared to males, especially in infectious diseases. However, this heightened immune response in females also correlates with a higher prevalence of autoimmune disease [43–45].

In the framework of this thesis, particular attention is directed towards monocytes and macrophages, both major components of the innate immune system, which play substantial roles in the immune responses associated with leishmaniasis.

1.2.1 Monocytes and macrophages

Monocytes and macrophages are mononuclear cell populations integral to innate immunity. Both fulfill important functions in maintaining tissue homeostasis and orchestrating inflammatory responses. However, due to their potential to initiate inflammatory reactions, they are also associated with the development of pathologies. Consequently, they represent interesting subjects for research in the context of immunopathology [46].

Monocytes originate in the bone marrow, where they arise from hematopoietic stem cells before entering the blood circulation. In mice, they constitute 4 % of all nucleated cells in the blood, while in humans, they comprise 10 %. Additionally, monocytes can be mobilized from populations in the spleen and lungs [47,48]. In mice, all monocytes express the myeloid marker CD11b, while two functionally distinct subsets are recognized, based on their expression levels of lymphocyte antigen 6 C (Ly6C) and CX₃C motif chemokine receptor (CX₃CR) 1. Classical monocytes, characterized by high Ly6C expression (Ly6C^{hi}) and low amounts of CX₃CR1, are recruited to sites of infection, inflammation, or tissue remodeling, where they migrate into tissues and differentiate into monocyte-derived DCs and monocyte-derived macrophages [46,49]. Egress from the bone marrow as well as recruitment into tissues is mediated by the C-C chemokine receptor (CCR) 2, highly expressed on classical monocytes, and its respective ligand chemokine (C-C motif) ligand 2 (CCL2) [50]. Under steady-state conditions, classical monocytes in the blood stream can differentiate into non-classical monocytes, characterized

by low Ly6C (Ly6C^{lo}) and CCR2 expression, as well as high expression of CX₃CR1. However, non-classical monocytes can also directly develop in the bone marrow. This subset functions in patrolling endothelial surfaces for integrity and recruiting neutrophils in response to tissue damage [51,52]. Comparable subsets of monocytes have been identified in humans, with CD14⁺CD16⁻ representing classical monocytes and CD14^{low}CD16⁺ representing non-classical monocytes. The expression levels of CCR2, as well as functions seem equivalent to murine counterparts. Additionally, an intermediate subset of monocytes is defined in humans as CD14⁺CD16⁺ [53,54].

The trafficking of monocytes guided by chemokines is a crucial process essential for their functionality. Apart from the previously mentioned CCL2, numerous other chemokines play roles in this process. Chemokines such as CCL7 and CCL12, akin to CCL2, facilitate the egress of monocytes from the bone marrow via the common receptor CCR2 especially under inflammatory or infectious conditions. Consequently, this results in an elevation of Ly6C^{hi} monocytes in the bloodstream, due to high expression of CCR2. Recruitment into or within inflamed or infected tissues primarily relies on receptors CCR1 and CCR5 and their respective ligands, including CCL3 and CCL5. Additionally, the upregulation of C-X-C motif ligand 1 (CXCL1) under inflammatory conditions predominantly leads to increased recruitment of neutrophils. However, monocytes also express the corresponding (C-X-C motif) receptor 2 (CXCR2), which contributes to their recruitment. Overall, dysregulation of monocyte recruitment can contribute to the development of immunopathology, underscoring chemokines as targets for therapeutic interventions [55–57].

In contrast to monocytes, macrophages represent a heterogeneous group of cells dispersed throughout various tissues in the entire body. Even under homeostatic conditions, macrophages can constitute a significant proportion, ranging from 10-15 % of total cellular constituents within a given tissue, which can increase further during inflammatory conditions. The heterogeneity among macrophages stems from the disparate microenvironments across different tissue types. Interestingly, despite executing similar functions, macrophages exhibit substantial differences at the transcriptomic level depending on their tissue of residence. Macrophages are therefore referred to differently, depending on their tissue localization, e.g. as Kupffer cells in the liver or osteoclasts in the bones [58,59]. Monocytes have long been considered as the sole progenitors of macrophages. However, further understanding revealed that macrophages predominantly originate from embryonic precursors within the tissue and are capable of self-renewal, for their maintenance. The contribution of monocytes in replenishing macrophage populations appears to be confined to inflammatory conditions [46,60].

Based on the activation state of macrophages and their specific microenvironment, two major subpopulations have been described: the classically activated M1 and the alternatively activated M2 macrophages [61]. The induction of the M1 phenotype is mainly facilitated by LPS and interferon- (IFN) γ , commonly referred to as the pro-inflammatory phenotype, due to the secretion of key pro-inflammatory cytokines, such as IL-1 β and TNF as well as expression of inducible nitric oxide synthase (iNOS) [62,63]. Consequently, M1 macrophages exert pro-inflammatory effects through antigen presentation, pathogen elimination and anti-tumor responses [64,65]. Conversely, polarization into M2 macrophages, referred to as the anti-inflammatory phenotype, is induced by IL-4 and IL-13. This classification arises from the secretion of primarily anti-inflammatory cytokines, including IL-10, transforming growth factor- β (TGF- β) and expression of arginase 1 (Arg1). Therefore M2 macrophages are pivotal in promoting tissue remodeling, preventing overly inflammatory conditions and parasitic

infections, while also participating in processes such as angiogenesis, tumor progression and immune regulation [64]. Overall, M1 and M2 macrophages assume contrasting roles in the onset and progression of various diseases. The balance or imbalance in M1/M2 polarization plays a crucial role in modulating immune responses, with an imbalance potentially leading to either excessive or insufficient immune responses [65].

1.2.2 Immune response to *L. infantum* infection

The immune mechanisms triggered by *L. infantum* transmission via sandflies are complex and remain incompletely understood. A large part of the current understanding is based on animal models and transfer to VL in humans is constrained. However, some parts of human immunological dynamics, as well as the interplay between innate and adaptive immune components can be recapitulated in experimental models of VL [66,67].

Upon entry of metacyclic promastigotes into the host's skin during a blood meal of an infected sandfly, the parasites are taken up by phagocytes, such as dermal dendritic cells, macrophages and rapidly recruited neutrophils. Notably, up to 90 % of the injected parasites are lysated as a result of opsonization by complement components [68–70]. Neutrophils, considered as the first line of defense, employ phagocytosis and the production of reactive oxygen species (ROS) or neutrophil extracellular traps (NETs) to capture and eliminate parasites [71,72]. However, parasites have evolved mechanisms to evade neutrophil-mediated killing by counteracting oxidative stress, inhibiting phagolysosome biogenesis and delaying neutrophil apoptosis [73–75]. Infected neutrophils release a variety of cytokines, including IL-8, IL-1 β , macrophage inflammatory protein- (MIP) 1 β and TNF, thereby orchestrating the recruitment of additional host cells, primarily monocytes and macrophages, thus promoting infection establishment [76–78]. Ultimately, macrophages phagocytose apoptotic neutrophils including viable parasites. In this context, neutrophils serve as “Trojan Horses”, transmitting parasites to macrophages without inducing an immediate immune response [38,77].

Additionally, resident dermal macrophages directly phagocytose promastigote or amastigote parasites, establishing them as the predominant infected cell type within the initial 24 h after infection [79]. Parasites within macrophages reside in phagosomes, which undergo maturation into phagolysosomes to acquire anti-microbicidal properties. However, parasites can inhibit this process, primarily mediated by the parasitic surface molecule lipophosphoglycan (LPG), which additionally shields parasites from the enzymatic activity within the phagolysosome [80,81]. Effective control of parasite proliferation and the elicitation of a protective immune response is decisive for the further course of infection. Here, DCs play a crucial role in the initiation of the adaptive immune response, serving as primary influencers of T helper (T_H) polarization of CD4⁺ T-cells, through IL-12 secretion. A pro-inflammatory immune response is associated with the polarization of CD4⁺ T-cells into T_H1-cells following antigen recognition. T_H1-cells, in turn promote M1 polarization in macrophages, by secretion of cytokines, such as IFN- γ , IL-2 and TNF. M1 polarization correlates with the efficient elimination of intracellular parasites, primarily facilitated by the production of NO through iNOS [82–84].

Conversely, an anti-inflammatory environment upon antigen recognition, favors the polarization of CD4⁺ T-cells into T_H2-cells. These subsequently secrete anti-inflammatory factors, including transforming growth factor- (TGF) β , IL-10 and IL-4, ultimately associated with M2 macrophage polarization and parasite survival, predominantly driven by enhanced polyamine synthesis through arginase upregulation. While in mice a predominant T_H1 response facilitates the elimination of parasites, in humans a combination of T_H1 and T_H2 responses is more commonly observed [82–84].

The precise mechanism underlying the transfer of *Leishmania* parasites from the inoculated skin to the visceral organs during VL remains incompletely elucidated. However previous studies suggest that infected macrophages and DCs leave intradermal injection sites via lymphatic vessels. Additionally, the presence of free amastigotes in the bloodstream suggests a direct transport to the visceral organs [85,86]. Interestingly, the murine immune response to *Leishmania* infection is organ specific. While the infection is controlled and ultimately resolved in the liver, parasites persist in the spleen [87]. The underlying mechanisms of these distinct immune responses are not yet fully understood.

1.2.2.1 Cytokine dynamics in the liver during VL

In the context of developing new therapies for VL, cytokines have emerged as potential targets for immunotherapeutic interventions. To advance these strategies, a thorough understanding of cytokine dynamics during VL is essential [88]. In the framework of this thesis, a primary focus was placed on the processes occurring in the liver.

Upon invasion of the liver, tissue-resident macrophages, namely Kupffer cells as well as DCs phagocytose parasites. Subsequently, infected cells secrete chemokines, primarily CCL3, CCL2 and IP-10 (CXCL10), facilitating the recruitment of immune cells to the liver [89]. This recruitment primarily includes monocytes and neutrophils, mediated by CCL2 and CCL3, as well as CD8⁺ and CD4⁺ T-cells guided by IP-10, which enhances prolonged IP-10-dependent recruitment of additional T-cells as the infection progresses [90,91]. Here, the interaction between DCs and parasite-specific CD4⁺ T-cells triggers the production of T_H1 cytokines such as IL-2, TNF and IFN- γ . These cytokines induce M1 polarization in macrophages, as well as encapsulation of parasites by granuloma formation, ultimately leading to infection resolution in the liver [88,92] (Figure 2). These processes represent the primary mechanisms underlying infection resolution in the liver of murine models of VL, predominantly characterized by T_H1 immune responses. Thus, infection with *Leishmania* parasites in various murine models is controlled and asymptomatic, contrasting with the potentially lethal outcome in humans, which often involves components of both T_H1 and T_H2 immune responses [93]. *Leishmania* parasites are recognized for their ability to modulate the immune response by inducing heightened expression of cytokines like IL-10 and suppressing IL-12 production, thus promoting their survival through enhanced M2 polarization. The balance and regulation of these responses might be decisive for disease resistance and susceptibility in humans. However, murine models might not adequately reflect the underlying mechanisms in humans [94].

Interestingly, previous studies on *L. donovani* infection in mice have highlighted the immunopathological potential of the chemokines CCL2 and CCL3, which facilitate monocyte recruitment to the infected liver. Notably, studies have demonstrated that repression of CCL2 or CCL3-mediated monocyte recruitment resulted in a significant decrease in parasite burdens within the liver, suggesting a detrimental role of monocytes in disease progression [95,96]. Conversely, other investigations have demonstrated, that *in vivo* administration of CCL2 and CCL3 led to diminished parasite loads in the liver and spleen through induction of T_H1 and suppression of T_H2 responses [97]. Overall, the dual role of chemokines CCL2 and CCL3 during VL and their potential application in immunotherapeutic treatment approaches remains to be further elucidated.

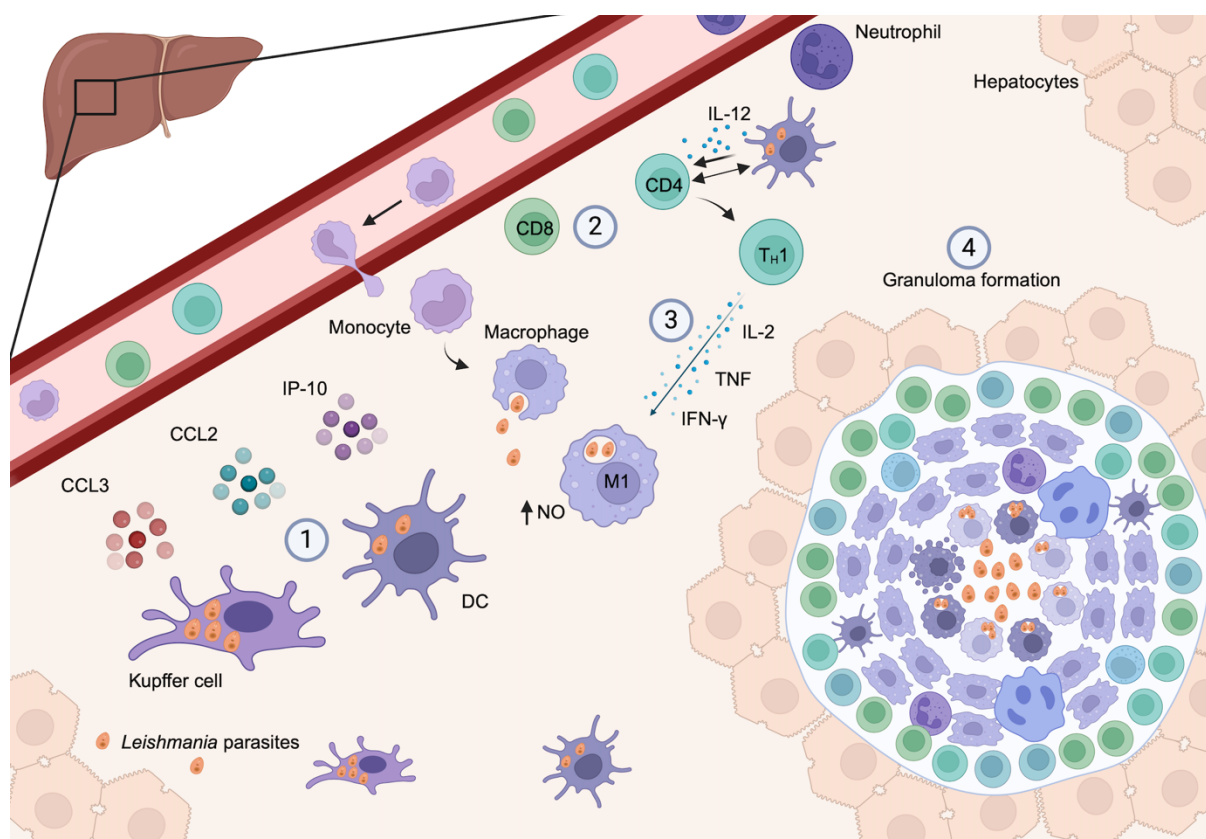


Figure 2: Immune dynamics during VL in the liver.

Schematic and simplified representation of immune dynamics during VL in the liver: **1.** Upon infiltration of macrophages and DCs with *Leishmania* parasites (shown in orange), cells secrete chemokines, primarily CCL3, CCL2 and IP-10. **2.** These chemokines cause the recruitment of monocytes, neutrophils, CD4⁺ T-cells and CD8⁺ T-cells. **3.** Interaction of infected DCs with CD4⁺ T-cells and IL-12 secretion, leads to polarization into TH1 cells and subsequent secretion of TH1 cytokines, such as IFN- γ , TNF and IL-2. Associated responses include M1 polarization of macrophages and ultimately granuloma formation **4.**, leading to resolution of the infection. Based on Oghumu, *et al.* [98] and Samant, *et al.* [88]. Figure created with BioRender.

1.3 Organoids

The increasing constraints on animal experiments and the limited transferability of findings from animal models to humans highlights the need for novel models. Especially in the field of infection biology, where specific host-pathogen dynamics are studied. Organoid models have emerged as a powerful tool to investigate these human-specific disease stages, as well as developmental processes [99]. Organoids have been defined by Marsee, *et al.* [100] as follows: “Three-dimensional structure derived from (pluripotent) stem cells, progenitor and/or differentiated cells that self-organize through cell-cell and cell-matrix interactions to recapitulate aspects of the native tissue architecture and function *in vitro*”. Although organoid models have been in existence for several decades, more recent advancements in the understanding of cellular self-organization, extracellular matrix (ECM) interactions and pluripotent stem cell (PSC) biology, have led to the rapid progress in organoid research [101]. So that organoids were recognized as the “Method of the year 2017” by *Nature Methods* [102].

The cultivation of 3D cell cluster cultures primarily relies on embedding the cells within an ECM-rich hydrogel, which functions as a supporting scaffold. These 3D cell clusters offer a closer representation of *in vivo* tissue physiology compared to traditional 2D cultures. This is

due to several factors, including the intricate cell-cell and cell-matrix interactions in three dimensions. Additionally, 3D cultures allow for the recreation of gradients of soluble molecules, such as nutrients, waste products or signaling factors to a certain extent, a capability lacking in 2D cultures. These more physiological conditions, support *in vivo*-like cell migration, proliferation, differentiation, morphogenesis and survival [103]. Consequently, organoid models might be suitable to bridge the gap between conventional cell cultures and animal models.

Based on their distinct characteristics and levels of complexity, various organoid types can be distinguished, including epithelial organoids, multi-tissue organoids and multi-organ organoids [100]. Epithelial organoids, representing the least complexity, consist of cells derived from a single germ layer of endoderm, mesoderm or ectoderm. Under appropriate culture conditions, these epithelial cells exhibit long-term proliferative capacity from a single cell, allowing culture expansion. Interestingly, these organoid cultures show the ability to regenerate organoids following enzymatic or mechanical fragmentation, highlighting their self-organizational capacity [104,105]. Multi-tissue organoids encompass cell types originating from at least two distinct germ layers, commonly endoderm and mesoderm. Characterized by greater complexity, these organoids integrate diverse cell types either through co-cultivation or PSC-based co-differentiation, followed by intra-organ self-organization. Unlike epithelial organoids, multi-tissue organoids lack the ability to regenerate upon fragmentation due to their higher complexity [106,107]. The highest level of complexity is observed in multi-organ organoids, which exhibit a high degree of interconnectivity among different organ domains and inter-organ self-organization [108]. Although currently underexplored, these organoids are expected to play a major role in future research fields. However, increased levels of complexity come at the expense of reduced reproducibility. Therefore, current limitations in organoid research revolve around achieving both complexity and reproducibility in the applied models [100].

Generating organoids with diverse levels of complexity and originating from various cell types and organs has unlocked great application potential. Notable, several well-established human organoid models currently exist, including skin, brain, lung, liver, kidney and intestine, among others [109]. The predominant applications of organoids are in research and personalized medicine. In the context of research, human organoid models present opportunities to study developmental processes and the functionalities of diverse organs in more detail than previously possible. Additionally, organoids offer a versatile platform for modeling a broad spectrum of disease, based on both healthy or diseased human material. In the domain of personalized medicine patient-specific organoids emerge as potent tools for drug screening and gene therapy, which can facilitate the development of needs-oriented treatment options [99].

1.3.1 Liver organoids

The liver is a highly vascularized organ, which performs crucial functions in the detoxification of the body. The primary epithelial cell types in the liver are hepatocytes and ductal cells. While ductal cells line the bile ducts, hepatocytes govern the majority of liver-specific functions, including metabolic regulation, synthesis of essential serum proteins and detoxification of endogenous and exogenous substances [110]. Interestingly, an exceptional regenerative capacity is observed in the liver, allowing for the regeneration of up to two-thirds of its mass within two weeks following surgical removal (partial hepatectomy, PHx). This regenerative process is characterized by a vast entry of mature hepatocytes into the cell cycle, without evident dedifferentiation into progenitor or stem cell-like states. This phenomenon underscores the replicative capacity of hepatocytes upon liver damage. Despite these *in vivo* regenerative

capabilities, reproducing the proliferative potential of human hepatocytes *ex vivo*, has remained elusive for decades, causing limitations in respective research fields [111].

In 2019, Hu and colleagues introduced a protocol demonstrating the long-term proliferative capacity of murine and human hepatocytes within 3D hepatocyte organoids (HepOrgs) [112]. Their study displayed the successful generation of HepOrgs from single mature hepatocytes embedded in ECM-rich hydrogel, which could be sustained in culture for several months. Notably, the transcriptional profiles of these HepOrgs remained stable over time and were comparable to those of proliferative hepatocytes following PHx. The addition of hepatocyte-specific mitogen hepatocyte growth factor (HGF), as well as activation of the Wnt pathway, by addition of high amounts of R-spondin1 to the culture medium, emerged as crucial factors in maintaining hepatocyte proliferation [112]. Noteworthy, these described HepOrgs represent structural complex epithelial organoids comprising a single cell type, the hepatocytes. While cholangiocyte organoids (CholOrgs) can emerge within HepOrg cultures, these are not functionally integrated with HepOrgs and therefore essentially represent a form of co-culture of two distinct organoid types. Recent advancements have led to the establishment of liver organoids derived from induced PSCs (iPSCs) [113]. These models exhibit increased complexity as stepwise iPSC differentiation enables the generation of organoids incorporating cells from multiple germ layers, yielding vascularized liver organoids [114]. Additionally, iPSC-derived liver organoids circumvent the limitations posed by the availability of scarce human tissue samples, thus allowing for simplified upscaling of organoid-based studies [115]. The next steps in further enhancing the relevance of liver organoids for disease modeling, especially involve the incorporation of immune cells, as well as further stromal components, such as fibroblasts.

1.3.2 Application of organoids in immunological research

Abundant populations of immune cells reside within diverse epithelial tissues throughout the body. Consequently, immune and epithelial cells engage in direct interactions within their respective tissue microenvironment, profoundly influencing the maturation and activation of immune cells. This interplay is particularly pivotal during infection processes, where epithelial cells are the first to be exposed to the pathogen. Thus, the direct communication with immune cells is crucial to induce and regulate rapid immune responses, while maintaining tissue homeostasis [116,117].

As previously addressed, human epithelial organoids can closely mimic *in vivo* tissue conditions and therefore provide powerful tools for investigating the development, functionality and pathology of their tissue of origin. These characteristics also render them very useful in the field of immunological research, where organoid infection models and organoid immune cell co-cultures are increasingly utilized. Here, researchers focus particularly on the direct effects of pathogens on epithelial cells and their subsequent immunomodulatory responses, to assess their impact on downstream immune responses [118]. Based on these findings, previous studies have established infection models in epithelial organoids, followed by the addition of immune cells or immune system derived-components to establish triple co-cultures [119,120]. A large part of this research has centered on bacterial and viral infections, whereas investigations into parasitic infections remain relatively scarce [121]. Overall, co-culture systems enable the study of interactions between epithelial cells and immune cells during inflammatory disease, tissue regeneration, tissue development and homeostasis, as well as in the context of tumor biology [121]. Noteworthy, organoid immune cell co-cultures provide a reductionist approach compared to animal models, to closely examine the interplay of specific immune and epithelial cells using human-derived cells [122].

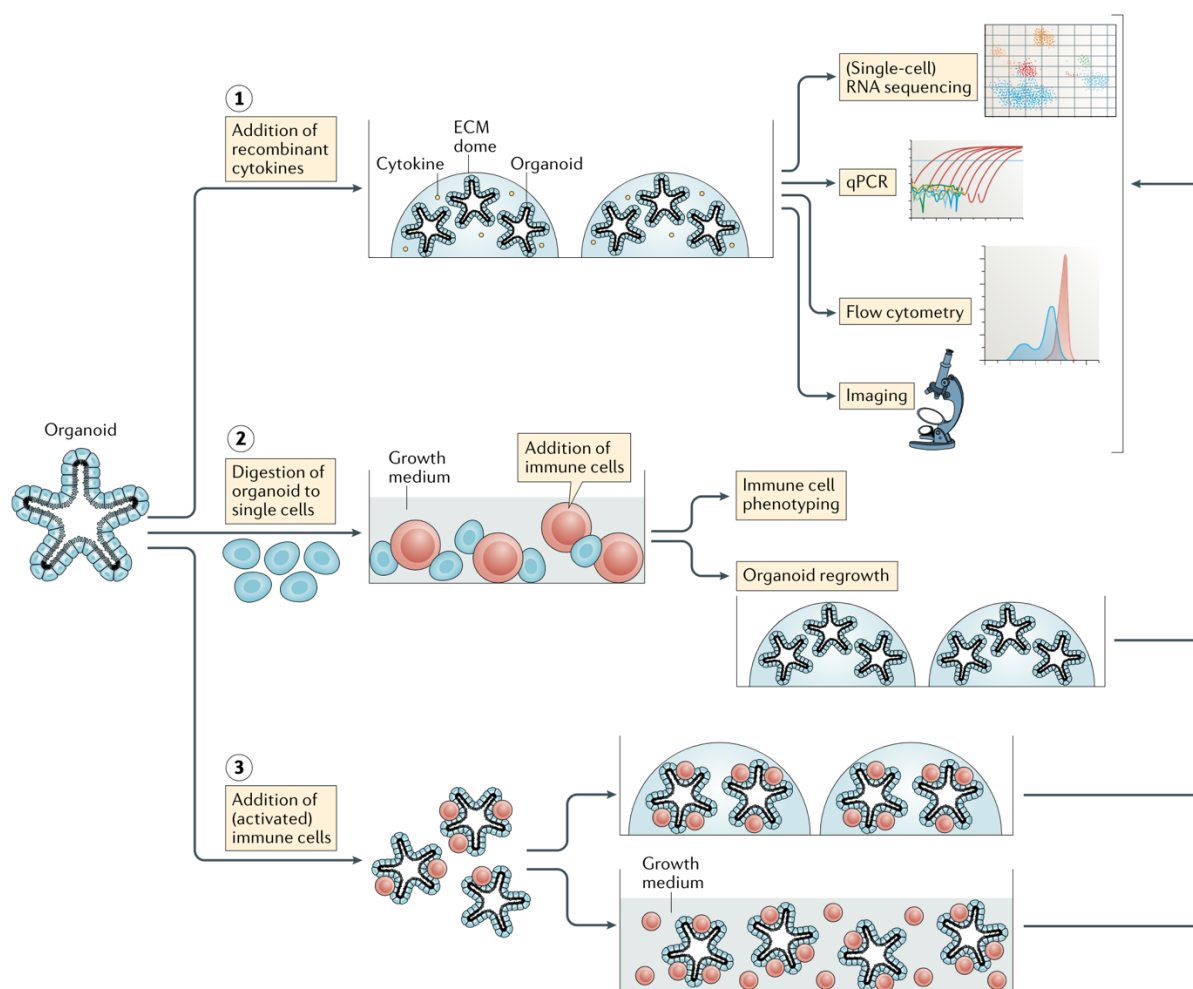


Figure 3: Co-culture systems to study the interaction of epithelial cells and immune cells.

Established co-culture systems involving cytokines or immune cells with epithelial organoids, to study their reciprocal interaction. **1.** The addition of cytokines to ECM-embedded organoids enables the study of the influence of soluble immune cell-derived factors on epithelial organoids. **2.** Organoids are digested into single cells, followed by the addition of immune cells and regrowth in ECM domes, to assess the impact of immune cells on organoid differentiation and formation, as well as their effect on immune cell activation. **3.** The direct interaction between immune cells and epithelial cells is evaluated by introducing (activated) immune cells to intact organoids either embedded into ECM domes or in suspension culture. Analysis of these different methods is commonly facilitated by techniques such as RNA sequencing, qPCR, flow cytometry and imaging. Illustration: [121].

Different systems have been explored to facilitate the co-cultivation of immune cells and epithelial organoids (Figure 3). The optimal co-cultivation approach is heavily dependent on the specific organoid type and the immune cells involved. However, it should be noted that the chosen co-culture conditions commonly represent a trade-off between the ideal culture requirements of the organoids and those of the immune cells, especially with regard to the medium composition and the ECM type. When planning such co-cultures, it should be acknowledged that culture conditions exert a major influence on the behavior of the constituent cells. With further refinement of culture protocols, co-cultures comprising of epithelial organoids and immune cells hold great potential to unravel their reciprocal interactions under both homeostatic and diseased conditions [121].

1.3.3 Aim of this thesis

Visceral leishmaniasis develops from arthropod-borne infections with protozoan parasites belonging to the *Leishmania* species [2]. Upon inoculation into the host, parasites are phagocytosed by immune cells primarily by macrophages, in which the parasites spread to the spleen and liver [68,85]. In the liver, an effective immune response is characterized by the recruitment of immune cells such as monocytes and a variety of T_H1-dependent mechanisms ultimately leading to granuloma formation and parasite killing [88,92]. In this regard, past research has unveiled a detrimental role of monocyte recruitment on infection resolution, suggesting a dual role of monocyte recruitment [96]. While previous studies have largely relied on mouse models, discrepancies exist between mouse and human infections. Although many processes observed in mice parallel those in humans, *Leishmania* liver infection in mice is self-resolving, contrasting with the potentially lethal outcome in humans [30]. This discrepancy highlights the need for new models to elucidate the underlying mechanisms for pathology in human visceral leishmaniasis. Moreover, the majority of previous studies on VL in the liver have predominantly focused on the interactions among immune cells. Therefore, there is currently little understanding regarding the response of hepatic epithelial cells, such as hepatocytes, to *Leishmania* parasites and their role in shaping the immune response during liver infection.

Accordingly, the aim of this thesis was to establish co-culture models of monocytes / macrophages, *L. infantum* parasites and liver organoids. In particular, a focus was placed on revealing the immunomodulatory responses of 3D HepOrgs upon exposure to *L. infantum* parasites, utilizing transcriptomics and cytokine profiling. Based on this, various strategies for co-cultivating *L. infantum*-infected HepOrgs with monocytes were explored. Furthermore, two approaches for the co-culture of HepOrgs with *L. infantum*-infected macrophages, the primary host cells for *Leishmania* parasites, were evaluated.

Overall, the main aims of this thesis were:

- Generation of 3D hepatocyte organoids, based on primary murine and human hepatocytes, followed by analysis of functional and structural markers.
- Initiation of direct infection of HepOrgs with *L. infantum* parasites.
- Evaluation of immune responses in HepOrgs following *L. infantum* infection at both cytokine and transcriptome level.
- Development of a model system for *L. infantum* infection in HepOrg-immune cell co-cultures:
 - Co-cultivation of *L. infantum*-infected HepOrgs with monocytes followed by the analysis of cytokine profiles and the expression of specific genes of interest.
 - Co-cultivation of *L. infantum*-infected macrophages with HepOrgs followed by the analysis of cytokine profiles.

2 Material and Methods

2.1 Material

2.1.1 Laboratory equipment

Table 1: List of utilized instruments

Instrument	Supplier
2100 Bioanalyzer	Agilent Technologies, Inc.
BD Accuri™ C6 Flow Cytometer	BD® Biosciences
BD® LSR II Flow Cytometer	BD® Biosciences
Centrifuge 5810 R	Eppendorf
Centrifuge 5424 R	Eppendorf
EasySep™ Magnet	STEMCELL Technologies
EVOS® FL Auto Fluorescence microscope	Thermo Fisher Scientific™
Fume Hood	Werner Hassa
FV3000 Confocal Laser Scanning Microscope	Olympus Life Science
Incubator HERA Cell 150i CO ₂	Thermo Fisher Scientific™
Incubator New Brunswick TM Galaxy® 170S	Eppendorf
Heraeus Laminar/Safety workbench HB 2448 K	Heraeus instruments
LSR II™ Flow Cytometer	BD® Biosciences
MicroPulser Electroporator	BioRad
MrFrosty™ Freezing Container	Thermo Fisher Scientific™
MRX ^e Microplate Reader	DYNEX Technologies, Inc.
Multichannel pipet	Mettler Toledo©
Multisizer™ 3 Coulter counter	Beckmann Coulter
NanoDrop™ 2000 Spectralphotometer	Thermo Fisher Scientific™
NextSeq™ 550-System	Illumina, Inc.
Opera Phenix High content screening system	revivvty
Pipet-Lite XLS electric pipette	Mettler Toledo©
Pipets (0.1-2 µl, 1-10 µl, 2-20 µl, 10-100 µl, 50-200 µl, 100-1000 µl)	Mettler Toledo©
Plate shaker	IKA-Werke GmbH

Rotor-Gene 3000	Corbett Life Science
Sonorex Super ultrasonic bath	Bandelin electronic GmbH & Co. KG
Vortexer VF2	IKA-Werke GmbH
Waterbath 1002	Lauda GmbH&Co

2.1.2 Consumables

Table 2: List of utilized consumables

Product	Supplier
Bottle top filter (0.22 µl)	MerckMillipore
Cell scraper	SARSTEDT AG & Co. KG
Cell strainer, 70 µl, sterile	SARSTEDT AG & Co. KG
Cryopreservation tube 2 ml	SARSTEDT AG & Co. KG
Culture flask without filtered cap (T25 cm ²)	SARSTEDT AG & Co. KG
Culture flask with filter cap (T175 cm ²)	SARSTEDT AG & Co. KG
Disposable hypodermic needle, 0.4 x 20 mm	B. Braun
Eppendorf tubes (1.5 ml, 2 ml)	SARSTEDT AG & Co. KG
Falcons (15 ml, 50 ml)	SARSTEDT AG & Co. KG
LightCycler® 480 Multiwell Plate 96, white	F. Hoffmann-La Roche AG
Microplate, 96 well, PS, F-bottom, Microlon®, high binding	Greiner Bio-One GmbH
Parafilm M	Sigma-Aldrich
Phenoplates ultra+Lid (96-well)	revivvty
Pipette Tips surthob (filtered) (10 µl, 200 µl, 1000 µl)	Biozym Scientific GmbH
Pipette Tips (10 µl, 200 µl, 1000 µl)	Eppendorf
Pipette Tips for multichannel pipettes	Mettler Toledo©
Polystyrene tube 5 ml	SARSTEDT AG & Co. KG
Well plates flat bottom Standard (6-well, 24- well)	SARSTEDT AG & Co. KG
Well plates flat bottom Suspension (24-well, 48-well)	SARSTEDT AG & Co. KG
Well plates round bottom (96-well)	SARSTEDT AG & Co. KG

2.1.3 Chemicals and reagents

Table 3: List of utilized solutions

Solution	Supplier
ACCUTASE™	STEMCELL Technologies
Albumin bovine Fraction V, Protease-free (BSA)	SERVA Electrophoresis GmbH
1-Brom-3-chlorpropan	Sigma-Aldrich
CASYton	Beckmann Coulter
dPBS	PAN Biotech™
Ethanol	Carl Roth®
Ethylenediaminetetraacetic acid (EDTA) disodium salt dihydrate	Carl Roth®
Fc blocking solution	Kindly provided by the research group Protozoa Immunology (BNITM)
Glycerol	Sigma-Aldrich
Sulfuric acid (H ₂ SO ₄), 95 – 97 %, p.a.	Merck KGaA
TRIS PUFFERAN® ≥99.5 %, p.a.	Carl Roth®
TRIzol Reagent	Invitrogen™ by Thermo Fisher Scientific™
0.04 % trypan blue	Gibco™ Life Technologies
TrypLE Express Enzym (1x), Phenolrot	Gibco™ Life Technologies
TWEEN® 20	Sigma-Aldrich
4 % PFA	Thermo Fisher Scientific™
2-Propanol (Isopropanol)	Carl Roth®

2.1.4 Kits

Table 4: List of utilized Kits

Kit	Supplier
BD OptEIA™ Mouse IL-6 ELISA Set	BD® Biosciences
BD OptEIA™ Mouse MCP-1 ELISA Set	BD® Biosciences
BD OptEIA™ TMB Substrate Reagent Set	BD® Biosciences
EasySep™ Mouse Monocyte Isolation Kit	STEMCELL Technologies
ELISA MAX™ Standard Set Mouse MCP-1	BioLegend, Inc.
ISOLATE II Genomic DNA Kit	Bioline
LEGENDplex™ Mouse Anti-Virus Response Panel	BioLegend, Inc.

LEGENDplex™ Mouse M1 Macrophage Panel (8-plex)	BioLegend, Inc.
Maxima First Strand cDNA Synthesis Kit for RT-qPCR	Thermo Fisher Scientific™
Maxima SYBR Green/ROX qPCR Master Mix (2X)	Thermo Fisher Scientific™
Mouse CCL3/MIP-1 alpha DuoSet ELISA	R&D Systems, Inc.
Mouse CXCL1/KC DuoSet ELISA	R&D Systems, Inc.
NextSeq 500/550 Mid Output Kit v2.5 (150 Cycles)	Illumina, Inc.
RNeasy® MinElute™ Cleanup Kit (50)	QIAGEN

2.1.5 Antibodies

Table 5: List of primary antibodies utilized for IFA

Antibody	Host	Provider	Catalog number	Dilution
α-mouse ZO-1	Rabbit	Affinity Biosciences	AF5145	1:500
α-mouse Albumin	Goat	Novusbio	NB600-41532	1:500
α-mouse Ki67	Rabbit	Abclonal	A20018	1:500
α-mouse CYP3A4	Rabbit	Abclonal	A2544	1:200
α-LHSP90	Mouse	Produced at BNITM		1:500
α-mouse F4/80	Rat	BioRad	MCA497RT	1:500

Table 6: List of conjugated antibodies

Reactivity	Host	Fluorochrome	Provider	Catalog number	Dilution
Rabbit	Goat	AF488	Invitrogen	A-11008	1:500
Rabbit	Goat	AF594	Invitrogen	A-11012	1:500
Goat	Donkey	AF488	Abcam	Ab150129	1:500
Mouse	Goat	AF594	Invitrogen	A-11005	1:500
Mouse	Goat	AF647	Invitrogen	A-21236	1:500
Rat	Goat	AF488	Invitrogen	A-11006	1:500
DAPI			Sigma-Aldrich	D9542	1:100
α-mouse Ly6C	Rat	APC	Biolegend	128016	1:200
α-mouse Ly6G	Rat	PE	Biolegend	127608	1:400
α-mouse CD11b	Rat	AF488	Biolegend	557672	1:400

2.1.6 Culture media and buffers

Table 7: List of buffers and media supplements

Buffer/Supplement	Supplier	Catalog number
A 83-01	Sigma Aldrich	SML0788
Adult Bovine Serum, sterile filtered	Capricorn Scientific GmbH	ABS-1D
Advanced DMEM/F-12	Gibco™ Life Technologies	12634028
B-27™ Supplement (50x), minus Vitamin A	Gibco™ Life Technologies	12587001
CHIR 99021	Tocris	4423
Cultrex™ RGF Basement Membrane Extract, Type 2, Select	R&D Systems	3536-005-02
DMEM	PAN™ Biotech	P04-01550
Diamond Vitamin Tween 80 Solution, 40x	BioConcept Ltd.	5-78F00-I
DPBS w/o Calcium, Magnesium	PAN™ Biotech	P04-361000
EGF, animal-free recombinant human	Peprtech	AF-100-15
Fetal Bovine Serum (FBS) Advanced	Capricorn Scientific GmbH	FBS-11A
FGF-7, recombinant human	Peprtech	100-19
FGF-10, recombinant human	Peprtech	100-26
Gastrin I (human)	Tocris	3006
GlutaMAX™ Supplement	Thermo Scientific™	35050038
HGF, recombinant human (HEK293 derived)	Peprtech	100-39H
IMDM	PAN™ Biotech	P04-20250
L-Glutamine (200 mM, sterile filtered)	Sigma Aldrich	G7513
Liberase™ TH, research grade	Roche	5401135001
N-Acetyl-L-Cystein	Sigma Aldrich	A9165-100G
Nicotinamide	Sigma Aldrich	N0636
Penicillin/Streptomycin Solution (100x)	AppliChem GmbH	A8943,0100
RPMI 1640	PAN™ Biotech	P04-17500
TGF- α , recombinant human	Peprtech	100-16A

Y-27632 dihydrochloride	Abmole	M1817
-------------------------	--------	-------

Table 8: Composition of utilized buffers and media

Buffer/Medium	Composition
AD ⁺	10 mM HEPES (pH 7.4) 1 % GlutaMAX 1 % Penicillin/Streptomycin (100x) In Advanced DMEM F12
Blocking solution (IFA)	2 % BSA 0.1 % Triton X-100 In 1x PBS, adjust pH to 7.4
cDMEM	10 % FCS-AC (activated charcoal treated) 1 % Penicillin/Streptomycin (100x) 300 µl/ml Zeocin In DMEM
Clearing Solution (IFA)	60 % glycerol 2.5 M fructose In dH ₂ O
Coating Buffer (ELISA)	8.4 g/l NaHCO ₃ 3.56 g/l Na ₂ CO ₃ in dH ₂ O, adjust pH to 9.5
cRPMI	10 % FCS-AC (activated charcoal filtered) 1 % Penicillin/Streptomycin (100x) In RPMI 1640
Hep medium (murine)	10 mM HEPES (pH 7.4) 1 % Penicillin/Streptomycin (100x) 1 % GlutaMAX 1x B27 15 % R-spondin1-conditioned medium 3 mM CHIR99021 1.25 mM N-acetyl-L-cysteine 10 mM Nicotinamide 10 nM recombinant Gastrin 50 ng/ml recombinant EGF 50 ng/ml recombinant human FGF7 50 ng/ml recombinant human FGF10 25 ng/ml recombinant human HGF

	<p>1 mM A83-01 10 μM Y-27632 In Advanced DMEM F12</p>
Hep medium (human)	<p>Hep medium murine 20 ng/ml TGF-α</p>
IMDM ⁺	<p>10 % LADMAC-Supernatant 10 % FBS-AC 5 % Horse serum 1 % L-glutamine 50 μg/ml Gentamycin</p>
M199 ⁺ medium	<p>20 % heat-inactivated FCS 1 % Penicillin/Streptomycin (100x) 2 mM L-Glutamine 40 mM HEPES (pH 7.4) 0.1 mg/ml Streptomycin 15.3 μM Hermin 100 μM Adenine 5 μM 6-Biopterin In M199</p>
PBS (20x)	<p>4 g KCl 4 g KH₂PO₄ x 2 H₂O 160 g NaCl In 1 l dH₂O, adjust pH to 7.4</p>
Permeabilization buffer (IFA)	<p>50 mM NH₄Cl 0.1 % Triton-X-100 In 1x PBS</p>
PM buffer	<p>400 mg KCl 190 mg MgSO₄ x 7 H₂O 190 mg MgCl₂ x 6 H₂O 60 mg Na₂HPO₄ x 2 H₂O 2.38 mg HEPES 8 g NaCl 60 mg KH₂PO₄ 2 g Glucose 220 mg CaCl₂ 2 g BSA In 1 l dH₂O, adjust pH to 7.4</p>
PPML buffer	<p>400 mg KCl</p>

	58 mg KH ₂ PO ₄ 350 mg NaHCO ₃ 8.06 mg NaCl 68 mg Na ₂ HPO ₄ x 2 H ₂ O 1 g Glucose 190 mg EDTA 11.91 g HEPES In 1 l dH ₂ O, adjust pH to 7.35
3x Roditi buffer	15 mM KCl 150 mM HEPES (pH 7.5) 70 mM NaH ₂ PO ₄ 200 mM NaHPO ₄ In 50 ml dH ₂ O
1x Roditi buffer	17.5 ml 3x Roditi buffer 5 ml 1.5 mM CaCl ₂ 30 ml dH ₂ O
Wash buffer (ELISA)	0.5 % Tween-20 in 1x PBS
Wash buffer (IFA)	0.1 % Triton-X-100 in 1x PBS

2.1.7 Oligonucleotides

Table 9: List of utilized primers for RT-qPCR

Target	Primer	Sequence	Primer efficiency
<i>Leishmania β-Actin</i>	forward	CGCCAGAGCGAAAATACAGC	1.972
	reverse	CAGACTCGTCGTACTIONCGCTC	
<i>Nod2</i>	forward	ACGAGGGCTACTCTCTGTGT	1.706
	reverse	GCGAGACTGAGTCAACACCA	
<i>Tlr2</i>	forward	GAAACCTCAGACAAAGCGTCA	1.961
	reverse	GCAGAACAGCGTTTGCTGAA	
<i>Nos2</i>	forward	CCACCTTGGTGAAGGGACTG	2.028
	reverse	CGTTCTCCGTTCTCTTGACAG	
<i>Arg1</i>	forward	AGCTCTGGGAATCTGCATGG	2.396
	reverse	ATGTACACGATGTCTTTGGCAGATA	

2.1.8 Organisms

Table 10: List of utilized organisms

Species	Strain/Clone	Origin
<i>Leishmania infantum</i> belonging to MON-1 zymondeme	3511	Annie Sulahian, Centre National de Reference des Leishmanioses Montpellier (France)
<i>Mus musculus</i>	C57BL/6J	BNITM animal facility

2.1.8.1 Human samples

Primary human hepatocytes for the generation of liver organoids were obtained from donor material from the Human Tissue & Cell Research Foundation (HTCR). The handling of previously anonymized human body materials for research purposes does not require a vote of the ethics committee (processing number Ärztekammer Hamburg: 2022-300218-WF).

2.1.9 Software and Databases

Table 11: List of utilized software

Software	Manufacturer/Developer
BD FACSDiva™ v6.1.3	BD® Biosciences
Excel	Microsoft
Fiji v2.1.0	ImageJ
FlowJo™ version 10.7.1	BD® Biosciences
FV3000 Super Resolution Software	Olympus Life Science
Harmony software v4.6	PerkinElmer
LEGENDplex™ Cloud-based Data Analysis Software	BioLegend
LightCycler® 96 SW 1.1	F. Hoffmann-La Roche AG
NanoDrop™ 2000/2000c 3.0	Malvern instruments Ltd.
NextSeq 550 System	Illumina, Inc.
Prism version 9.1.0	GraphPad
Revelation™ G 3.2	Dynex® Technologies GmbH
Rotor-Gene real time Analysis 6.0	Corbett Life Science
SpectroFlo® version 3.1.0	Cytek® Biosciences
Word	Microsoft

Table 12: List of utilized Websites

Name	URL
BioRender	https://www.biorender.com/
Heatmapper	http://heatmapper.ca/
InteractiVenn	http://www.interactivenn.net/
ShinyGO	http://bioinformatics.sdstate.edu/go74/

2.1.10 List of utilized tools

Name	URL
ChatGPT v3.5*	https://chat.openai.com/auth/login
DeepL Translator	https://www.deepl.com/translator
DeepL Write	https://www.deepl.com/write
Leo dictionary	https://dict.leo.org/englisch-deutsch/
Linguee	https://www.linguee.de/

*ChatGPT was utilized exclusively for the purpose of making linguistic corrections based on independently written texts. At no time was content generated by ChatGPT.

2.2 Cell Biology Methods**2.2.1 Isolation of murine hepatocytes**

Primary hepatocytes were isolated from male and female C57Bl/6J mice at the age of 10-12 weeks, by enzymatic liver perfusion. Prior to isolation all buffers were preheated to 42 °C and the tubes of the pump system were thoroughly sterilized with 70 % ethanol and dH₂O. Subsequently the mice were euthanized with CO₂ gas. The abdominal wall of the mice was opened up and fixed, exposing the internal organs. After cutting through the diaphragm the upper blood vessels were carefully tied off with a surgical knot. The liver was folded upwards without damaging it, while the other abdominal organs were moved to the right side, exposing the portal vein. A needle was added to the tube of the pump system, allowing a steady flow of droplets to appear at the bevel of the needle, which was then carefully inserted 1 to 2 mm deep into the portal vein. The needle was fixated using a clamp. The lower blood vessels were cut, and the liver flushed with 10 ml PPML buffer at a low speed, successful perfusion of the liver was indicated by decolorization of the liver tissue. A 1 mg Liberase containing solution was diluted in 25 ml preheated PM buffer and pumped through the liver. Regular compression of the lower blood vessels allowed the liver to be flooded with the enzymatic solution. After complete perfusion the liver was excised from the mouse and placed in a petri dish containing PM buffer. Upon removal of the gallbladder, the liver was shaken in the buffer, to release the hepatocytes from the digested tissue. Lastly the hepatocyte suspension was filtered through a 100 µm cell strainer and transferred to a 50 ml tube. After 20 min most cells sedimented at the bottom of the tube and 25 ml of the PM supernatant were replaced by a cold 90 % Percoll solution, mixed with 10x PBS. The suspension was centrifuged for 10 min, at 50 g and 4 °C. The supernatant was discarded, and the cells were taken up in 10 ml 1x dPBS. The cell

concentration was determined with a Neubauer chamber using a 1:10 dilution in 0.04 % trypan blue solution (see 2.2.11).

2.2.2 Handling of isolated primary human hepatocytes

The primary human hepatocytes were provided by Human Tissue and Cell Research (HTCR) foundation. The hepatocytes were isolated from human liver tissue and the cell suspension was shipped over night on ice. Upon arrival the cell suspension was mixed with 20 ml AD⁺ buffer, centrifuged for 5 min at 300 g and 4 °C and the cell pellet was resuspended in 10 ml AD⁺. The cell concentration was determined (see 2.2.11) and the hepatocytes were cultured as 3D organoids, as described in section 2.2.3.

2.2.3 Cultivation of murine and human 3D hepatocyte organoids

Isolated hepatocytes were washed with AD⁺ buffer and resuspended on ice in a mixture of cold Hep medium (murine or human) and BME (1:4). Per well of a 24 well plate 1x10⁵ cells per 50 µl droplet BME mixture were seeded. After BME was solidified, 500 µl of prewarmed Hep medium were added to each well and the cells were incubated at 37 °C and 5 % CO₂. Hep medium was refreshed every two to three days.

14 days after the initial seeding organoids were split by mechanic fragmentation. Therefore, Hep medium was removed from the wells and 1 ml cold AD⁺ buffer was added, to dissolve the BME droplet. The organoid solution from four wells was collected in 15 ml tubes and centrifuged for 5 min at 300 g and 4 °C. The supernatant was discarded, the organoid pellet resuspended in 300 µl AD⁺ and transferred to a 1.5 ml tube. To fragment the organoids the suspension was quickly pipetted up and down 50 to 100 times, first with a 100 µl pipette volume, afterwards with a 10 µl pipette volume. AD⁺ was added up to 1 ml and the tubes were centrifuged for 1 min in the benchtop centrifuge. The supernatant was discarded, and the pellet re-seeded in new Hep medium and BME (1:4). After the initial seeding, HepOrgs were seeded in 30 µl BME droplets. The split ratio was dependent on the organoid density within the BME droplets and ranged between 1:1.5 to 1:2.5. After initial passage, the organoids were usually passaged again every 7-14 days.

For cryopreservation the organoids were released from the BME droplets and fragmented, as before and the content of up to four wells (depending on organoid density) was resuspended in 500 µl Recovery™ Cell Culture Freezing Medium and transferred into cryotubes. The cryotubes were initially stored at -80 °C within Mr. Frosty™ freezing containers, for 2-3 days and then transferred to liquid N₂ for long-term storage.

To recover frozen HepOrgs from liquid N₂, 10 ml AD⁺ were prewarmed. Upon removal of cryotubes from the N₂ tank, 500 µl of the prewarmed AD⁺ were added to the tubes and the mixture was carefully pipetted up and down to thaw the frozen organoid suspension. Finally, the thawed suspension was transferred to 10 ml prewarmed AD⁺ and the cryotube was rinsed once with 500 µl AD⁺, before centrifugation for 5 min at 300 g and 4 °C. The supernatant was discarded and the pellet taken up in 300 µl AD⁺ and transferred to a 1.5 ml tube. The organoids were pipetted up and down, as described above for mechanical fragmentation. Subsequently, AD⁺ was added up to 1 ml and organoids were pelleted in the benchtop centrifuge for 1 min. The supernatant was discarded and the pellet resuspended in BME and Hep medium mixture as describe above.

2.2.4 Production of R-Spondin1 conditioned medium

R-spondin1 conditioned medium, a component of human and murine Hep medium, was produced in-house, utilizing 293t-HA-Rspon1-Fc cells. After liquid nitrogen storing, cells were thawed in a hot water bath and subsequently transferred to a 50 ml tube. Cells were washed with 20 ml cDMEM and centrifuged for 5 min, at 500 *g* and RT. The supernatant was discarded and the cell pellet was resuspended in 40 ml cDMEM, zeocin was added as selection antibiotic in a concentration of 300 μ l/ml. The cell suspension was seeded into a T175 flask with filter cap and incubated for three days at 37 °C and 5 % CO₂. When the cells reached close to 100 % confluency, the medium was removed and the cells were washed with 10 ml preheated 1x dPBS. 2 ml Accutase were added to detach the cells from the culture vessel and incubated for 5 min at 37 °C. Subsequently 18 ml cDMEM were added and cells were washed off from the bottom of the culture vessel. After centrifugation for 5 min, at 300 *g* and 4 °C, the supernatant was discarded and the cell pellet was resuspended in 10 ml cDMEM. The cell concentration was determined, as described in section 2.2.11. 5×10^6 cells were seeded into new T175 culture flasks with 40 ml cDMEM + zeocin and cultured for four days, or until the cells reached 100 % confluency. The cells were then removed from the flask, counted and seeded out again in new T175 flasks as before, although here no zeocin was added to the cDMEM medium. The cells were cultured again for four days. Afterwards, the medium was carefully removed from the cells with a serological pipet to avoid disruption of the confluent cell layer. 40 ml of AD⁺, the basal organoid medium, were added to the cells and cultured for a total of 8 days to enrich AD⁺ with R-Spondin1. To harvest the R-Spondin1 conditioned medium (RCM) the supernatants were collected in 50 ml tubes and centrifuged for 5 min, at 500 *g* and 4 °C. Finally, the supernatants were filtered through a 0.2 μ m sterilize filter and stored at -20 °C until use.

2.2.5 Cultivation of *Leishmania* parasites

Promastigote *Leishmania* parasites were cultivated at 25 °C in 10 ml M199+ (pH 7,4) medium in T25 culture flasks, with an airtight cap. Culture progression was microscopically monitored biweekly and cultures were diluted accordingly in fresh medium to 1×10^5 - 1×10^6 parasites/ml. To ensure parasites in stationary growth phase for infection experiments, dense parasite cultures were split with a ratio of 1:10 4 days prior to infection.

Cell counting of parasites was performed with the Beckmann Coulter cell counter, in 1:1000 dilutions of *Leishmania* culture in CASYton solution. Measurements were generally performed in duplicates.

2.2.6 Transfection of *Leishmania* parasites

To generate fluorescent *Leishmania* parasites, a vector facilitating mCherry expression was transfected into the parasites. An electroporation protocol was used for this purpose. Initially 1x Roditi buffer was freshly prepared from 3x stock solution and sterile filtered. *L. infantum* parasites in the exponential growth phase with 1×10^7 parasites per ml were used for transfection. Parasites were counted (refer to 2.2.5) and 5×10^7 parasites were transferred to a 15 ml tube, for both the mock control and the transfection approach. Tubes were centrifuged for 8 min at 600 *g* for 5 min and supernatants were discarded. Parasite pellets were washed with 10 ml cold 1x PBS and centrifuged as before. Supernatants were thoroughly removed and cell pellets resuspended in cold 1x Roditi buffer on ice. The suspension was briefly mixed and centrifuged as before. Cell pellet was taken up in 400 μ l 1x Roditi buffer and mixed by pipetting. The electroporation cuvette was placed on ice and 50 μ g DNA of the vector solution were added to the cuvette, followed by 400 μ l parasite suspension in Roditi buffer. No vector DNA was added to the mock control. The suspension was carefully mixed within the cuvette and

placed in BioRad's MicroPulser Electroporator. Electroporation was performed by pulsing 3 times at 1.5 kV and 200 Ω . Afterwards the cuvette was placed on ice for 10 min. T25 culture flask with airtight cap was prepared by addition of 10 ml M199+ supplemented with additional 1 % penicillin-streptomycin + L-glutamine. The parasites were transferred from the cuvette to the culture flask and incubated for 24 h at 25 °C. Subsequently the selection antibiotic neomycin was added at a concentration of 50 $\mu\text{g/ml}$ and parasites were cultivated for another 24 h at 25 °C, after which the culture was split at a ratio of 1:10. Mock control parasites and transfected parasites were cultured simultaneously, until all parasites were dead in the mock control (10-14 days).

2.2.7 Isolation of murine bone marrow cells

Murine bone marrow cells were isolated from C57BL/6J mice aged 10 – 12 weeks. Following CO₂ euthanasia, front and hind legs of the mice were excised and freed from muscular tissue. The bones were sterilized with 70 % isopropanol for 2 minutes and set aside to dry. The ends of each bone were cut off with scissors and the bone marrow was flushed out repeatedly with 1x dPBS, utilizing 0.4 mm hypodermic needles and 5 ml syringes. The collected cell suspension was filtered through a 70 μm cell strainer and centrifuged for 5 min, at 300 g and 4 °C. The supernatant was discarded, and the cell pellet was resuspended in 1 ml 1x dPBS. The cell concentration was determined (2.2.11). The isolated bone marrow cells were subsequently used for monocyte isolation (2.2.8) or macrophage differentiation (2.2.9).

2.2.8 Isolation of monocytes from murine bone marrow cells

Antibody-mediated negative selection with the EasySep™ Mouse Monocyte Isolation Kit from StemCell Technologies, was utilized to purify monocytes from isolated bone marrow cells. Procedure was in accordance to the manufacturer's guidelines. Following cell count determination of the isolated bone marrow cells, 2×10^5 cells were set aside for the purification control as "unstained" and "pre MACS" samples respectively. The residual cell suspension was centrifuged again for 5 min, at 300 g and 4 °C and the cell pellet was resuspended in 2 % FBS/DPBS + 1 mM EDTA to a cell concentration of 1×10^8 cells/ml. A selection cocktail was produced by combining components A and B from the EasySep™ kit, containing antibodies for all cell types excluding monocytes, and stored on ice. 50 μl of F_C-Block per 1×10^8 cells were added to the cell suspension and additionally 100 μl of the selection cocktail. The mixture was incubated for 5 min at 4 °C. 75 μl RapidSpheres were added and the suspension incubated for 3 min at 4 °C. Subsequently 2 % FBS/DPBS + 1 mM EDTA were added to a total volume of 2.5 ml. The suspension within a sterile flow cytometry tube was inserted into the EasySep™ magnet and incubated at RT for 3 min. The suspension was transferred to a new flow cytometry tube, while maintaining the first tube in the magnet. The suspension in the fresh tube was inserted into the magnet again and incubated for additional 3 min. The resulting cell suspension was again transferred to a fresh tube and centrifuged for 5 min, at 300 g and 4 °C. The supernatant was discarded and the cell pellet resuspended in 1 ml cRPMI. The cell concentration was determined (2.2.11). 2×10^5 isolated monocytes were set aside for the purification control as "post MACS" samples. Monocytes were further processed by CMFDA staining, described in section 2.2.10.

2.2.9 Differentiation of murine bone marrow cells into macrophages (BMDMs)

Previously isolated murine bone marrow cells (see 2.2.7) were seeded into a T175 culture flask with filter cap at a density of $1-2.5 \times 10^7$ cells per 50 ml IMDM⁺ medium and cultivated for 3 days at 37 °C with 5 % CO₂. 50 ml prewarmed IMDM⁺ were added after 3 days and half of the culture medium was exchanged on day 5. On the 7th day the cells were removed from the culture flask

by discarding the medium and adding 50 ml cold 1x dPBS, followed by incubation on ice for 10 min to detach cells. Subsequently a cell scraper was used to aid this process. The cell suspension was collected in a 50 ml tube and centrifuged for 5 min at 300 g and 4 °C. The supernatant was discarded and the cell pellet was resuspended in 1 ml IMDM⁺ medium to count cells, as described in section 2.2.11. Cells were seeded into distinct well plates at different densities. For HCS infection quantification 6x10⁴ BMDMs per well were seeded into 96-well Phenoplates and cultured in 200 µl IMDM⁺ (2.5.4). For the co-cultivation of dissociated HepOrgs with macrophages (2.3.4a), 1x10⁶ cells per 6-well were seeded out in 5 ml IMDM⁺. For the co-cultivation of intact HepOrgs with macrophages (2.3.4b), 3x10⁵ cells per 48-well were seeded in 200 µl IMDM⁺. BMDMs were further cultivated until day 10, followed by infection with *Leishmania* parasites, as outlined in section 2.3.3.

2.2.10 CMFDA staining

Monocytes were stained with CMFDA prior to co-culture with HepOrgs (2.3.2). A 10 mM stock solution of CellTracker™ Green CMFDA Dye was prepared by addition of 11 µl DMSO per tube. Upon dissolution of the dye 3 µl of the stock solution were added to 2 ml cRPMI medium. The quantity of monocytes to be stained was centrifuged for 5 min, at 300 g and 4 °C and the cell pellet was resuspended in 2 ml cRPMI with CMFDA. The cell suspension was transferred to a low adhesion 24-well plate and incubated for 30 min at 37 °C. Subsequently cells were collected and washed twice with 2 ml 1x dPBS, before addition to HepOrgs.

2.2.11 Determination of cell count

The cell count of single cell suspensions was determined utilizing a Neubauer counting chamber (depth = 0.1 mm, area = 0.0025 m²). Cell suspensions were diluted as indicated in ratios from 1:2 to 1:100 in 0.04 % trypan blue solution. 10 µl were added to the Neubauer chamber and the viable cells in all four larger squares were counted. Dead cells, indicated by trypan blue staining, were not included in the cell count. The final cell concentration (C in cells/ml) was calculated by including the mean number of viable cells per square (n), the dilution factor (D) and the Neubauer chamber-specific correction factor (10⁴), as follows:

$$C = n \times D \times 10^4$$

2.2.12 Staining of murine cells for FACS analysis – Monocyte purity control

Monocyte purity control was conducted subsequently to monocyte isolation from murine bone marrow cells (2.2.8). Flow cytometry staining was performed with the indicated cell suspensions set aside during monocyte isolation as “unstained”, “pre MACS” and “post MACS” samples. Initially all samples were transferred to flow cytometry tubes and 1 ml flow cytometry buffer (1 % FBS in 1x PBS) was added. Cells were centrifuged for 5 min at 300 g and 4 °C. Antibodies Alexa Fluor (AF) 488-conjugated anti-CD11b (1:400), allophycocyanin (APC)-conjugated anti-Ly6C (1:200) and phycoerythrin (PE)-conjugated anti-Ly6G (1:400) were diluted in Fc blocking solution. Following centrifugation of the cells, the supernatants were discarded and the cell pellets resuspended in 50 µl antibody master mix. The “unstained” sample was taken up in solely Fc blocking solution. Samples were incubated for 30 min, at 4 °C in the dark. The cells were washed twice with 1 ml 1x PBS and centrifuged as stated above. Finally, cell pellets were resuspended in 150 µl 1x PBS. The subsequent measurement was performed at the Accuri C6 flow cytometer.

2.3 Cellular Assays

2.3.1 *L. infantum* infection of murine HepOrgs in suspension

Murine and human HepOrgs were generated as described in section 2.2.3, organoids in passage P3 and onwards were used for infection experiments. To infect the organoids with *L. infantum* parasites, organoids were initially released from BME embedding by addition of 1 ml cold AD⁺ buffer to each well. Organoids were collected in 15 ml tubes and pelleted by centrifugation for 5 min at 200 *g* and 4 °C. To determine the cell count for MOI calculation, organoids from one reference well were dissociated into single cells using Gibco™ TrypLE™ dissociation reagent, the single cell suspension was counted as before (2.2.11). Simultaneously, stationary phase *L. infantum* parasites were counted (refer to 2.2.5) and a suitable culture volume for the intended multiplicity of infection (MOI) of 20:1 was sedimented by centrifugation for 10 min at 600 *g* and 4 °C. The supernatant was discarded and the parasite pellet was resuspended in the respective volume of Hep medium. The pelleted organoids were then resuspended in Hep medium containing parasites, while uninfected controls were taken up in standard Hep medium. An organoid suspension equivalent to 1x10⁵ single cell hepatocytes was seeded in 250 µl medium per well of a low attachment 48-well plate and incubated with or without parasites for 4 h at 37 °C and 5 % CO₂. Afterwards, organoid suspensions were collected in 15 ml tubes, wells were washed once with 0,5 ml AD⁺ buffer and further 5 ml AD⁺ were added to the 15 ml tubes. Organoids were washed carefully by pipetting up and down with a serological pipette and centrifuged at 200 *g* for 5 min at 4 °C, to remove unattached parasites. Supernatants were discarded and organoids were resuspended in fresh Hep medium. An organoid suspension equivalent to 1x10⁵ single cell hepatocytes was seeded in 250 µl Hep medium per well of a 48-well plate and incubated for further 24 h at 37 °C and 5 % CO₂. Subsequently, organoids were collected in 1.5 ml tubes and centrifuged as before. The supernatants were collected and stored at -80 °C for cytokine measurements, while pellets were resuspended in 1x dPBS. Uninfected and infected organoids were further processed by RNA isolation (2.4.3) for RNA sequencing, whole mount immunostaining (2.5.3) for parasite detection or subsequent co-cultivation with monocytes (2.3.2).

2.3.1.1 Alternative murine HepOrg infection approaches

For the infection of HepOrgs with *L. infantum* parasites in BME, HepOrgs were released from BME and a reference well was dissociated into single cells and counted as described before, to calculate MOIs. Parasites were simultaneously prepared for infection. The parasites were added to the HepOrgs at an MOI of 20:1 in 1.5 ml tubes and centrifuged in a bench top centrifuge. The supernatant was discarded and the cell pellet was resuspended on ice in a 1:4 mixture of Hep medium and BME. 30 µl droplets were seeded per well of a 24-well plate and incubated at 37 °C to solidify. Afterwards 500 µl prewarmed Hep medium were added to each well and incubated for 24 h at 37 °C and 5 % CO₂.

For the addition of *L. infantum* parasites to the supernatants of BME embedded HepOrgs, a reference well of HepOrgs was released from BME, dissociated into single cells and counted as described before to calculate MOIs. Parasites were simultaneously prepared for infection. Upon resuspension of an appropriate amount of parasites in prewarmed Hep medium, medium was removed from the embedded HepOrgs and replaced by parasite containing Hep medium. HepOrgs were incubated with parasites for 24 h at 37 °C and 5 % CO₂.

2.3.2 Co-culture of murine *L. infantum*-infected HepOrgs with monocytes

For the co-cultivation of *L. infantum*-infected HepOrgs with monocytes, previously described protocols for the infection of HepOrgs with *L. infantum* parasites (refer to 2.3.1) and the isolation of monocytes from murine bone marrow cells (2.2.8) were followed. All co-cultures were performed with cells derived from male mice.

Subsequently to the infection of murine HepOrgs with *L. infantum* parasites (refer to 2.3.1), these were co-cultivated with monocytes. Therefore, monocytes were isolated from murine bone marrow cells as described in section 2.2.8 and stained with CMFDA (2.2.10). Finally, monocytes were resuspended in AD⁺ buffer. After organoids were incubated with parasites for 24 h and washed as described, monocytes were added to the tubes containing uninfected or infected organoids at a ratio of 1:3 hepatocytes (equivalent to the counted single cell suspension from one reference well) to monocytes. Consequently, each co-culture consisted of HepOrgs equivalent to 1×10^5 single cells and 3×10^5 monocytes. The suspension was centrifuged for 5 min at 300 g and 4 °C. Depending on which co-culture approach was applied, different procedures followed:

- a) For the co-cultures embedded in BME, the cell pellets were taken up in a 1:4 mixture of Hep medium and BME. 30 µl droplets were seeded per well of a 24-well plate and incubated at 37 °C to solidify. Subsequently 500 µl of prewarmed Hep medium were added to each well and incubated for 24 h. After 2 h, 6 h and 24 h of incubation co-cultures were monitored using EVOS® FL Auto Fluorescence microscope. Afterwards, the supernatants were collected and stored at -80 °C for cytokine measurements.
- b) For the co-cultures in semi-suspension, the cell pellets were taken up in a mixture of cold Hep medium and 10 % BME. Cells were seeded in 200 µl medium per well of a low attachment 48-well plate and incubated for 24 h. After 2 h, 6 h and 24 h of incubation co-cultures were monitored using EVOS® FL Auto Fluorescence microscope. Afterwards the entire contents of the wells were transferred to 1.5 ml tubes and centrifuged for 5 min at 200 g and 4 °C. The supernatants were stored at -80 °C for cytokine measurements.
- c) For the co-cultivation in suspension, the cell pellets were taken up in 200 µl Hep medium. 200 µl of the suspension were added to each well of a low attachment 48-well plate and incubated for 24 h. Subsequently the entire contents of the wells were transferred to 1.5 ml tubes and centrifuged for 5 min at 200 g and 4 °C. The supernatants were collected and stored at -80 °C for cytokines measurements. The co-culture pellet was resuspended in 1x dPBS and further processed by RNA isolation (2.4.3).

2.3.3 *L. infantum* infection of murine macrophages (BMDMs)

Stationary phase *L. infantum* parasites were counted (refer to 2.2.5) and a suitable culture volume for the intended multiplicity of infection (MOI) of 20:1 was sedimented by centrifugation for 10 min at 600 g and 4 °C. The supernatant was discarded and the parasite pellet was resuspended in the respective volume of prewarmed IMDM⁺ medium. The medium from the macrophage wells was discarded and the cells were washed once by addition of prewarmed 1x dPBS. The parasite suspension was added to the macrophages in a volume of 100 µl, corresponding controls were treated equally without added parasites. Cells were incubated for 4 h at 37 °C and 5 % CO₂. Following the incubation, medium was removed from the macrophages and discarded. The macrophages were washed twice with 1x dPBS, to remove extracellular parasites. Finally, prewarmed IMDM⁺ was added and macrophages were further

cultivated for 24 h. The infected (and uninfected) macrophages were used for the quantification of the infection parameters (2.5.4) or employed in co-cultivation with murine HepOrgs (2.3.4).

2.3.4 Co-cultivation of murine HepOrgs with *L. infantum*-infected macrophages

Two different approaches for the co-cultivation of murine HepOrgs with *L. infantum*-infected macrophages were employed. In both approaches, cells derived exclusively from male mice were utilized.

- a) For the co-cultivation of dissociated HepOrgs with infected macrophages in BME, initially macrophages were seeded into 6-well plates at a density of 1×10^6 per well in 5 ml IMDM⁺ medium and infected as described in section 2.3.3, whereby the infection was performed in a volume of 2 ml IMDM⁺ medium. Organoids were released from BME droplets by removal of the liquid medium and subsequent addition of 1 ml cold AD⁺ buffer. The organoids were collected in 15 ml tubes and further 5 ml AD⁺ buffer were added prior to centrifugation at 300 g for 5 min at 4 °C. The supernatants were discarded, the organoid pellet was resuspended in 1 ml prewarmed TrypLE™ dissociation reagent by Gibco™ and incubated for 20 min at 37 °C. Upon sufficient dissociation of cell clusters, single cells were transferred to 15 ml tubes and 5 ml AD⁺ were added. Cells were centrifuged for 5 min at 500 g and 4 °C. The supernatants were discarded and the pellet was resuspended in 1 ml AD⁺. The cell count was determined as described in section 2.2.11. The cells were stored on ice until further processing. In the meantime, medium was removed from uninfected and infected macrophages. The well plate was placed on ice and 2 ml cold 1x dPBS were added to each well and incubated for 5 min. Cells were carefully removed from the well plate by usage of a cell scraper. The cell suspension was collected in 15 ml tubes and centrifuged for 5 min at 300 g and 4 °C. The cell pellet was resuspended in 1 ml IMDM⁺ medium and the cells were counted as before. Appropriate amounts of macrophages and the single cell suspension of hepatocytes were combined and centrifuged. The cell pellet was resuspended in a 1:4 mixture of Hep medium and BME and seeded as 30 µl droplets containing 6×10^4 hepatocytes and 3×10^4 macrophages. Upon solidification of the droplets, 500 µl of a 1:1 prewarmed mixture of Hep medium and IMDM⁺ were added to each well. Supernatants were collected every two days and cultures supplied with fresh medium. After 4 and 8 days, the supernatants were collected as before and stored at -80 °C for cytokine measurements. 1 ml cold AD⁺ buffer was added to each well, to dissolve the BME droplets. Cells were transferred to 1.5 ml tubes and centrifuged at 200 g and 4 °C for 5 min. The supernatants and BME residues were discarded and the cells washed with 1x dPBS. Cells were further processed by immunofluorescence staining (2.5.3) or gDNA isolation (2.4.1) to quantify parasite burden.
- b) For the co-cultivation of intact HepOrgs in suspension with macrophages, initially macrophages were seeded into 48-well plates at a density of 3×10^5 macrophages per well and infected as described in section 2.3.3, in a volume of 200 µl. Upon removal of the medium, the macrophages were washed once with prewarmed 1x dPBS. Simultaneously the organoids were released from BME as before and collected in 15 ml tubes. HepOrgs from one reference well were dissociated into single cells using Gibco™ TrypLE™ dissociation reagent, the single cell suspension was counted. Intact organoids were pelleted for 5 min at 200 g and 4 °C and subsequently resuspended in Hep medium. 200 µl of the organoid suspension were added to each macrophage well, containing organoids equivalent to 1×10^5 single cells. The co-culture was incubated for

24 h. Afterwards supernatants were collected and stored at -80 °C until cytokine measurements.

Co-culture experiments involving macrophages and HepOrgs were conducted as part of Marko Lo Piparo's master thesis [123], which was supervised within the scope of this doctoral thesis.

2.4 Molecular Biology Methods

2.4.1 Isolation of gDNA from *Leishmania*-infected macrophages

To quantify parasites within organoid-macrophage co-cultures, initially gDNA was isolated by employing the ISOLATE II Genomic DNA Kit from Bioline. Starting from the co-cultures embedded in BME, first the medium was removed and the BME droplets were dissolved in 1 ml cold AD⁺ buffer. After transferring the cell suspension to 1.5 ml tubes, these were centrifuged for 5 min at 300 *g* and 4 °C. The supernatant was discarded and the pellet was washed 3 times with 1 ml 1x dPBS. After the last centrifugation, the cell pellet was taken up in 200 µl lysis buffer GL and incubated for 5 min at room temperature (RT). 200 µl lysis buffer G3 and 25 µl protein kinase were mixed on ice prior to addition to the cell suspension. The suspension was thoroughly mixed and incubated for 15 min at 70 °C. Subsequently samples were mixed again and centrifuged for 5 min at 300 *g*. Samples were stored at -20 °C until proceeding further.

210 µl 100 % ethanol were added to each sample and then carefully mixed. The complete mixture was added onto the silica membrane of the provided spin columns within 2 ml tubes and incubated for 5 min at RT. The column was centrifuged for 1 min at 11000 *g* and RT before the addition of 500 µl wash buffer GW1, followed by another centrifugation step. The filtrate was discarded and another 600 µl wash buffer GW1 were added to the column and centrifuged again. The filtrate was discarded and the membrane dried by another centrifugation step. Finally, 50 µl of the elution buffer G preheated to 70 °C was added to the silica membrane and incubated for 5 min at RT. The spin column was placed in a new 1.5 ml tube and centrifuged for 1 min at 11000 *g* and RT to elute the gDNA. The gDNA concentration was assessed via NanoDrop™ measurement. The samples were stored at 4 °C until use in TaqMan real-time PCR (2.4.2).

2.4.2 *Leishmania* quantification by TaqMan real-time PCR

Leishmania-specific gDNA was quantified by TaqMan-qPCR, with the use of specific primers for *Leishmania* β -Actin gDNA. Therefore, previously isolated gDNA was combined with provided qPCR agents, as detailed below in Table 13. Both dH₂O and MgCl₂ were exposed to UV-light prior to use, to destroy unwanted DNA residues. gDNA was substituted by dH₂O in negative controls. Samples were prepared under benchtop fume hood and measured in triplicates in RotorGene6 cyclers. Quantification was carried out by means of the Δ CT method using the measured CT values.

Table 13: TaqMan qPCR sample set up

Agent	Volume [µl]
Bioline Mastermix	10
dH ₂ O	4.6
MgCl ₂ (25 mM)	1.2
Leish-Ac-F2 (900 nM)	0.3

Leish-Ac-R (900 nM)	0.3
Leish-Ac Probe (200 nM)	0.5
Murine-Ac β -F2 (900 nM)	0.3
Murine-Ac β -R2 (900 nM)	0.3
Murine-Ac β Probe (200 nM)	0.5
gDNA	2

2.4.3 RNA isolation

RNA was extracted from *L.infantum*-infected HepOrgs (2.3.1) and suspension co-cultures with monocytes (2.3.2) using MinElute Kit from QIAGEN. All cell suspensions were thoroughly washed with 1x dPBS prior to uptake in 500 μ l prewarmed TRIzol® under the fume hood. After homogenization by pipetting up and down, the samples were stored at -80°C until further processing. To prepare for the RNA isolation samples were thawed at RT. 50 μ l of 1-bromo-3-chloropropane (BCP) were added and samples were vigorously shaken before incubation for 3 min at RT. Tubes were centrifuged for 15 min at 12000 g for 4 °C. The upper aqueous phase containing RNA was transferred to a new RNase free 1.5 ml tube and stored on ice. Samples were mixed 1:1 with 70 % sterile filtered ethanol and vigorously shaken. The MinElute kit was used according to the manufacturer's guidelines. Initially total sample volume was added to MinElute columns, tubes were centrifuged for 15 s at 8000 g and RT, subsequently the flow-through was discarded. 350 μ l RW1 buffer were added to the column and tubes were centrifuged as before. Columns were transferred to new collection tubes and 80 μ l DNase digestion mix, consisting of 10 μ l DNase diluted in 70 μ l RDD buffer, were added. DNase digestion was incubated for 30 min at RT. Subsequently 350 μ l RW1 buffer were added and tubes were centrifuged as before. Columns were transferred to new collection tubes and 500 μ l RPE buffer were added, followed by centrifugation as before and addition of 500 μ l 80 % sterile filtered ethanol. Again, tubes were centrifuged and columns transferred to new collection tubes. To dry the membrane, columns were centrifuged with open lids for 5 min at maximum speed. Finally, columns were transferred to RNase-free 1.5 ml tubes and 20 μ l RNase-free H₂O were added to the center of the membrane. Upon incubation for 2 min at RT, samples were centrifuged for 2 min at maximum speed. This step was repeated with the RNA containing flow-through. RNA concentration was assessed with NanoDrop™. Aliquots of 2 μ l were stored separately for analysis of RNA integrity (2.4.4). All other samples were stored at -80 °C until further processing, repeated freeze-thaw cycles were avoided. RNA samples were further used for either RNA sequencing (2.4.5) or RT-qPCR (2.4.8)

2.4.4 RNA integrity control using Bioanalyzer Agilent 2100

RNA integrity and precise concentration were determined using on-chip automated electrophoresis with Agilent 2100 Bioanalyzer and Agilent RNA 6000 Pico Kit, analysis was performed with 2100 Expert Software. Following the manufacturer's guidelines, RNA samples were diluted to a concentration between 0.2 ng/ μ l and 5 ng/ μ l with RNase free water, following concentration measurement with NanoDrop™. Prior to chip loading, all diluted samples were denatured for 2 min at 70 °C. 1 μ l per sample were loaded onto the chip. RNA quality was assessed using the RNA Integrity Number (RIN), a value calculated by the software and used as a measure of RNA intactness. A value between 1 and 10 is determined, whereby a value of 10 is equal to intact RNA, while 1 indicates degraded RNA. RIN values could not be determined

in *Leishmania*-infected samples, since RIN calculation was disturbed by additional *Leishmania*-specific 16S and 23S RNA peaks. Therefore, the electropherogram was examined manually for signs of RNA degradation. Within the samples analyzed, all RIN values were above 7 and there were no signs of excessive RNA degradation in the infected samples based on the electropherograms, thus all samples were used for RNA sequencing (2.4.5).

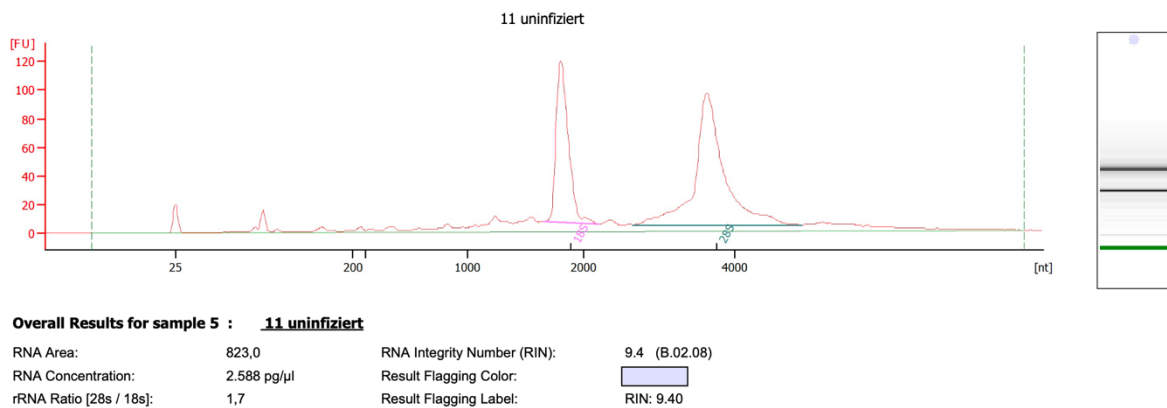


Figure 4: Agilent 2100 Bioanalyzer output.

RNA samples were diluted to recommended concentration range and RNA integrity was assessed by Agilent 2100 Bioanalyzer with Agilent 6000 Pico Kit and 2100 Expert Software. Depicted is an exemplary electropherogram of an uninfected sample with a RIN of 9.4.

2.4.5 RNA sequencing

RNA sequencing was performed at the NGS core facility of the BNITM under the direction of Daniel Cadar. RNA samples were used to prepare the library utilizing QIAseq Stranded mRNA Lib Kit UDI-A according to the manufacturer's guidelines. The library created was loaded onto a NextSeq 500/550 Mid Output (150 Cycles) Kit v2.5 cartridge and sequenced using the Illumina NextSeq 550 system. This sequencing run generated 75 bp paired-end reads with an average sequencing depth of 5 million reads per sample. The obtained raw data was further processed as described in section 2.4.6.

2.4.6 Analysis of RNA sequencing results

The obtained sequencing data was processed utilizing Nextflow RNAseq (v.3.8) pipeline. Initially a quality control was performed with FastQC and corresponding reports were generated with MultiQC (v1.11). Processed reads were aligned to the murine genome GRCm38 obtained from iGenomes [124]. R package DESeq2 (v1.34) was used to normalize the expression data using variance stabilizing transformation (VST). Principal component analysis (PCA) was performed based on sex and infection status of the analyzed samples, by applying VST data employing the scikit-learn (v1.2) package by Python. Additionally, DESeq2 (v1.34) package was utilized for differential expression analyses between sex and infection state, p-value correction for multiple testing was performed with Benjamini-Hochberg method. To define a gene as differentially expressed between two sample sets, an adjusted p-value (FDR) < 0.05 was defined. In the first analysis of the complete data set, a comparison was made both between samples of one sex in different conditions and between different sexes in the same condition. In the following analysis of the sample subset, only a comparison between the conditions uninfected and infected was made, to ensure a samples size of at least 4 individuals.

The data was presented graphically using the VST normalized data. A volcano plot was generated using R package EnhancedVolcano (v1.12). In addition, the freely accessible tools Heatmapper (<http://heatmapper.ca/>) and InteractiVenn (<http://www.interactivenn.net/>) were employed to generate Heatmap and Venn diagram. ShinyGo (v0.8) (<http://bioinformatics.sdstate.edu/go/>) was used for GO-term enrichment of all differentially expressed genes, with default settings.

2.4.7 cDNA synthesis

RNA isolated from murine co-cultures of *L. infantum*-infected HepOrgs and monocytes (2.3.2) was transcribed into cDNA for RT-qPCR using Thermo Fisher Maxima First Strand cDNA Synthesis Kit according to the manufacturer's guidelines. In brief, in an RNase-free tube 200 ng template RNA was combined with 2 μ l Maxima Enzyme Kit and 4 μ l 5x Reaction Mix. RNase-free H₂O was added up to a final volume of 20 μ l. Initially the mixture was incubated for 10 min at 25 °C, followed by 15 min at 50 °C. Lastly the reaction was terminated through incubation for 5 min at 85 °C. The synthesized cDNA was employed in RT-qPCR as described in section 2.4.8.

2.4.8 Quantitative Real-Time Polymerase Chain Reaction (RT-qPCR)

To quantify target mRNA isolated from co-cultures of *L. infantum*-infected HepOrgs and monocytes (refer to 2.3.2), initially RNA was isolated (see 2.4.3) and cDNA was synthesized (2.4.7). Previously established primer pairs (see Table 9) [100 pmol/ μ l] were diluted at a ratio of 1:10 with RNase-free H₂O. Employing Thermo Fishers Maxima SYBR Green/ROX qPCR Master Mix (2x) following the manufacturer's guidelines, a master mix was prepared in an RNase-free tube containing 0.3 μ l of the primer dilutions (forward and reverse respectively), 3.4 μ l RNase-free H₂O per reaction. For each sample a housekeeping control encoding for 40S ribosomal protein S9 (*Rps9*) was amplified. 9 μ l of this master mix was combined with 1 μ l of the synthesized cDNA in a LightCycler Multiwell 96-well plate. Negative controls for each primer pair contained RNase-free H₂O instead of cDNA. Reactions were performed in duplicates. The plate was sealed and shortly centrifuged. RT-qPCR was performed with LightCycler® 96, employing the following program:

Table 14: Cyclor program for RT-qPCR

Step	Temperature	Time	Repetition
Preincubation	95 °C	300 s	
3-step amplification	95 °C	10 s	60 x
	58 °C	10 s	
	72 °C	10 s	
Melting	95 °C	10 s	
	65 °C	60 s	
	97 °C	1 s	
Cooling	37 °C		

LightCycler® 96 SW 1.1 software was utilized to process the obtained data. Within Microsoft Excel the mean Cq values were calculated from duplicates. Based on these values, the fold changes in the expression of the respective genes of interest in the analyzed co-culture conditions as compared to the control condition (uninfected HepOrgs) were calculated using the following equation based on [125].

$$\text{fold change} = \frac{(E_{\text{target}})^{\Delta\text{Cq target (control-sample)}}}{(E_{\text{reference}})^{\Delta\text{Cq reference (control-sample)}}$$

E_{target} = primer efficiency of gene of interest

$E_{\text{reference}}$ = primer efficiency of housekeeping gene (*Rps9*)

$\Delta\text{Cq}_{\text{target}}$ = Cq control condition – Cq co-culture condition (gene of interest)

$\Delta\text{Cq}_{\text{reference}}$ = Cq control condition – Cq co-culture condition (housekeeping gene)

2.5 Biochemical Methods

2.5.1 Enzyme-Linked Immunosorbent Assay (ELISA)

2.5.1.1 IL-6 ELISA

To detect IL-6 in supernatants of murine HepOrgs, BD OptEIA™ Mouse IL-6 ELISA Set was employed. The assay was performed as described by the manufacturer's guidelines, with minor adjustments. The day before the assay was performed, a Nunc MaxiSorp flat-bottom 96-well plate was coated with 50 µl per well of the capture antibody diluted 1:250 in coating buffer and incubated overnight at 4 °C. On the next day, the supernatants were discarded and the wells were washed three times with 300 µl wash buffer (0.05% Tween-20/PBS). After the washing solution had been removed from all wells residual liquid was blotted of on absorbent paper. Unspecific binding sites were blocked through addition of 100 µl assay diluent (10 % FBS/PBS) per well and incubated for 1 h at RT. Supernatants were discarded and the wells were washed as before. The provided standard was diluted in assay diluent to a maximum concentration of 1000 pg/ml, from which as serial 2-fold dilution series was generated. Assay diluent served as blank. 50 µl of standard dilutions or samples were added to the wells, each in duplicates. The well-plate was covered and incubated for 2 h at RT. Afterwards, the plate was washed three times as before. The detection antibody was diluted 1:500 in assay diluent, along with 1:250 diluted enzyme reagent. 50 µl of the mixture were added to each well and incubated for 1 h at RT. Subsequently the well plate was washed seven times, with the washing solution soaking the plate for 30 s each time. The substrate solution was prepared by mixing Tetramethylbenzidine (TMB) with hydrogen peroxide in a ratio of 1:1, 50 µl were added to each well and incubated for 30 min in the dark. The color reaction was stopped by the addition of 50 µl 2N H₂SO₄, which resulted in a color change from blue to yellow. The absorbance was measured at a wavelength of 450 nm, using MRX^e plate reader.

2.5.1.2 CCL2 ELISA

To detect CCL2 (or monocyte chemoattractant protein-1 (MCP-1)) in supernatants of murine HepOrgs, BioLegend ELISA MAX™ Standard Set Mouse MCP-1 was employed. The assay was performed as described by the manufacturer's guidelines, with minor adjustments. The day before the assay was performed, a Nunc MaxiSorp flat-bottom 96-well plate was coated with 50 µl per well of the capture antibody diluted 1:200 in coating buffer and incubated overnight at 4 °C. On the next day, the supernatants were discarded and the wells were

washed four times with 300 μ l wash buffer (0.05% Tween-20/PBS). After the washing solution had been removed from all wells, residual liquid was blotted of on absorbent paper. Unspecific binding sites were blocked through addition of 200 μ l assay diluent (10 % FBS/PBS) per well and incubated for 1 h at RT. Supernatants were discarded and the wells were washed as before. The provided standard was diluted in assay diluent to a maximum concentration of 4000 pg/ml, from which as serial 2-fold dilution series was generated. Assay diluent served as blank. 50 μ l of standard dilutions or samples were added to the wells, each in duplicates. The well-plate was covered and incubated for 2 h at RT. Afterwards the plate was washed four times as before. The detection antibody was diluted 1:200 in assay diluent. 50 μ l of the dilution were added to each well and incubated for 1 h at RT. Subsequently the well plate was washed four times as before. Avidin-HRP was diluted 1:1000 in assay diluent and 50 μ l were added to each well to incubate for 30 min at RT. The plate was washed five times, with the washing solution soaking the plate for 30 s each time. The substrate solution was prepared by mixing Tetramethylbenzidine (TMB) with hydrogen peroxide in a ratio of 1:1, 50 μ l were added to each well and incubated for 30 min in the dark. The color reaction was stopped by the addition of 50 μ l 2N H₂SO₄, which resulted in a color change from blue to yellow. The absorbance was measured at a wavelength of 450 nm, using MRX^e plate reader.

2.5.1.3 CCL3 ELISA

To detect CCL3 (or macrophage inflammatory protein 1- α (MIP-1 α)) in supernatants of murine HepOrgs, R&D SYSTEMS Mouse CCL3/MIP-1 alpha Quantikine ELISA Kit was employed. The assay was performed as described by the manufacturer's guidelines, with minor adjustments. The day before the assay was performed, a Greiner high binding flat-bottom 96-well plate was coated with 50 μ l per well of the capture antibody diluted 1:250 in 1x PBS and incubated overnight at RT. On the next day, the supernatants were discarded and the wells were washed three times with 300 μ l wash buffer (0.05% Tween-20/PBS). After the washing solution had been removed from all wells, residual liquid was blotted of on absorbent paper. Unspecific binding sites were blocked through addition of 150 μ l reagent diluent (1 % BSA/PBS) per well and incubated for 1 h at RT. Supernatants were discarded and the wells were washed as before. The provided standard was diluted in reagent diluent to a maximum concentration of 500 pg/ml, from which as serial 2-fold dilution series was generated. Reagent diluent served as blank. 50 μ l of standard dilutions or samples were added to the wells, each in duplicates. The well-plate was covered and incubated for 2 h at RT. The plate was washed three times as before. The detection antibody was diluted 1:60 in reagent diluent. 50 μ l of the dilution were added to each well and incubated for 2 h at RT. Subsequently the well plate was washed three times as before. Streptavidin-HRP was diluted 1:40 in reagent diluent and 50 μ l were added to each well to incubate for 20 min at RT. The plate was washed three times as before. The substrate solution was prepared by mixing Tetramethylbenzidine (TMB) with hydrogen peroxide in a ratio of 1:1, 50 μ l were added to each well and incubated for 20 min in the dark. The color reaction was stopped by the addition of 25 μ l 2N H₂SO₄, which resulted in a color change from blue to yellow. The absorbance was measured at a wavelength of 450 nm, using MRX^e plate reader.

2.5.1.4 CXCL1 ELISA

To detect CXCL1 in supernatants of murine HepOrgs, R&D SYSTEMS Mouse CXCL1/KC Quantikine ELISA Kit was employed. The assay was performed as described by the manufacturer's guidelines, with minor adjustments. The day before the assay was performed, a Greiner high binding flat-bottom 96-well plate was coated with 50 μ l per well of the capture antibody diluted 1:120 in 1x PBS and incubated overnight at RT. On the next day, the supernatants were discarded and the wells were washed three times with 300 μ l wash buffer

(0.05% Tween-20/PBS). After the washing solution had been removed from all wells, residual liquid was blotted on absorbent paper. Unspecific binding sites were blocked through addition of 200 μ l reagent diluent (1 % BSA/PBS) per well and incubated for 1 h at RT. Supernatants were discarded and the wells were washed as before. The provided standard was diluted in reagent diluent to a maximum concentration of 1000 pg/ml, from which a serial 2-fold dilution series was generated. Reagent diluent served as blank. 50 μ l of standard dilutions or samples were added to the wells, each in duplicates. The well-plate was covered and incubated for 2 h at RT. Afterwards the plate was washed three times as before. The detection antibody was diluted 1:60 in reagent diluent. 50 μ l of the dilution were added to each well and incubated for 2 h at RT. Subsequently the well plate was washed three times as before. Streptavidin-HRP was diluted 1:40 in reagent diluent and 50 μ l were added to each well to incubate for 20 min at RT. The plate was washed three times as before. The substrate solution was prepared by mixing Tetramethylbenzidine (TMB) with hydrogen peroxide in a ratio of 1:1, 50 μ l were added to each well and incubated for 20 min in the dark. The color reaction was stopped by the addition of 25 μ l 2N H₂SO₄, which resulted in a color change from blue to yellow. The absorbance was measured at a wavelength of 450 nm, using MRX^e plate reader.

2.5.2 Multiplex Immunoassay - LEGENDplex™

Multiplex Immunoassay was performed using the indicated LEGENDplex™ pre-defined panels from BioLegend® (refer to Table 4), to simultaneously detect multiple cytokines in cell culture supernatants. Cytokine detection relied on the application of analyte-specific antibody-covered beads. Respective beads are differentiated by size and signal intensities. Prior to assay conduction, a 6-fold 1:4 serial dilution of the supplied top standard was performed, assay buffer served as blank. The procedure was based on the manufacturer's guidelines. Within 96-well V-bottom-plates, 10 μ l of sample / standard, beads and assay buffer respectively were combined in each well, covered opaque to light and incubated over night at 4°C on a plate shaker (800 rpm). 200 μ l 1x wash buffer were added to each well and the samples were washed for 5 min, at RT on a plate shaker. Subsequently, the well plates were centrifuged for 5 min, at 250 g and RT. The supernatant was discarded and 10 μ l detection antibody were added to each well, the plate was sealed opaque to light and incubated for 1 h on a plate shaker, at RT. 10 μ l SA+PE were directly added to each well and incubated for further 30 min on a plate shaker. Finally, 200 μ l 1x washing buffer were added to each well and the samples were washed for 5 min, at RT on a plate shaker, followed by centrifugation for 5 min, at 250 g and RT. The supernatant was discarded and the bead pellet was resuspended in 150 μ l 1x wash buffer. The measurement was carried out at the LSR II™ flow cytometer, using PE and APC channels. 500 events per analyte were recorded and the data output was analyzed with LEGENDplex™ Cloud-based analysis software (legendplex.qognit.com).

2.5.3 Whole mount immunostaining of organoids

To stain organoids or organoid containing co-cultures, these were initially released from BME embedding or surrounding liquid media, collected in 15 ml tube in AD⁺ buffer, centrifuged for 5 min at 200 g and 4 °C and washed twice in 2 ml 1x dPBS followed by centrifugation as before. The organoid pellet was resuspended in 1 ml 4 % paraformaldehyde (PFA) to fix the cells and incubated at RT for 15 min. 2 ml of the IFA wash buffer were added and fixed organoids were centrifuged for 5 min at 300 g and 4 °C. This process was repeated. Finally, the cell pellet was resuspended in 200 μ l of the wash buffer and transferred to 1.5 ml tubes, centrifuged again as before and the supernatants were thoroughly removed and discarded. Organoids were resuspended in permeabilization buffer and incubated for 30 min at RT on a shaker. Subsequently tubes were centrifuged as before and organoid pellet was taken up in 200 μ l

blocking solution and incubated for 30 min at RT on a shaker. Tubes were centrifuged as before and washed twice with 200 µl wash buffer. Primary antibodies were appropriately diluted in blocking solution as outlined in Table 5, before addition to the organoids in a final volume of 100 µl and incubated overnight at 4 °C on a shaker. Negative controls were incubated in blocking solution without added antibodies. On the next day, samples were washed three times through addition of 200 µl wash buffer and subsequent centrifugation for 5 min at 300 g. Conjugated antibodies were diluted in blocking solution as outlined in Table 6 and combined with 4,6-Diamidin-2-phenylindol (DAPI) at a dilution of 1/100 of the total volume of the solution. Samples, including negative controls, were resuspended in 100 µl of the antibody solution and incubated overnight at 4 °C on a shaker. Organoids were washed three times as before and the supernatants were thoroughly removed after the last centrifugation step. Organoids were resuspended carefully in Fructose-Glycerol clearing solution and incubated for 20 min at RT on a shaker. Subsequently organoids were mounted on glass slides, covered with cover slips and sealed with nail polish to prevent drying out or leakage. Slides were stored at 4 °C until analysis by confocal microscopy. Stained organoids were imaged with OLYMPUS FV3000 Confocal Laser Scanning Microscope and processed with FIJI Version 2.1.0.

2.5.4 Analysis of the infection parameters of *L. infantum* infected macrophages using High Content Screening (HCS)

To prepare *L. infantum*-infected macrophages for high content screening, macrophages and parasites were stained using immunofluorescence. Macrophages were derived from murine bone marrow cells (2.2.9) in 96-well Phenoplates and infected with *L. infantum* parasites at an MOI of 20:1 (2.3.3). After an incubation of 24 h, the medium was discarded and cells were washed twice with prewarmed 1x dPBS. To fix cells, 100 µl 4 % PFA were added to each well and incubated for 20 min at RT. Subsequently supernatants were removed and cells washed with 150 µl warm 1x dPBS. Following removal of PBS, macrophages were further washed twice by addition of 200 µl IFA wash buffer. Cells were permeabilized by incubation in 150 µl permeabilization buffer for 15 min at RT. Upon removal 150 µl blocking solution were added to each well and incubated for 30 min at RT to block all unspecific binding sites. A 1:4000 dilution of the primary antibody targeting pan-*Leishmania* heat shock protein 90 (LHSP90) in blocking solution was prepared, 60 µl were added to each well and incubated for 1 h at RT on a shaker. Macrophages were washed three times using 200 µl IFA wash buffer. The secondary antibody a-mouse-IgG conjugated with AF647 was diluted 1:8000 in blocking solution and combined with 1:100 diluted DAPI, for nuclear staining. 60 µl of the solution were added to each well and incubated for 1 h at RT in the dark. Subsequently the cells were washed twice with 200 µl IFA wash buffer and once with 200 µl 1x PBS. Finally, cells were covered with 200 µl 1x PBS and stored at 4 °C until HCS analysis. HCS analysis was performed using confocal high content microscope Opera Phenix® with Harmony® 4.5 software from Perkin Elmer (refer to Supplementary data for details on image acquisition and analysis).

2.5.5 Statistics

Statistical analysis was done in GraphPad Prism 9.1.0. All data sets were tested for Normality using Shapiro-Wilk test. Accordingly, further analysis was performed utilizing the parametric or non-parametric version of the test, indicated in each figure legend. Significances are shown in graphics as follows:

* = $p < 0.05$

** = $p < 0.01$

*** = $p < 0.001$

**** = $p < 0.0001$

Potential trends were further indicated by numerical depiction of p-values.

3 Results

In order to implement novel models and decrease reliance on animal experiments in accordance with the 3R principle (Reduce, Refine, Replace) for studying liver-specific immune responses during *L. infantum* infection, this study centered on establishing co-culture systems involving hepatocyte organoids (HepOrgs) alongside monocytes or macrophages. For this purpose, initially 3D HepOrgs were generated using murine and human primary hepatocytes. These HepOrgs were subsequently exposed to *L. infantum* parasites, and infection dynamics were comprehensively examined through microscopic analyses, cytokine profiling and transcriptome sequencing. Based on these findings, diverse strategies for co-cultivation of HepOrgs, *L. infantum* parasites and monocytes or macrophages were implemented. The primary aim was to recapitulate observed *in vivo* dynamics *in vitro*. These innovative approaches might further enable the investigation of reciprocal interactions between human hepatocytes and monocytes or macrophages during *Leishmania* infection, unraveling the immune response within the human liver microenvironment.

3.1 Generation of functional 3D organoids

3.1.1 Implementation of murine 3D hepatocyte organoid culture

3D cultures of murine hepatocyte organoids were initially generated using freshly isolated primary hepatocytes (Figure 5 A). Hepatocytes were obtained from male and female C57BL/6J mice by liver perfusion. Following perfusion with Liberase solution, the liver was excised and transferred to a buffer solution, facilitating the release of hepatocytes from the digested tissue. Subsequently, a Percoll gradient centrifugation step was employed to further process the hepatocytes. Finally, the cells were suspended in Cultrex Basement Membrane Extract (BME) and seeded as droplets.

During the first days of culture, small organoids formed from the embedded hepatocytes (Figure 5 B) and expanded to an average diameter of 150 μm within two weeks. Subsequently, the organoids were passaged by mechanical fragmentation every 7-14 days, depending on organoid size and culture density. Upon passaging, the culture was slightly expanded with an average split ratio of 1:1.5. However, this process required adaptation to each individual culture, as organoid growth was sensitive to low culture density and often resulted in collapse after passaging.

Cystic CholOrgs (Figure 5 B) began to emerge at the end of passage 0 and spread throughout the culture in subsequent passages due to their rapid growth. The distinct organoid types could be clearly distinguished (Figure 5 G), with HepOrgs forming dense cell clusters (I) and CholOrgs forming cysts with a single cell layer and a lumen (II). Some organoids exhibited both cystic and dense cell structures (III).

In comparison hepatocyte organoids evidenced slower, but significant growth ($p < 0.001$; $p < 0.05$) during the first two passages, reaching an average diameter of 300 μm (Figure 5 F). Subsequent passages showed no significant growth, but the culture stabilized in terms of a reduced amount of single cells and a consistent ratio of HepOrgs to CholOrgs (Figure 5 D+E). Therefore, organoids from passage 3 onwards were utilized for subsequent studies.

Overall, a 3D cell culture of expanding murine HepOrgs was successfully generated employing freshly isolated primary hepatocytes.

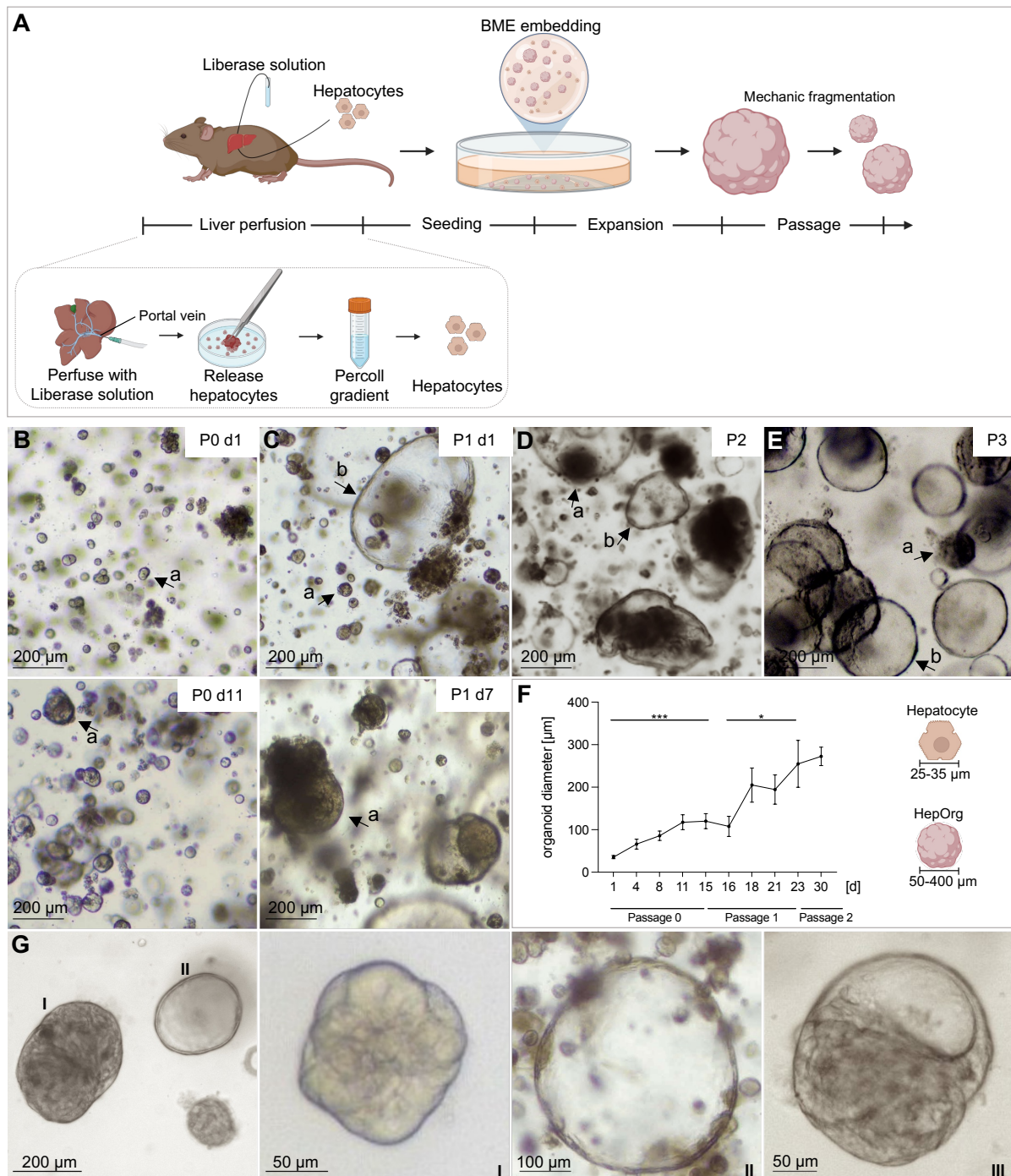


Figure 5: Seeding of primary murine hepatocytes into 3D liver organoids.

(A) Schematic workflow for the establishment of the 3D culture [Illustration:1, modified]: Liberase solution was pumped from the portal vein through the mouse liver. The hepatocytes were released from the digested tissue. Cells were further processed by Percoll gradient centrifugation and embedding in Basement Membrane Extract (BME). Expansion of forming organoids was regularly interrupted by mechanical fragmentation. (B-E) Representative light microscopy images of the 3D organoid culture at passage 0 (P0) day 1 and 11 (B), passage 1 (P1) at day 2 and 8 (C), passage 2 (P2) and passage 3 (P3) at day 7 respectively (D, E). Arrows indicate dense HepOrgs (a) and cystic CholOrgs (b). Images were acquired using Nikon ECLIPSE Ts2 Inverted Routine Microscope. (F) Quantification of the average HepOrg diameter in passages 0 to 2. The data is presented as mean \pm SEM of $n = 10$ individual HepOrgs. P-values were calculated using Unpaired Student's t-test (** $p < 0.001$; * $p < 0.05$). (G) Close-up images of different organoid types within the 3D culture (I HepOrg, II CholOrg, III HepOrg with cystic structure). Images were acquired using EVOS® FL Auto Fluorescence microscope.

3.1.2 Characterization of murine hepatocyte organoids

Following the successful generation of 3D murine HepOrg cultures, these organoids were analyzed for the expression of functional and structural markers, to demonstrate properties of HepOrgs. Therefore, the HepOrgs were fixed and whole-mount immunostaining was performed to visualize the expression of the analyzed markers at the protein level.

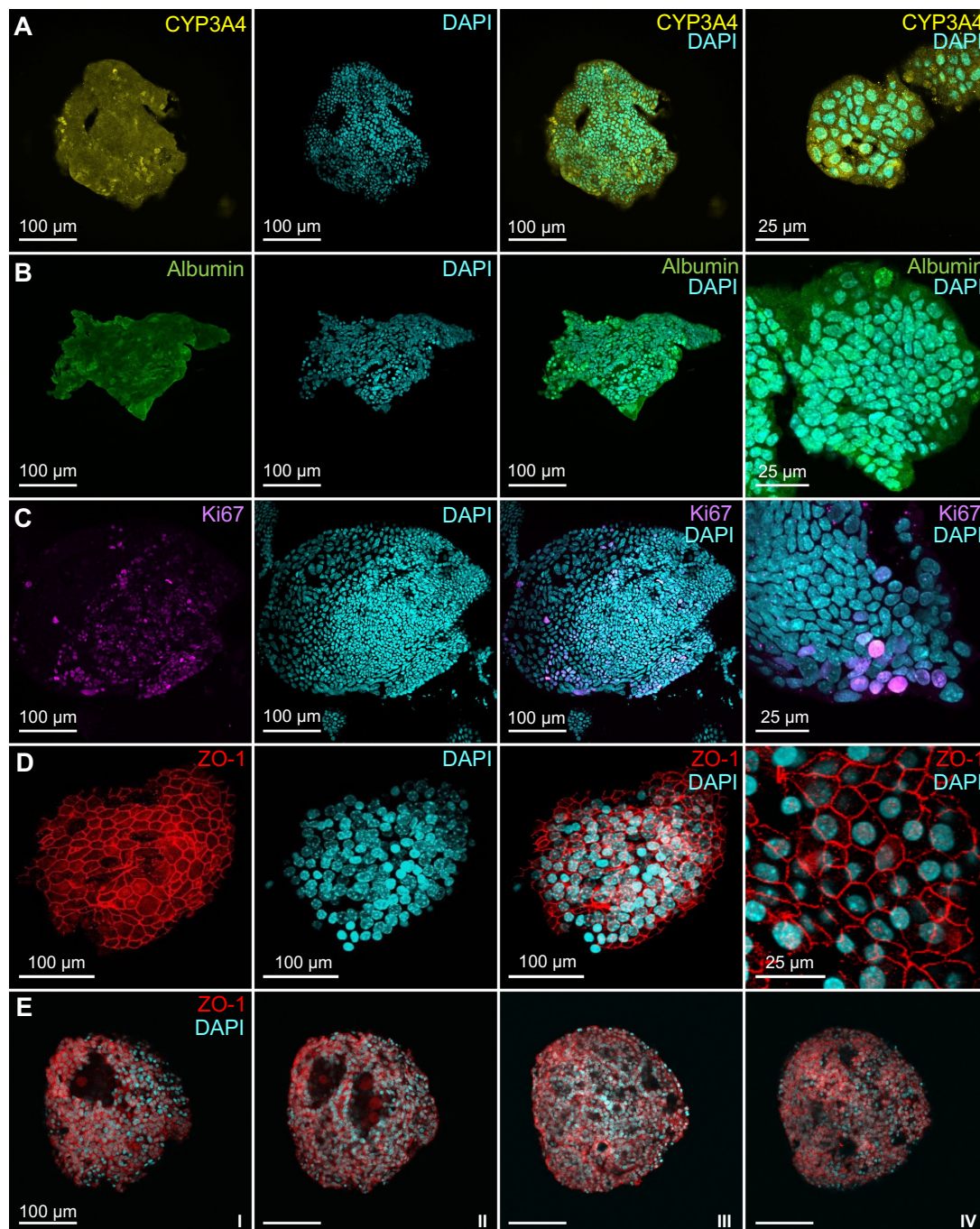


Figure 6: Immunofluorescence-based characterization of hepatocyte organoids.

HepOrgs were harvested from 3D culture, fixed and whole mount immunostaining was performed. Shown are confocal z stack images of the expression of hepatocyte markers (A) CYP3A4 (yellow) and (B) Albumin (green), proliferation marker (C) Ki67 (magenta) and tight junction marker (D) ZO-1 (red) at different magnifications. Images of individual channels are shown in the two left columns plus overlay with DAPI staining (blue, nuclei) in the two right columns. (E) Single plane images showing overlay of ZO-1 and DAPI stained HepOrgs at different z-levels (I – IV). Images were acquired using OLYMPUS FV3000 Confocal Laser Scanning Microscope.

The results obtained from confocal microscopy demonstrated the expression of both analyzed hepatocyte markers CYP3A4 (Figure 6 A) and albumin (Figure 6 B) throughout the entire HepOrgs, lacking discernible specific expression patterns. Ki67 expression, analyzed as a marker of proliferative activity within the HepOrgs, was identified in a substantial proportion of cells within the depicted organoid (Figure 6 C). Consistently, the Ki67 fluorescence signal localized to the nuclei, evident from the overlay with DAPI. The expression pattern of the tight junction marker ZO-1 (Figure 6 D) was confined to the cell membrane. Here, the staining illustrates both the dense structure of the HepOrgs, as well as the interconnectivity of hepatocytes within the organoids. Cross-sectional images depicted in Figure 6 E provided a more comprehensive visualization of the organoid structure. Notably, the organoids displayed areas with missing nuclei, indicative of a non-uniform cellular distribution within the organoids.

In summary, immunofluorescent staining of murine 3D HepOrgs confirmed the expression of functional markers CYP3A4 and albumin, along with the expression of the proliferation marker Ki67, indicating the presence of functional, proliferative hepatocytes. Furthermore, analysis of the tight-junction marker ZO-1 revealed a densely organized structure, as well as a non-uniform cellular distribution within the organoids.

3.1.3 Establishment and characterization of human 3D hepatocyte organoids

Following the establishment of murine HepOrgs, a 3D culture of human HepOrgs was generated using primary human hepatocytes. These hepatocytes were obtained from surplus liver tissue following tumor resections or biopsies and were provided as isolated single cells by the Human Tissue and Cell Research Foundation (HTCR). The cells were then seeded to form 3D organoids based on the published protocol by Hu, *et al.* [112].

Analogous to murine organoid cultures, dense HepOrgs and cystic CholOrgs were identified upon embedding of human hepatocytes in BME (Figure 7 A). Both the shape and size resembled those of murine HepOrgs. Notably, cystic CholOrgs manifested as rapidly growing structures as early as Passage 0 and maintained even distribution throughout subsequent passages of the 3D culture (Figure 7 B, C). Overall, the handling of the culture closely paralleled those for murine organoids. However, the human organoid culture appeared to exhibit more robust and faster growth, although these observations were not quantitatively assessed.

Characterization through immunofluorescence analysis (IFA) revealed abundant expression of the hepatocyte-specific marker albumin (Figure 7 D), along with the tight-junction marker ZO-1 (Figure 7 E) and the proliferation marker Ki67 (Figure 7 F). As expected, these findings are in concordance with the previous findings on murine HepOrgs, confirming the successful generation of functional and proliferating human HepOrgs.

In summary, a 3D culture of human hepatocyte organoids was implemented utilizing primary human hepatocytes. The characteristics of these organoids closely resembled their murine counterparts in terms of culture handling and expression of specific markers.

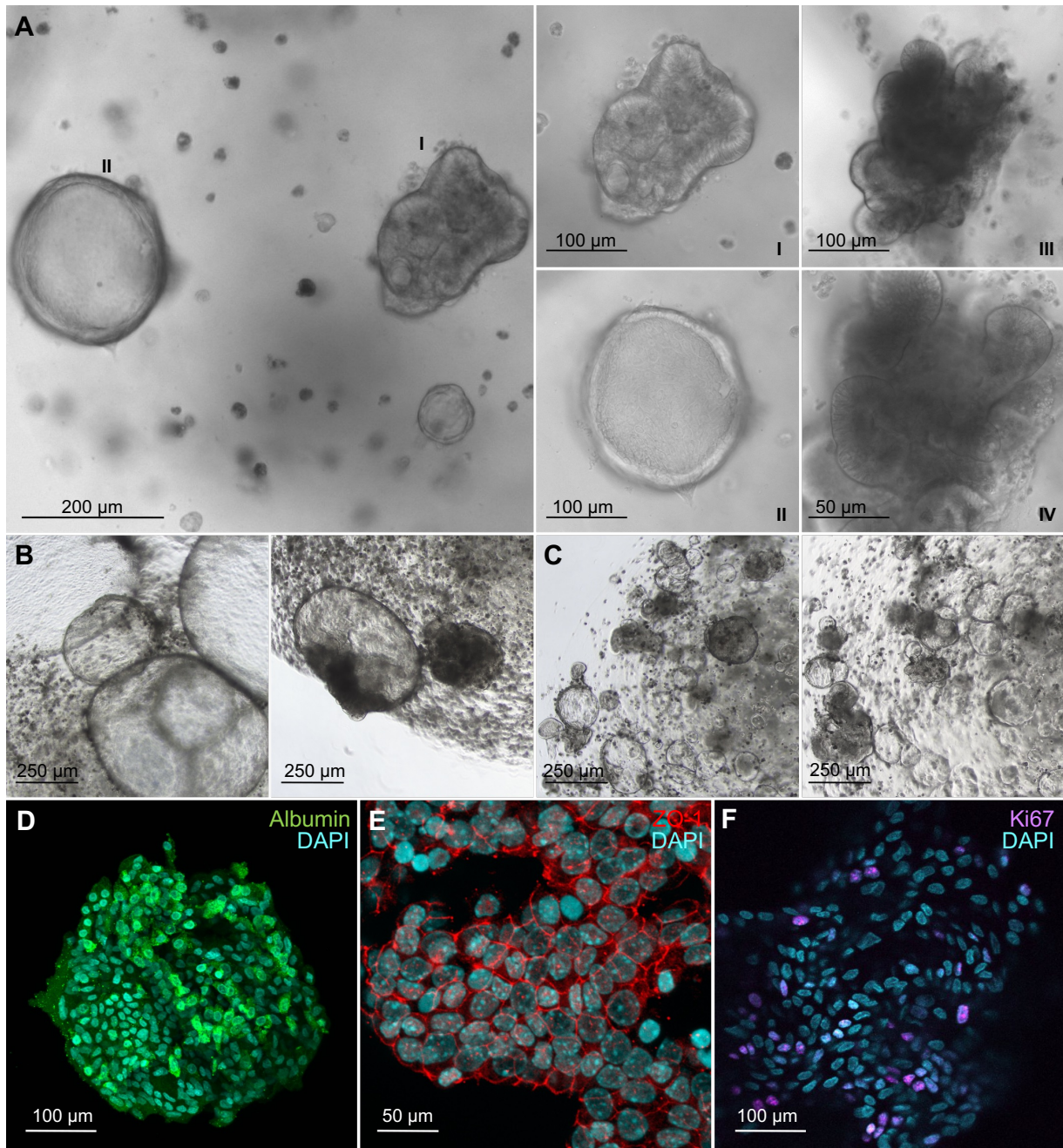


Figure 7: Establishment of human 3D hepatocyte organoids.

Human primary hepatocytes were seeded as 3D HepOrgs and characterized by phase contrast microscopy and immunofluorescence staining. (A) Representative images of human organoids at passage 2, including HepOrgs (I, III, IV) and cholangiocyte organoids (II) in different magnifications. Images were acquired using EVOS® FL Auto Fluorescence microscope. (B, C) Overview images of human 3D organoid culture at low magnification in passage 0 (B) and passage 3 (C). Images were acquired using Nikon ECLIPSE Ts2 Inverted Routine Microscope. (D-F) Confocal z-stack images of human HepOrgs, immunofluorescence-stained targeting hepatocyte marker (D) albumin (green), (E) tight junction marker ZO-1 (red) and proliferation marker (F) Ki67 (magenta) as overlay with DAPI (blue). Images were acquired with OLYMPUS FV3000 Confocal Laser Scanning Microscope.

3.2 Establishment of *L. infantum* infection in hepatocyte organoid immune cell co-cultures

Addressing the need for novel models to dissect liver-specific immune responses during VL in humans and the absence of data elucidating the involvement of hepatocytes in the underlying immune mechanisms, this study aimed to establish an infection model for *L. infantum* parasites in co-cultures of HepOrgs and immune cells (monocytes, macrophages).

To this end, the project is structured into three main parts, which are summarized in Figure 8:

In the initial phase (Figure 8, I.) a protocol for infecting HepOrgs with *L. infantum* parasites was established. HepOrgs are cultivated embedded into BME to facilitate organoid growth and prevent the disintegration of cell clusters. Therefore, in a first infection approach, parasites were embedded in BME along with HepOrgs (a). Alternatively, parasites were introduced into the liquid media surrounding the BME-embedded HepOrgs (b). Lastly, HepOrgs were released from the embedding by dissolving the BME, enabling co-cultivation of both HepOrgs and parasites in liquid media.

In the second phase of this study, illustrated in Figure 8 (Part II.), strategies for co-cultivating HepOrgs with monocytes were investigated, based on the previous infection of HepOrgs with *L. infantum* parasites. The employed approaches were primarily based on the methods previously outlined for co-cultures of epithelial organoids and immune cells (see Figure 3). Monocytes were either collectively embedded with *L. infantum*-infected HepOrgs in BME (a) or co-cultured in liquid media supplemented with (b) or without (c) 10 % BME.

Given that not hepatocytes but macrophages serve as the primary host cells for *Leishmania* parasites, two co-culture strategies were examined to combine HepOrgs with *L. infantum*-infected macrophages in the third phase of this thesis (Figure 8, III.). The aim was to establish a model that more closely mimics the *in vivo* conditions during *Leishmania* infection. Initially, HepOrgs were dissociated into single cells and collectively re-embedded into BME with *L. infantum*-infected macrophages (a). Additionally, HepOrgs were introduced in suspension to adherent macrophages previously infected with *L. infantum* parasites (b).

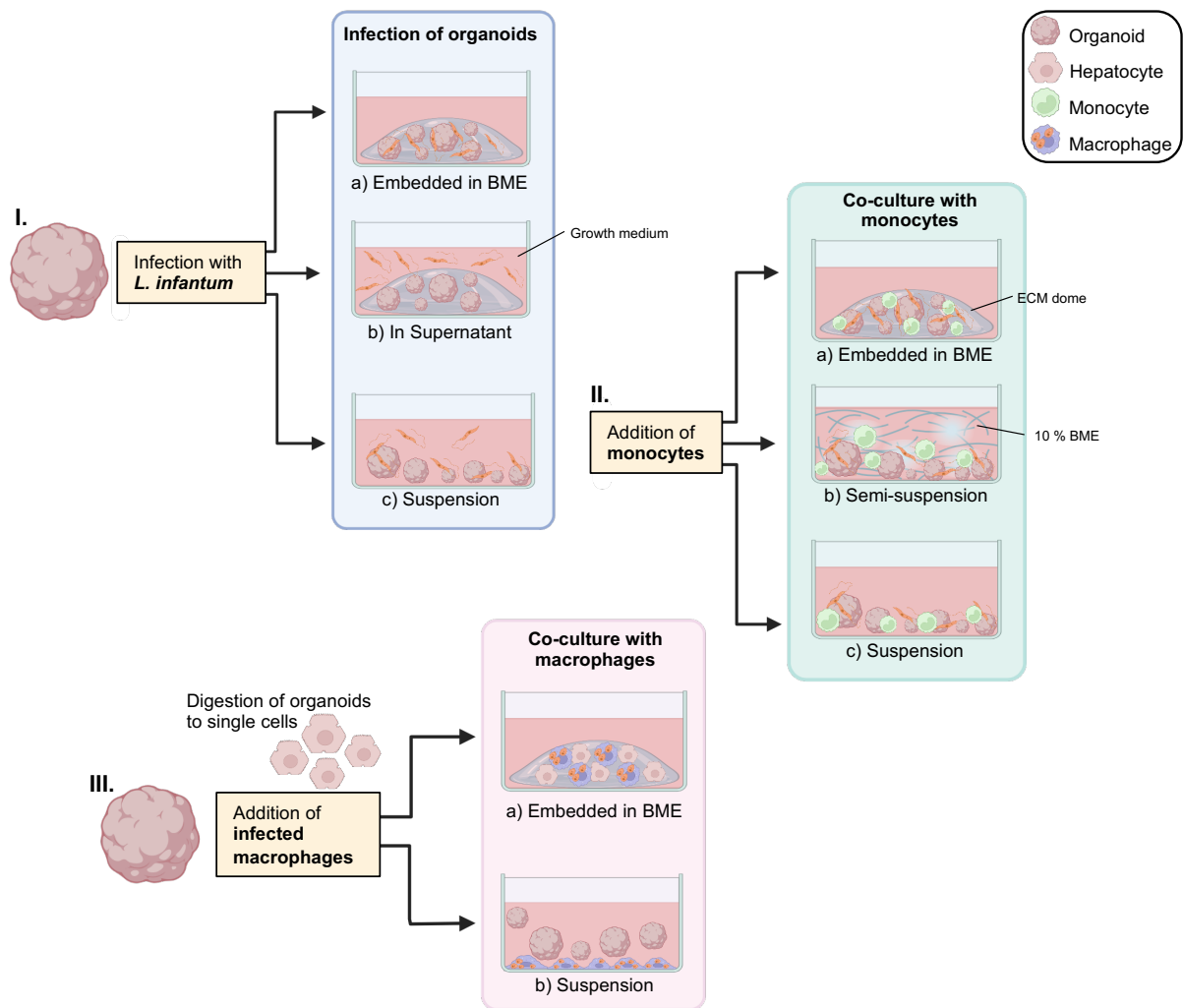


Figure 8: Scheme for establishing co-cultures of hepatocyte organoids with immune cells.

I.) Scheme showing different approaches for the infection of intact HepOrgs with *L. infantum* parasites. Parasites were embedded with HepOrgs in BME (a), added to the supernatant of embedded HepOrgs (b) or HepOrgs and parasites were co-cultured in suspension (c). II.) Illustration of the addition of monocytes to *L. infantum*-infected HepOrgs. Monocytes were embedded with infected HepOrgs in BME (a), co-cultured in semi-suspension with 10 % BME added to liquid media (b) or co-cultured in suspension (c). III.) Representation of the co-culture of *L. infantum*-infected macrophages and HepOrgs. a) HepOrgs were digested into single cells and embedded with infected BMDMs in BME. b) Intact HepOrgs were introduced in suspension to adherent infected BMDMs.

Overall, a variety of methods was evaluated to initiate *L. infantum* infection in co-cultures of hepatocyte organoids and immune cell. The advantages, limitations and applicability of these methods are subject of this study and will be elucidated in the following chapters.

3.3 Implementation of *L. infantum* infection in hepatocyte organoids

To establish a protocol for infecting HepOrgs with *L. infantum* parasites (project part I.), suitable co-culture conditions for both cell types had to be ensured. Therefore, the proliferation of *L. infantum* parasites was evaluated under HepOrg culture conditions.

Within the first 24 h of culture the parasite count per ml did not differ between M199+ *Leishmania* medium and HepOrg-specific Hep medium. However, a notable decrease in parasite count was observed within cultivation in Hep medium at subsequent time points (Figure 9 A), indicating compromised reproduction of the parasites. Consequently, infection experiments were limited to an incubation period of 24 h.

In the following infection experiments, it was investigated which of the methods represented, facilitated direct interactions between parasites and HepOrgs to enable subsequent infection. A primary focus was set on the necessity of the matrix and its influence on the infectivity of the parasites.

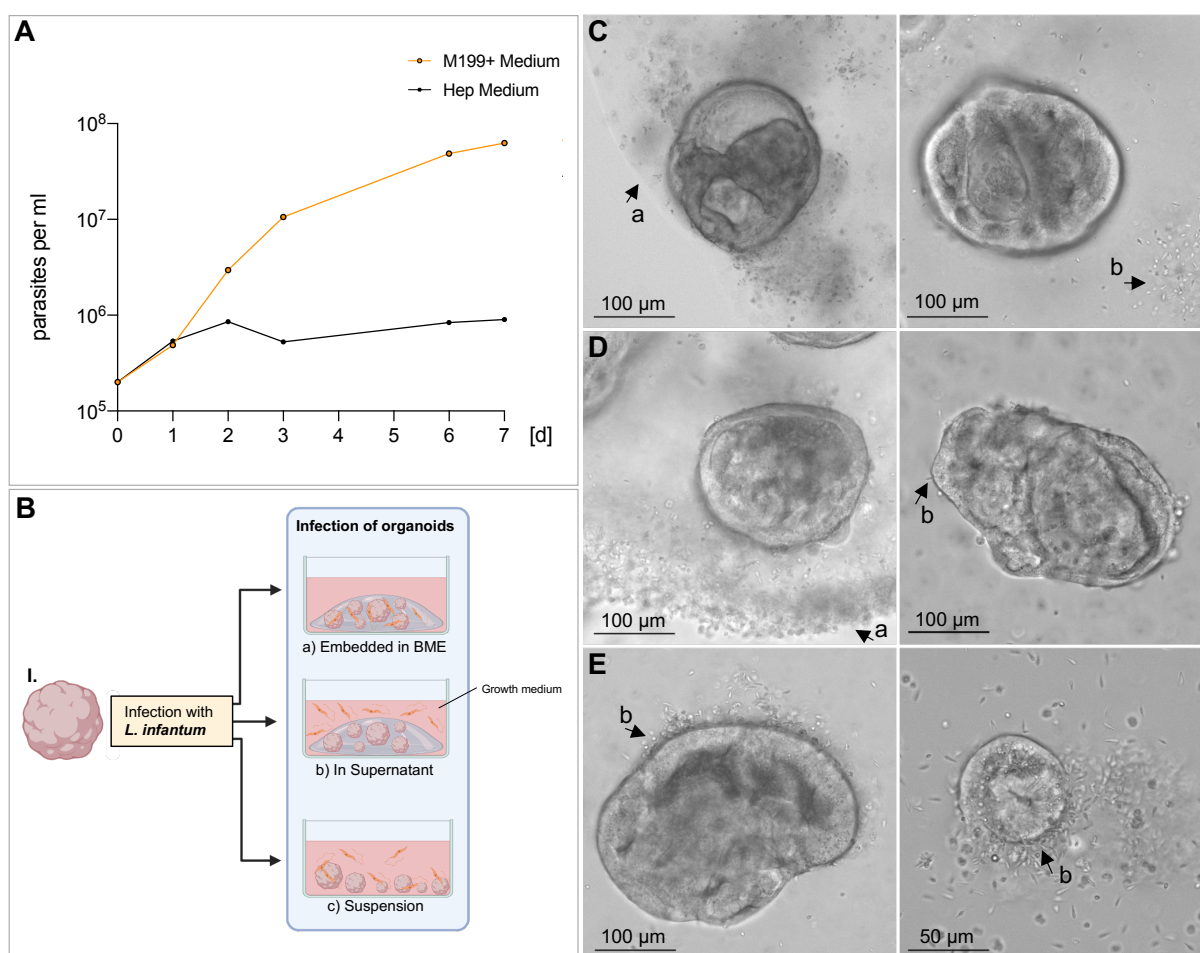


Figure 9: Evaluation of different hepatocyte organoid infection protocols.

(A) *L. infantum* parasites in the exponential growth phase were seeded in M199+ medium (standard *Leishmania* culture medium) and Hep medium (HepOrg culture medium) at 2×10^5 parasites per ml. Cell count was determined at 24 h intervals for 7 days. (B) Schematic representation of the infection approaches. *L. infantum* metacyclic promastigotes were added to the HepOrgs at an MOI of 20:1 (20 parasites per individual hepatocyte) for 24 h. The infection process was examined by phase contrast microscopy (C-E). Arrows indicate outer edge of the BME droplet (a) and individual or accumulated *L. infantum* parasites (b). (C) Representative images of HepOrgs and *L. infantum* parasites embedded in BME. (D) Images of HepOrgs following addition of parasites to the culture supernatant. (E) Images of HepOrgs infected in suspension. Images were acquired using EVOS® FL Auto Fluorescence microscope.

BME embedding of *L. infantum* seemed to result in complete immobilization of parasites. While movements of the flagellum were still observable (not shown), the parasites were unable to migrate through the BME. Upon addition of the parasites to the supernatant of the embedded HepOrgs, the parasites appeared to accumulate on the surface of the BME droplet (Figure 9 D). Whereas only a small fraction of parasites infiltrated the droplet. Both approaches failed to facilitate sufficient contact between parasites and organoids.

Only when parasites and HepOrgs were co-cultured in suspension both cell types seemed to exhibit direct interaction, as parasites aggregated around organoids, indicating tropism towards hepatocytes (Figure 9 E). Of note, the organoids largely remained intact in suspension, with only minor shedding of single cells becoming evident towards the end of the incubation period.

In summary, *L. infantum* parasites were unable to directly interact with BME embedded HepOrgs, due to the BME impeding the targeted movement of the parasites. However, when both HepOrgs and parasites were cultured in suspension, the cell types appeared to establish direct contacts, potentially facilitating infection.

3.3.1 Generation of fluorescent *L. infantum* parasites

To assess the potential infiltration of *L. infantum* parasites during infection, fluorescent parasites were generated through transfection with a vector facilitating mCherry expression in parasites.

Accordingly, an mCherry construct (Figure 10 A) was introduced into *L. infantum* parasites by electroporation, followed by selection under neomycin pressure. A fraction of the resultant transfectants demonstrated mCherry expression throughout living parasites, as evidenced by fluorescence microscopy. However, differential interference contrast (DIC) imaging revealed a prominent proportion of transfectants devoid of mCherry expression (Figure 10 B). Quantitative analysis of mCherry⁺ *L. infantum* indicated an average percentage of 30 % fluorescent parasites across all transfectants (Figure 10 C).

In summary, mCherry-expressing *L. infantum* transfectants were successfully generated, although only 30 % exhibited fluorescence.

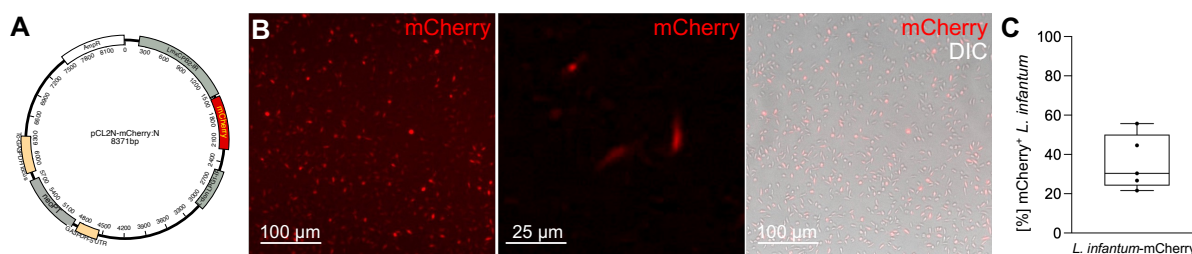


Figure 10: Generation of mCherry *L. infantum* transfectant.

(A) Plasmid pCL2N-mCherry:N (donated from J. Clos), employed for transfection into promastigote *L. infantum* parasites. (B) Fluorescence microscopy imaging of *L. infantum*-mCherry parasites, showing mCherry (red) channel in different magnifications plus overlay of mCherry and DIC image. Images were acquired using EVOS® FL Auto Fluorescence microscope. (C) Quantification of fluorescent *L. infantum* parasites upon transfection, based on images depicted in B. Evaluation was performed in FIJI. The data is presented as boxplot.

3.3.2 Evaluation of the infiltration of murine hepatocyte organoids by *L. infantum* parasites

To validate the established infection protocol, confocal microscopy was employed to visualize the potential invasion of the parasites into HepOrgs. Consequently, organoids were infected with mCherry-expressing *L. infantum* transfectants and processed for confocal microscopy. HepOrgs were counterstained targeting albumin and DAPI.

Confocal microscopy analysis revealed parasites attached to and infiltrated into HepOrgs. Notably, parasites evidenced mCherry fluorescence signal and displayed a characteristic promastigote morphology. Predominantly, parasites were localized at the outer edge of the organoids, indicating either attachment or concurrent invasion. Interestingly, individual parasites were discernible within the HepOrgs (Figure 11 A), as shown in cross-sectional images obtained at different z-levels (Figure 11 B). While parasites were distinctly observable amidst the organoid nuclei, determination regarding the invasion into hepatocytes or intercellular localization remained elusive (Figure 11 C).

Subsequently, non-transfected parasites were employed to infect HepOrgs and visualization of parasites was facilitated through immunostaining targeting Hsp90. The results of confocal microscopy were comparable to those obtained from the infection with mCherry-expressing transfectants. However, it was found that a prominent proportion of detected parasites appeared to be attached to structures external of the depicted organoids, such as BME residues (Figure 11 D).

Overall, the obtained results demonstrate the capacity of *L. infantum* parasites to infiltrate murine HepOrgs utilizing the established infection protocol. However, the parasites were predominantly located at the outer edge or external to the organoids, suggesting a limited direct interaction between parasites and hepatocytes.

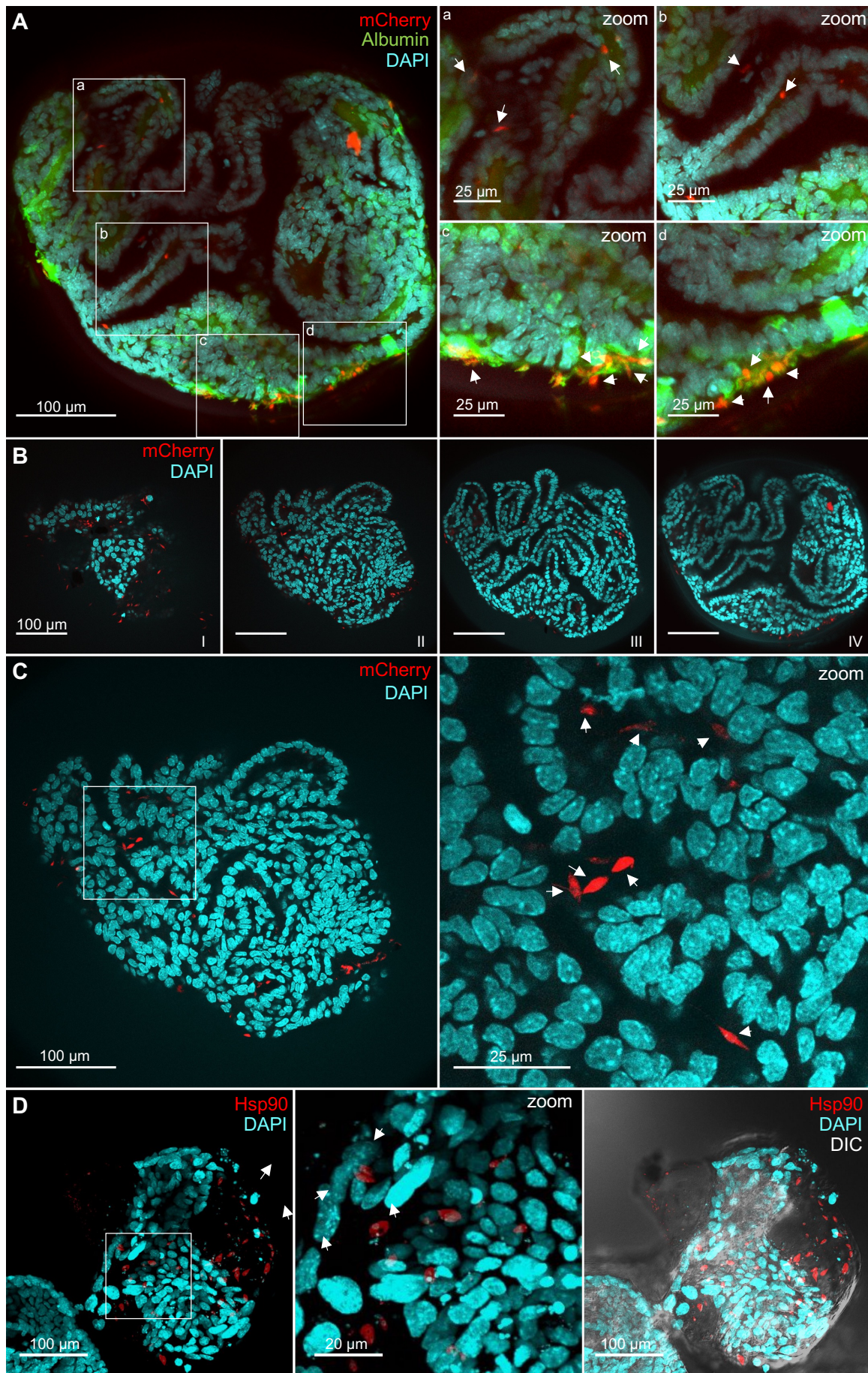


Figure 11: Imaging of the infiltration of hepatocyte organoids by *L. infantum* parasites.

HepOrgs were infected with *L. infantum*-mCherry or non-transfected *L. infantum* metacyclic promastigotes at an MOI of 20:1 (20 parasites per individual hepatocyte) for 24 h. HepOrgs were fixed and stained in preparation for confocal microscopy. (A) Confocal z stack images of *L. infantum*-mCherry-infected HepOrgs showing Albumin (green), mCherry (red) and DAPI (blue) channels as overlay, in different magnifications. Arrows indicate detected parasites. (B) Single plane images of *L. infantum*-mCherry infected HepOrgs showing mCherry (red) and DAPI (blue) channels as overlay, at different z-levels (I – IV). (C) Confocal z stack images of *L. infantum*-mCherry infected HepOrgs showing mCherry (red) and DAPI (blue) channels as overlay. Arrows indicate detected parasites. (D) Confocal z stack images of *L. infantum*-infected HepOrgs, showing Hsp90 (red) (*Leishmania* parasites) and DAPI (blue) channels as overlay, plus overlay with DIC. Images were acquired using OLYMPUS FV3000 Confocal Laser Scanning Microscope.

3.3.3 The cytokine profile of *L. infantum*-exposed hepatocyte organoids

The cytokine release triggered by HepOrgs upon exposure to *L. infantum* parasites, as well as potential sex-specific differences in the response of HepOrgs was evaluated by assessing cytokine levels in the culture supernatants. To this end, HepOrgs were derived from both male and female mice and infected with *L. infantum* parasites for 24 h employing the established suspension approach (Figure 12 A+B). Subsequently, the culture supernatants were subjected to cytokine measurements. A total of 12 cytokines were analyzed utilizing a multiplex immunoassay panel focusing on proinflammatory cytokines, including GM-CSF, IL-27, IL-23, IL-12p70, IL-1 α , IL-1 β , IL-10, IFN- β , IL-6, CCL2, TNF and IFN- γ . The data are presented as the mean fluorescent intensity (MFI), which directly correlates with the concentration of the respective cytokines, considering that the concentration of some analyzed cytokines was outside the detection range.

A notable trend in cytokine levels was observed with regard to sex, revealing elevated levels of GM-CSF, IL-1 β , IL-6, TNF and CCL2 in the supernatants of female-derived organoids compared to male-derived counterparts, regardless of infection status. Additionally, a tendency towards increased levels of IFN- γ in the supernatants of female-derived HepOrgs compared to male-derived ones was observed solely following *L. infantum* infection ($p = 0.088$). However, within the analysis of the multiplex results, no prominent infection-dependent differences were observed in either sex. Notably, considerable variance was evident across samples from different individuals for GM-CSF, IL-1 β , IL-6, TNF and CCL2, making potential trends less distinct. Conversely, the levels of the remaining cytokines were comparable to negative controls of the standard, suggesting low to negligible production by HepOrgs.

Furthermore, the concentrations of IL-6, CCL2 and CXCL1 were assessed via ELISA to quantify minor differences more accurately in these cytokines, which can serve as biomarkers during VL [126]. In contrast to the multiplex results, IL-6 concentration appeared to be consistently higher in supernatants of male-derived HepOrgs compared to female-derived counterparts, independent of infection status. Furthermore, exposure to *L. infantum* led to a decrease in IL-6 concentrations in both sexes, although this decline was more pronounced in male-derived samples. However, due to the low sample size this tendency could not be evaluated as statistically significant (Figure 12 D). High concentrations of both CCL2 and CXCL1 were detected. The concentration of CCL2 appeared to be higher in the supernatants of female-derived HepOrgs, irrespective of *L. infantum* exposure (Figure 12 E). Regarding CXCL1, increased cytokine levels were observed in the supernatants of female-derived HepOrgs compared to male-derived counterparts, both in uninfected and infected samples, whereby this effect was significant following *L. infantum* infection ($*p < 0.05$). Notably, CXCL1 levels appeared to decrease upon *L. infantum* exposure, particularly in the supernatants of female-derived HepOrgs (Figure 12 F).

In summary, the infection had a minor effect on the levels of the detected cytokines, although some trends were observed. Following *L. infantum* infection of HepOrgs levels of IL-6 and CXCL1 exhibited a decrease, while GM-CSF appeared to increase. Additionally, sex-specific differences were evident. Specifically, levels of GM-CSF, IL-1 β , CCL2, TNF and CXCL1 were elevated in supernatants of female-derived HepOrgs compared to male-derived counterparts. The measurement data for IL-6 presented contradicting trends between the multiplex immunoassay and ELISA with regard to sex-specific differences.

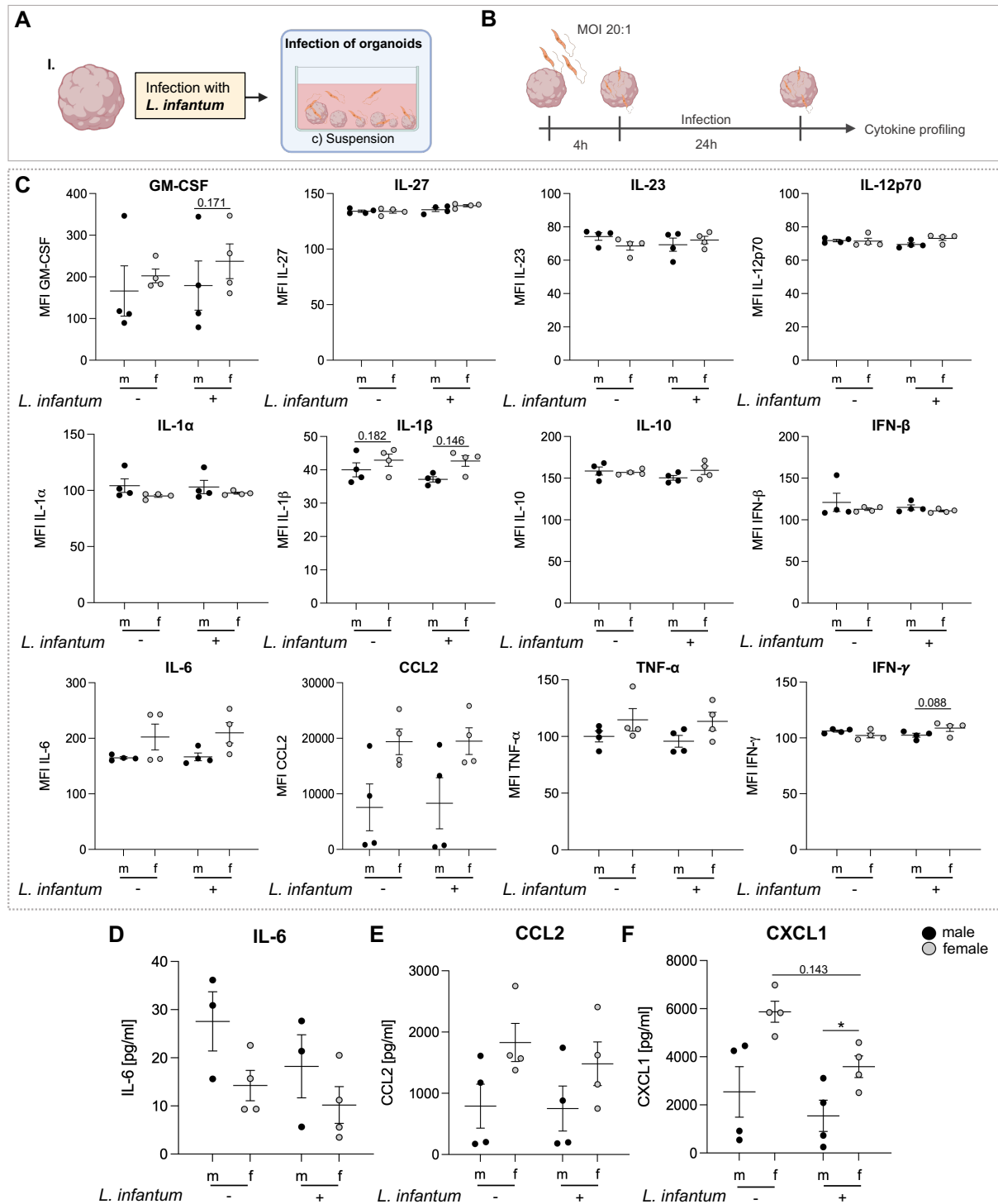


Figure 12: Cytokine profiling of hepatocyte organoids exposed to *L. infantum* parasites.

(A) Schematic representation of the infection of HepOrgs in suspension. (B) HepOrgs were generated from male and female mice and infected with *L. infantum* metacyclic promastigotes at an MOI of 20:1 (20 parasites per individual hepatocyte) for 4 h. Excess parasites were removed from the supernatant

and organoids were incubated for further 24 h. The infection was analysed by cytokine profiling. Uninfected HepOrgs served as controls. Cytokines were detected in cell culture supernatants by multiplex immunoassay (LEGENDplex™) (C) and ELISA for IL-6 (D), CCL2 (E) and CXCL1 (F). The data is presented as mean \pm SEM of $n = 4$ individuals per sex. P-values were calculated using Students t-test, followed by Holm-Šídák correction.

3.3.4 Application of the established infection protocol to human hepatocyte organoids

Next, the established protocol for the infection of murine HepOrgs with *L. infantum* parasites was applied to human organoids. Accordingly, human HepOrgs were infected with *L. infantum* parasites at an MOI of 20:1 for 24 h (Figure 13 A). Parasites were detected through immunofluorescence staining targeting Hsp90, followed by confocal microscopy. As depicted in Figure 13 B, the obtained images illustrate the infiltration of *L. infantum* into the HepOrgs. Interestingly, human organoids seemed to exhibit a more pronounced infiltration of parasites throughout the HepOrg structure, contrasting with the infection of murine organoids where parasites predominantly accumulated at the outer edge. This suggests a higher proportion of hepatocytes directly engaging with parasites in human HepOrgs upon infection. The appearance of parasites within the organoids was further shown by microscopy of the infected HepOrgs at different z levels (Figure 13 C).

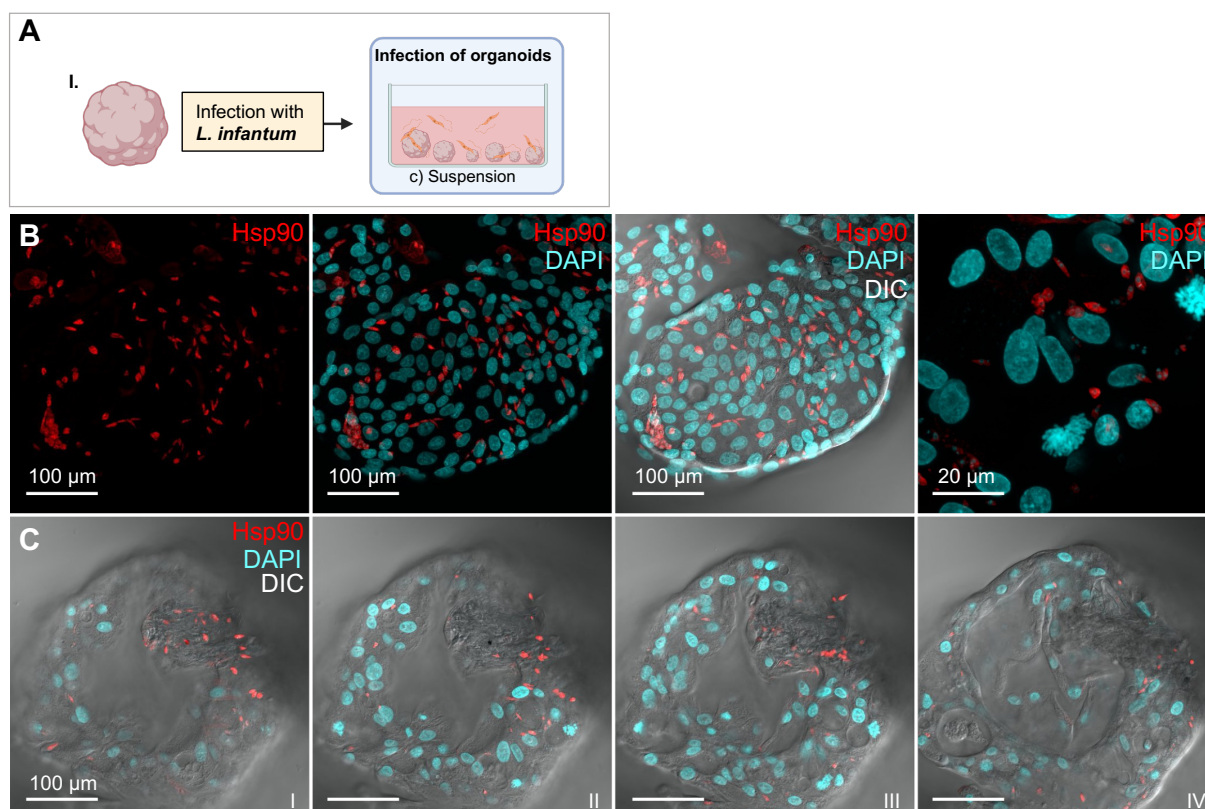


Figure 13: Microscopic evaluation of *L. infantum* infection in human hepatocyte organoids.

Human HepOrgs were infected with *L. infantum* metacyclic promastigotes at an MOI of 20:1 (20 parasites per individual hepatocyte) for 24 h. HepOrgs were fixed and stained in preparation for confocal microscopy. (A) Schematic representation of the infection of HepOrgs in suspension. (B) Confocal z-stack images of infected human HepOrgs, showing Hsp90 (red, *Leishmania* parasites) channel plus overlay with DAPI (blue) and DIC, in different magnifications. (C) Single plane images of infected human HepOrgs at different z-levels (I-IV). Shown are overlay images of Hsp90, DAPI and DIC channels. Images were acquired using OLYMPUS FV3000 Confocal Laser Scanning Microscope.

To assess the cytokine response of human HepOrgs following *L. infantum* infection, a comprehensive measurement of cytokines within the culture supernatant was conducted. Therefore, human HepOrgs derived from a single male donor were infected with *L. infantum* parasites at an MOI of 20:1 for 24 h. A multiplex assay targeting cytokines released in response to pathogens was utilized, which included the measurement of GM-CSF, IL-12p70, IL-1 β , IL-10, IFN- α , IFN- β , IFN- γ , IFN- λ 1, IFN- λ 2/ λ 3, IL-6, TNF, IL-8 and IP-10 (Figure 13 A-M). Additionally, an ELISA was used to quantify CXCL1 concentration in culture supernatants (Figure 13 N).

Overall, a significant decrease in the amounts of IL-1 β and IFN- α was observed in response to infection. Additionally, a discernible trend towards decreased cytokine levels post-infection was noted for IL-10, IFN- β , TNF, IL-8, IP-10 and CXCL1, although not statistically significant. No notable alterations in cytokine quantity were identified following infection for the remaining depicted cytokines, however these cytokines were scarcely detected at all, suggesting minimal or absent production by human HepOrgs.

In summary, the infection of human HepOrgs with *L. infantum* parasites, was validated through IFA, employing the established infection protocol. On cytokine level this resulted in a significant decrease of IL-1 β and IFN- α in culture supernatants, while IL-10, IFN- β , TNF, IL-8, IP-10 and CXCL1 showed a tendency towards decreased levels.

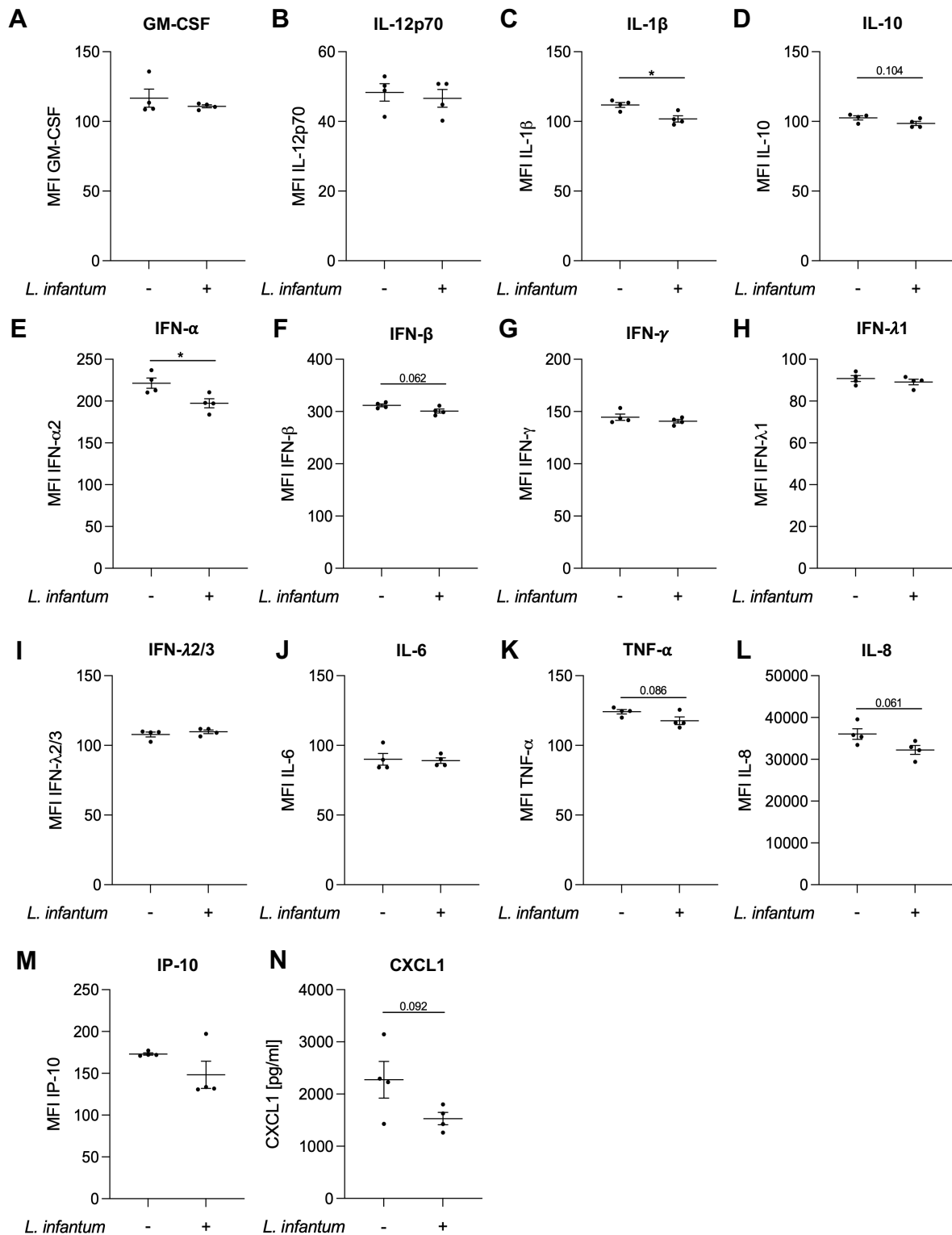


Figure 14: Cytokine profiling of human hepatocyte organoids infected with *L. infantum* parasites.

Human HepOrgs were infected with metacyclic promastigotes at an MOI of 20:1 (20 parasites per individual hepatocyte) for 24 h. The cell culture supernatants were collected and analysed for the indicated cytokines by multiplex immunoassay (LEGENDplex™) (A-M) and ELISA (N). The data is presented as mean \pm SEM of human HepOrgs derived from n = 1 donor, data points indicate technical replicates. P-values were calculated using Unpaired Students t-test (*p < 0.05).

samples). (C, D) PCA plots divided into female (C) and male derived samples (D). Different individuals are indicated by different node shapes.

In samples derived from females, 10 genes were differentially expressed between uninfected and infected conditions. However, in samples derived from males, no differentially expressed genes (DEGs) were identified. Additionally, upon comparing samples derived from male and female mice, primarily sex-specific genes were differentially expressed, irrespective of infection status (Figure 15B). These genes include *X inactive specific transcript (Xist)*, *Eukaryotic translation initiation factor 2, subunit 3, structural gene Y-linked (Eif2s3y)*, *DEAD box helicase 3, Y-linked (Ddx3y)*, *lysine demethylase 5D (Kdm5d)*, *ubiquitously transcribed tetratricopeptide repeat containing, Y-linked (Uty)*.

Separate PCAs were conducted for each sex to investigate the variability between conditions more comprehensively. Interestingly, it was notable once again that the variance in gene expression profiles among HepOrgs derived from different individuals outweighed the variance attributed to infection. Notably, distinct differences in PC 1 and PC 2 between uninfected and infected samples were evident solely in the data from female 3 (f3) (Figure 15 C, D).

At this point, comprehensive analysis of the entire data set was hindered by the heterogeneity of the samples. To enable a statistical evaluation of the infection-associated differences in gene expression profiles, a separate analysis was undertaken. Here, a cluster comprising two female and two male derived samples was defined (Cluster A, Figure 15 A), characterized by comparably low variance between HepOrgs derived from different individuals. Subsequent analysis focused exclusively on distinguishing between uninfected and infected samples, disregarding the distinction between male and female derived samples, to ensure an adequate sample size ($n = 4$).

PCA conducted on this defined subset revealed no distinct clustering into separate groups (Figure 16 A). However, upon comparison between uninfected and infected samples, differentially expressed genes were identified. The heatmap in Figure 16 B illustrates all genes exhibiting a log-fold change (FC) > 0 and a p-adjusted < 0.05 . Notably, the gene expression profiles were comparatively homogenous within the analyzed samples, irrespective of sex. Overall, 23 genes were found to be upregulated, while 25 were downregulated upon *L. infantum* infection of HepOrgs. The most prominent differences upon infection included the upregulated expression of *actin alpha 1, skeletal muscle (Acta1)* (FC = 3.96; padj < 0.01), *S100 calcium binding protein A14 (S100a14)* (FC = 1.49; padj < 0.0001), *tubulin, beta 3 class III (Tubb3)* (FC = 2.44; padj < 0.001), *interleukin 6 receptor, alpha (Il6ra)* (FC = 1.25; padj < 0.01) and the downregulated expression of *pleckstrin homology domain containing, family S member 1 (Plekhs1)* (FC = -1.26; padj < 0.0001), as well as *SAS-6 centriolar assembly protein (Sass6)* (FC = -1.37; padj < 0.05) (Figure 16 C). Notably, all other depicted DEGs exhibited a FC $< |1|$.

To assess the infection-dependent impact on cellular pathways, KEGG pathway analysis was conducted for the differentially expressed genes represented. The analysis revealed that *L. infantum* infection affects pathways associated with GO biological processes such as response to mechanical stimulus, inflammatory response, regulation of cell differentiation, defense response among others (Figure 16 D). Notably, due to the relatively low number of differentially expressed genes, both up- and downregulated genes were included in the KEGG pathway analysis. Consequently, it was not possible to identify signaling pathways based on these two groups separately.

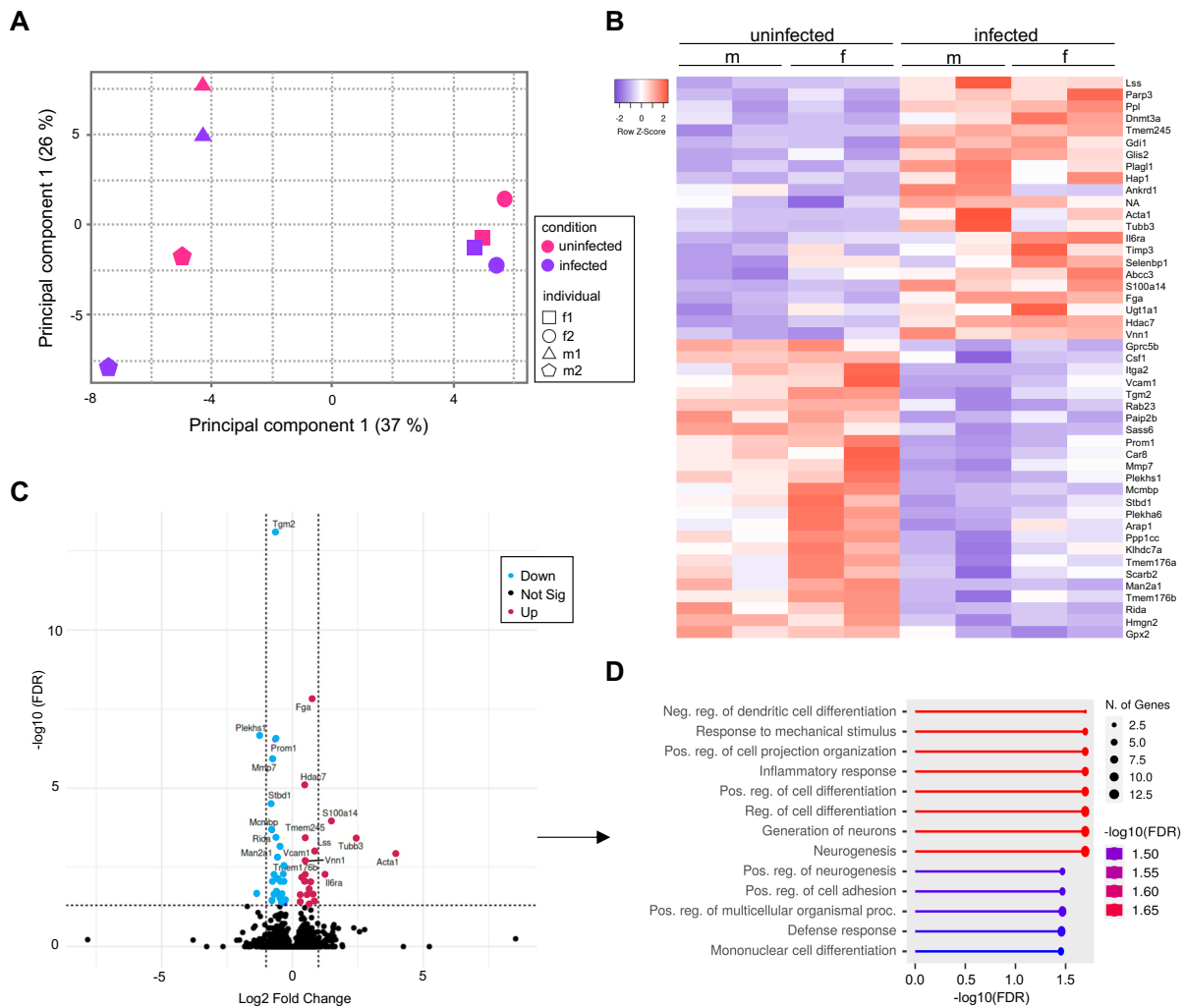


Figure 16: Transcriptome analysis of the defined sample subset.

Detailed analysis of Cluster A highlighted in Figure 8 (A), including samples derived from 2 male and 2 female individuals. Within the statistical analysis, samples were solely distinguished by infection status (irrespective of sex) to ensure adequate sample size ($n = 4$). (A) PCA plot distinguishing samples from different individuals by varying node shapes. Uninfected samples are depicted in pink and infected samples in purple. (B) Heatmap presents the z-scores of all genes differentially expressed between uninfected and infected samples (for $p\text{-adj} < 0.05$). (C) Volcano plot depicting differential expression of genes in infected samples compared to uninfected controls. Significantly regulated ($\log\text{-fold change (FC)} > 0$; $p\text{-adjusted} < 0.05$) genes are shown in blue (downregulated) or red (upregulated), not significantly regulated genes are shown in black. (D) Biological processes - GO term enrichment of genes that are significantly regulated in infected samples compared to uninfected controls.

To further assess the infection-dependent effects on specific genes of interest, the normalized read counts of these genes within the defined sample subset were evaluated. This analysis included genes known to be regulated in hepatocytes upon *L. infantum* exposure (*Nod1*, *Nod2*, *Tlr2*, *Tlr4*), cytokines and their respective receptors involved in immune responses in the liver during VL (*Cxcl1*, *Ccl2*, *Ccl5*, *Tnfrs1 α* , *Il10rb*, *Nos2*, *Arg2*), as well as hepatocyte specific functional markers (*Crp*, *Alb*, *Cyp3a13*).

Interestingly, further assessment revealed a discernible increase in *Nod2* mRNA levels. Conversely, the read counts for *CCL5* and *Tlr2* exhibited a decrease after exposure to parasites. The expression of all other depicted genes appeared to be independent of parasites exposure, as there was no prominent difference in transcript levels before and after infection (Figure 17).

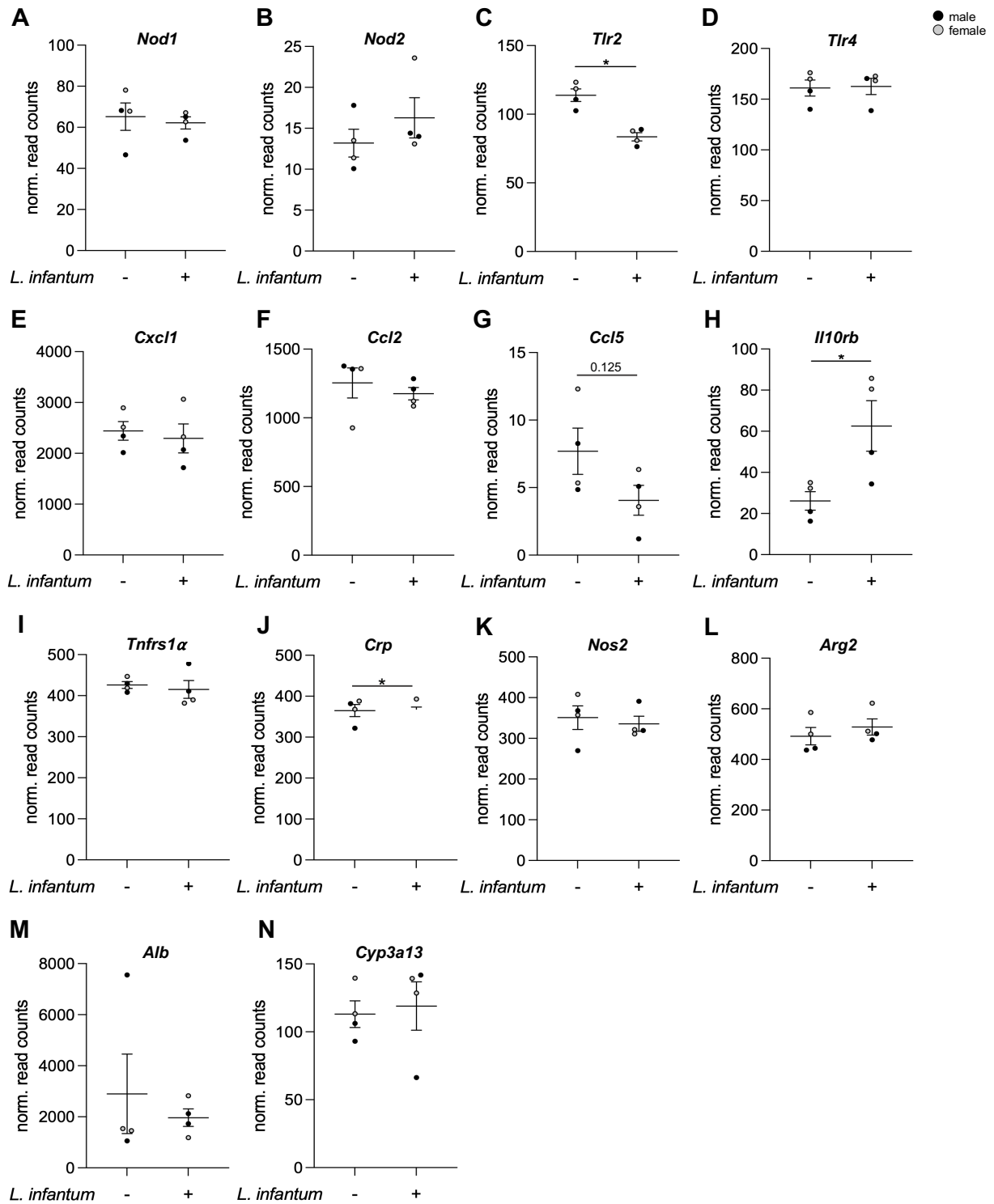


Figure 17: Analysis of relevant gene transcripts using the selected data set from *L. infantum*-infected organoids.

Shown are the normalized read counts of samples from Cluster A described in Fig. 9. Data is presented as mean \pm SEM of $n = 4$ independent experiments. P-values were calculated using Paired Student's *t*-test (* $p < 0.05$).

In summary, a comprehensive analysis of all sequencing data revealed a pronounced heterogeneity among the HepOrg samples obtained from different individuals. Only by defining a smaller sample subset, differentially expressed genes could be identified between uninfected and infected samples. The entirety of up- and downregulated genes following *L. infantum* infection of HepOrgs, could be assigned to several signaling pathways involved in biological processes such as response to mechanical stimulus, inflammatory response, regulation of cell differentiation and defense response. However, the relatively small number of differentially expressed genes upon *L. infantum* infection of HepOrgs suggests a rather weak response of the hepatocytes to parasite exposure.

3.4 Co-culture of murine monocytes with *L. infantum*-infected hepatocyte organoids

To model the interaction between hepatocytes, *L. infantum* parasites and monocytes, which are recruited to the liver during VL [89], monocytes were co-cultured with *L. infantum*-infected HepOrgs. Three distinct methods for the addition of monocytes to the infected organoids were utilized and evaluated regarding their capacity to replicate the underlying *in vivo* dynamics. Monocytes were either embedded collectively with infected organoids in BME, co-cultured in semi-suspension with the addition of 10 % BME, or co-cultured in suspension (Figure 18 A). These different methods were implemented in the established organoid infection model. Monocytes were introduced at a ratio of 1 to 3 individual hepatocytes to monocytes and co-cultured for 24 h. Evaluation of the methods involved live cell imaging and measurement of cytokine levels in the culture supernatants (Figure 18 B).

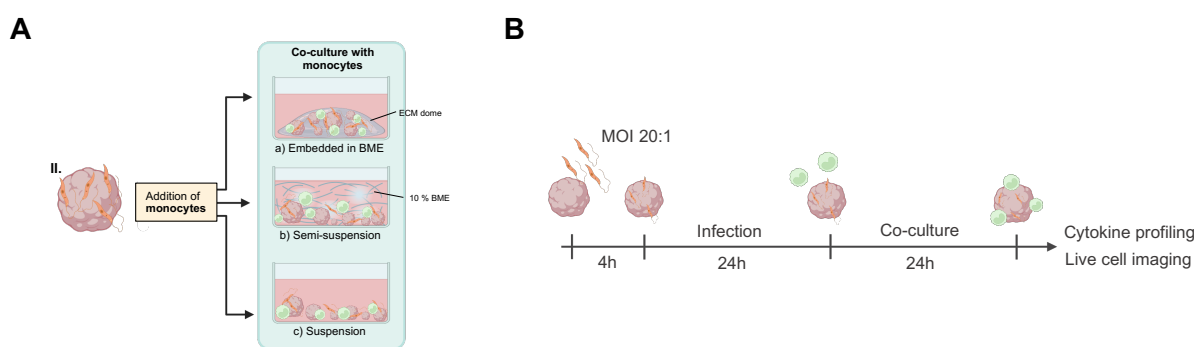


Figure 18: Schematic depiction of the co-cultivation of monocytes with *L. infantum*-infected hepatocyte organoids.

(A) Schematic representation of the co-culture approaches of *L. infantum*-infected HepOrgs and monocytes. (B) HepOrgs were infected with *L. infantum* metacyclic promastigotes at an MOI of 20:1 (20 parasites per individual hepatocyte) for 4 h. Excess parasites were removed from the supernatant and organoids were incubated for further 24 h. Monocytes were isolated from bone marrow, stained with CMFDA CellTracker™, added to the infected HepOrgs at a ratio of 1 to 3 (individual hepatocyte to monocyte) and co-cultured for 24 h. The co-cultures were analysed by cytokine profiling and Live cell imaging.

The monocytes utilized for co-cultivation experiments were isolated from mouse bone marrow via antibody-mediated immunomagnetic negative selection. A purification control was conducted using FACS to confirm successful isolation and ensure a sufficient purity of the monocyte population. Subsequently, the enrichment of monocytes was quantified. Overall,

there was a significant increase in the proportion of monocytes ($\text{Ly6C}^+\text{Ly6G}^-$) within all CD11b^+ cells, from on average 11 - 20 % pre MACS to 82 - 90 % post MACS. Only experiments in which monocytes with a purity exceeding 80 % were obtained, were employed in co-cultures with HepOrgs.

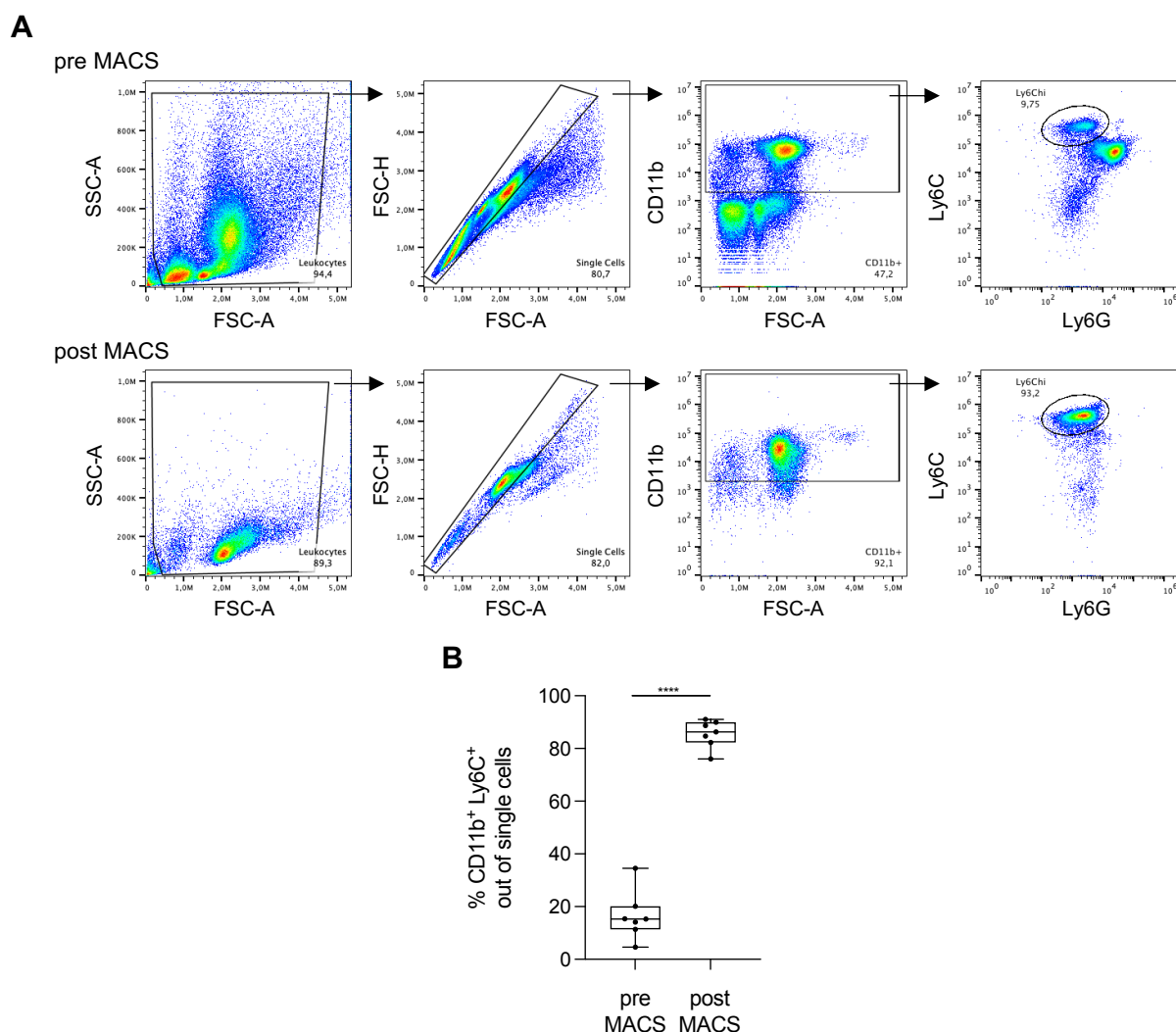


Figure 19: Purity control of monocytes isolated from murine bone marrow.

(A) Gating scheme to determine purity of monocytes after isolation. Cells were stained with anti-CD11b, anti-Ly6C and anti-Ly6G antibodies and analysed using BD Accuri™ C6 Plus Personal Flow Cytometer. Depicted are plots before (pre MACS) and after isolation (post MACS) from one representative experiment. (B) Quantification of Ly6C^+ cells from the total of CD11b^+ cells before and after monocyte isolation. The data is presented as boxplots of $n = 7$ independent experiments. P-value was calculated using Paired Student's t-test (**** $p < 0.0001$).

3.4.1 a) Co-culture of monocytes and infected organoids embedded in BME

In the initial experimental approach, freshly isolated and CMFDA-stained monocytes were embedded in BME with intact organoids for 24 h, post-infection with *L. infantum* (Figure 20 A). Uninfected HepOrgs served as controls, along with uninfected and infected organoids without monocytes, as well as monocytes co-cultured with *L. infantum* parasites without HepOrgs. Live cell imaging was utilized to monitor potential monocyte recruitment to the organoids after 2 h, 6 h and 24 h of co-culture. Additionally, comprehensive cytokine measurements were performed on the cell culture supernatants.

Representative images of the co-culture are shown in Figure 20 B. Based on these images, the quantification of monocytes per organoid was performed to assess potential recruitment. Overall, a tendency for a higher number of monocytes per organoid was observed following *L. infantum* infection as compared to uninfected controls, beginning after 6 h of co-culture. This trend was more prominent at the latest observation timepoint of 24 h. However, the data exhibited high variations particularly in the infected samples and could not be evaluated as statistically significant (Figure 20 C).

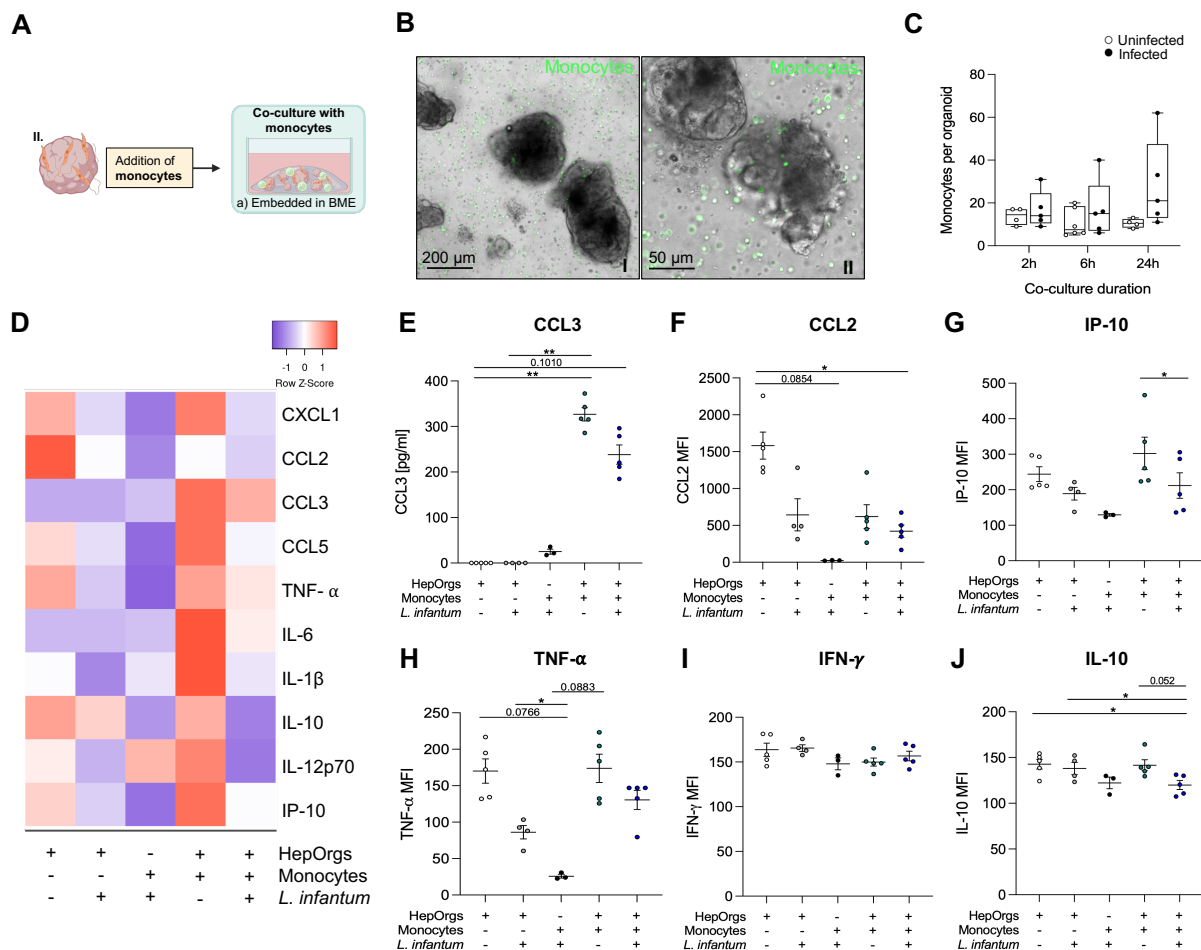


Figure 20: Co-culture of *L. infantum*-infected hepatocyte organoids with monocytes in BME.

CMFDA stained monocytes were added to *L. infantum*-infected HepOrgs, embedded in BME and co-cultivated for 24 h at a ratio of 1 to 3 (hepatocyte to monocytes). (A) Schematic representation of the co-culture embedded in BME. (B) Phase contrast microscopy images of co-cultures of infected HepOrgs and monocytes after 24 h incubation, in different magnifications (I, II). CMFDA stained monocytes are depicted in green. Images were acquired using EVOS® FL Auto Fluorescence microscope. (C) Quantification of the number of monocytes per organoid at different time points after co-culture initiation. The data was collected using microscopic images (representative shown in B) of $n = 4-6$ HepOrgs from one individual. Evaluation was performed in FIJI. The data is presented as boxplots. (D-J) Cytokines were detected in culture supernatants by ELISA (CCL3) and multiplex immunoassay (LEGENDplex™). The data was generated within a single experiment with $n = 3-5$ technical replicates. (D) Heatmap: the relative amounts of cytokines are given as row z-score of the indicated co-culture conditions. Purple indicates low levels of the cytokine, whereas red indicates high levels. (E-J) Graphs depict MFI or concentration (CCL3) of the identified cytokines. The data is presented as mean \pm SEM. P-values were calculated using one-way repeated measures ANOVA (* $p < 0.05$; ** $p < 0.01$).

Differences in cytokine levels were observed among the evaluated co-culture conditions, as shown in the heatmap in Figure 20 D. The results demonstrate that the cytokines CXCL1,

CCL3, CCL5, TNF, IL-6, IL-1 β , IL-12p70, IP-10 were predominantly elevated in the co-culture of uninfected HepOrgs and monocytes, as compared to the other conditions. Conversely, the co-culture of monocytes and *L. infantum* parasites exhibited the lowest levels of these cytokines. Notably, cytokine measurement further included IFN- α , IFN- β , IFN- γ and GM-CSF. However, cytokine levels appeared equal among all conditions and were therefore not included in the heatmap depiction.

The cytokines CCL3, CCL2, IP-10, TNF, IFN- γ and IL-10, which are known to be involved in liver stage leishmaniasis (refer to Figure 2), were presented separately to illustrate the dynamics across the different conditions more precisely and to evaluate the capability of the co-culturing method to mimic *in vivo* dynamics (Figure 20 E-J). A consistent trend was observed for CCL2, IP-10, TNF and IL-10, although to varying degrees. Cytokine levels were highest in uninfected organoids and decreased upon *L. infantum* exposure. A similar declining trend was shown in co-cultures of infected HepOrgs and monocytes, compared to uninfected controls. No clear difference in cytokine levels was observed in uninfected HepOrgs upon monocyte addition. Only CCL2 levels were higher without added monocytes. Conversely, respective cytokine levels were lowest in co-cultures of monocytes and *L. infantum*. Notably, CCL3 was not detected in the supernatants of solely cultured HepOrgs, regardless of infection, while low levels were found in the supernatants of monocytes and parasites. The addition of monocytes to HepOrgs led to a prominent increase in the overall CCL3 concentration, however, this concentration tended to decrease following HepOrg infection.

In summary, a co-culture of *L. infantum*-infected HepOrgs and monocytes embedded in BME was conducted. Live cell imaging demonstrated a trend towards increased numbers of monocytes in close proximity to infected HepOrgs, compared to uninfected organoids. Cytokine measurements revealed a decrease in cytokine levels of CCL2, IP-10, TNF and IL-10 upon parasite exposure of HepOrgs in both co-cultures of HepOrgs and monocytes and solely cultured HepOrgs. CCL3 was exclusively detected in cultures containing monocytes.

3.4.2 b) Co-culture of monocytes and infected organoids in semi-suspension

In the second co-culture approach, CMFDA stained monocytes and *L. infantum*-infected HepOrgs were co-cultured in a semi-suspension with the addition of 10 % BME to the liquid medium for 24 h (Figure 21 A), analogous to approach a) outlined in section 3.4.1. Live cell imaging was utilized to monitor potential monocyte recruitment after 2 h, 6 h and 24 h. In addition, cytokine profiling was employed to assess cytokine dynamics in the cell culture supernatant.

Imaging of the co-culture depicted aggregations of monocytes in close proximity to the organoids (Figure 21 B). Quantitative analysis of the number of monocytes per organoid evidenced a consistent trend of increased monocytes per organoid, following HepOrg infection across all observed timepoints (Figure 21 C).

Cytokine profiling demonstrated a distinct pattern, characterized by elevated levels of CXCL1, CCL2, CCL3, CCL5, TNF, IL-6, IL-1 β , IL-10, IL-12p70, IFN- α , and IFN- β in the co-culture supernatants of monocytes and uninfected or infected HepOrgs. The levels of these cytokines were markedly lower in all other conditions, while CXCL1 and CCL2 levels were comparable to the levels in the supernatants of uninfected and infected organoids without monocytes. IP-10 levels were overall higher in cultures without parasites. The cytokine profiles of IFN- γ and GM-CSF appeared less conclusive (Figure 21 D).

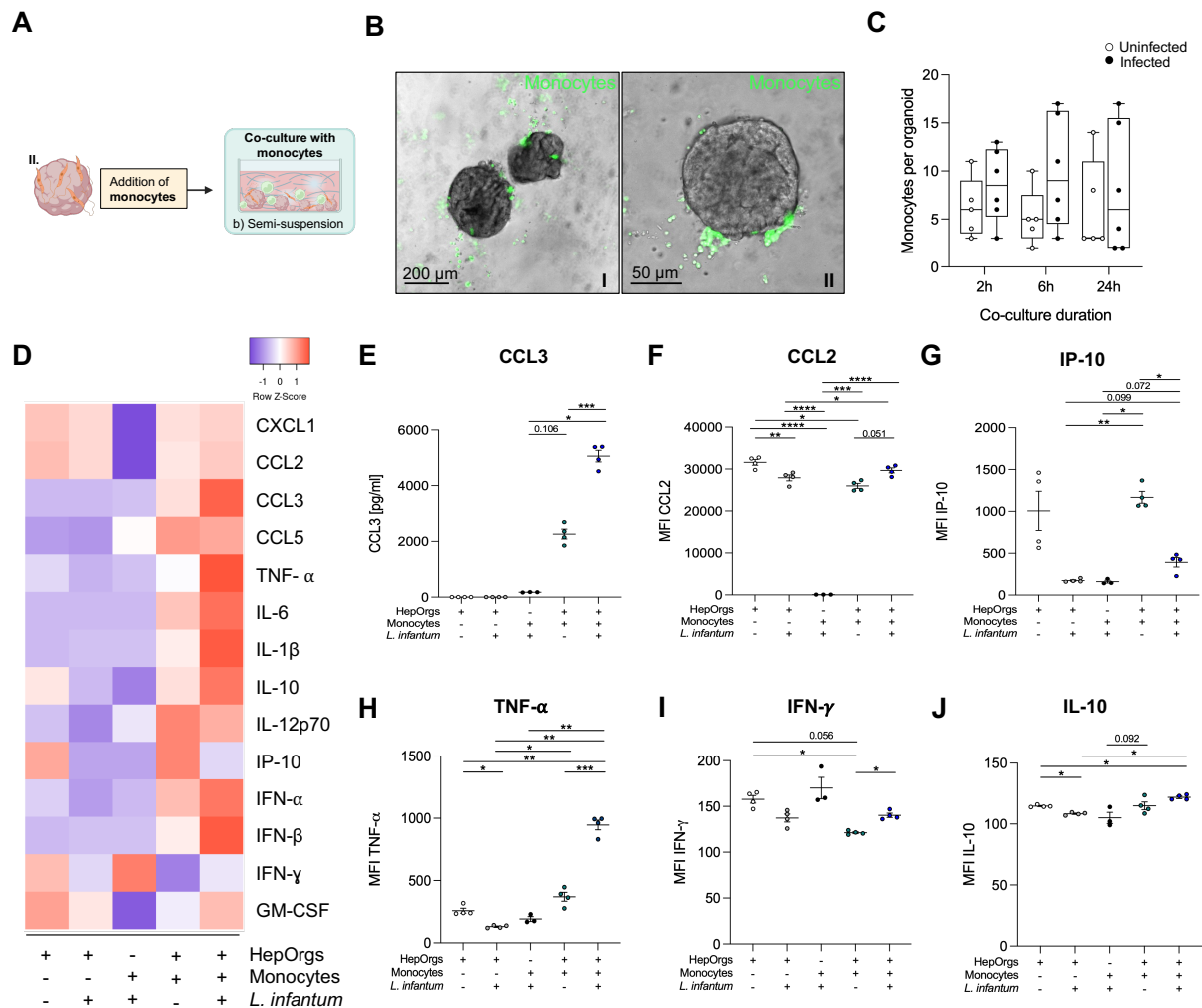


Figure 21: Co-culture of *L. infantum*-infected hepatocyte organoids with monocytes in semi-suspension.

CMFDA stained monocytes were added to *L. infantum*-infected HepOrgs, taken up in liquid medium + 10 % BME and co-cultivated for 24 h at a ratio of 1 to 3 (hepatocyte to monocytes). (A) Schematic representation of the co-culture in semi-suspension. (B) Phase contrast microscopy images of co-cultures of HepOrgs and monocytes after 24 h incubation, in different magnifications (I, II). CMFDA stained monocytes are depicted in green. Images were acquired using EVOS® FL Auto Fluorescence microscope. (C) Quantification of the number of monocytes per organoid at different time points after co-culture initiation. The data was collected using microscopic images (representative shown in B) of $n = 5-6$ HepOrgs from one individual. Evaluation was performed in FIJI. The data is presented as boxplot. (D-J) Cytokines were detected in culture supernatants by ELISA (CCL3) and multiplex immunoassay (LEGENDplex™). The data was generated within a single experiment with $n = 3-4$ technical replicates. (D) Heatmap: the relative amounts of cytokines are given as row z-score of the indicated co-culture conditions. Purple indicates low levels of the cytokine, whereas red indicates high levels. (E-J) Graphs depict MFI or concentration (CCL3) of the identified cytokines. The data is presented as mean \pm SEM. P-values were calculated using one-way repeated measures ANOVA (* $p < 0.05$; ** $p < 0.01$; *** $p < 0.001$; **** $p < 0.0001$).

Upon closer examination of specific cytokines (Figure 21 E-J), a significant infection-dependent increase in CCL3 (Figure 21 E, $***p < 0.001$), TNF (Figure 21 H, $***p < 0.001$) and IFN- γ (Figure 21 I, $*p < 0.05$) levels was observed in the supernatants of HepOrgs co-cultured with monocytes. A similar trend was shown for CCL2 and IL-10, although not statistically significant. Conversely, IP-10 levels exhibited a significant decrease in monocyte co-cultures following HepOrg infection (Figure 21 G, $*p < 0.05$). Interestingly, all mentioned cytokines evidenced a tendency to decrease upon infection, in supernatants of HepOrgs without added monocytes, with statistical significance reached for CCL2, TNF and IL-10 ($*p < 0.05$). CCL3 was only detected in culture supernatants containing monocytes. Except for IFN- γ , the levels of these cytokines were higher when organoids were co-cultured with monocytes compared to monocytes solely cultured with *Leishmania* parasites.

In summary, co-culturing monocytes and HepOrgs in a semi-suspension with 10 % added BME resulted in heightened aggregation of monocytes in close proximity to organoids after *L. infantum* infection, compared to uninfected controls. Furthermore, cytokine profiling revealed a significant infection-dependent increase in CCL3, TNF and IFN- γ levels in the culture supernatants of HepOrgs co-cultured with monocytes, as well as a significant decrease in IP-10.

3.4.3 c) Co-culture of monocytes and infected organoids in suspension

In the final approach, monocytes and *L. infantum*-infected HepOrgs were co-cultured in suspension (Figure 22 A). Therefore, the isolated and CMFDA-stained monocytes were added to the HepOrgs and co-cultured in standard organoid Hep medium for 24 h. Within this experimental setup, the potential recruitment of monocytes was not assessed. It was observed that monocytes tended to adhere to the culture vessel, while the organoids displayed mobility within the well plate, during co-culture handling (Figure 22 B). Consequently, conducting further analysis under these conditions could have led to misleading outcomes. Thus, only cytokine profiling was employed to evaluate the interaction between monocytes, HepOrgs and parasites.

Based on the heatmap shown in Figure 22 C, a clear picture of the cytokine profiles across the different conditions emerged, according to which the assessed cytokines CXCL1, CCL2, CCL3, TNF- α , IL-6, IL-1b, IL-10, IL-12p70, IFN- α , IFN- β , IFN- γ and GM-CSF exhibited elevated levels in co-cultures of monocytes and HepOrgs following *L. infantum* infection. Conversely, CCL5 and IP-10 evidenced higher levels in corresponding uninfected controls. The expression of these cytokines appeared lower in all the other analyzed conditions.

With regard to the cytokines illustrated in Figure 22 D-I, a significant infection-dependent difference was observed in the levels of CCL3, CCL2, IL-10 ($*p < 0.05$), TNF ($****p < 0.0001$), IFN- γ and IP-10 ($**p < 0.01$) after co-culture of monocytes and HepOrgs. Here, IP-10 cytokine levels were lower upon infection, while the other cytokines demonstrated an increase. Notably, the y-axis range for CCL3, CCL2, IP-10 and TNF underlines the prominent differences between the analyzed conditions. In the supernatants of uninfected and infected HepOrgs without added monocytes no infection-dependent differences were detected. Additionally, cytokine levels of monocytes co-cultured with *L. infantum* parasites were significantly lower for CCL3, IL-10 ($*p < 0.05$), CCL2 ($**p < 0.01$), TNF ($****p < 0.0001$) and tended to be lower for IP-10 and IFN- γ compared to co-cultures also containing HepOrgs.

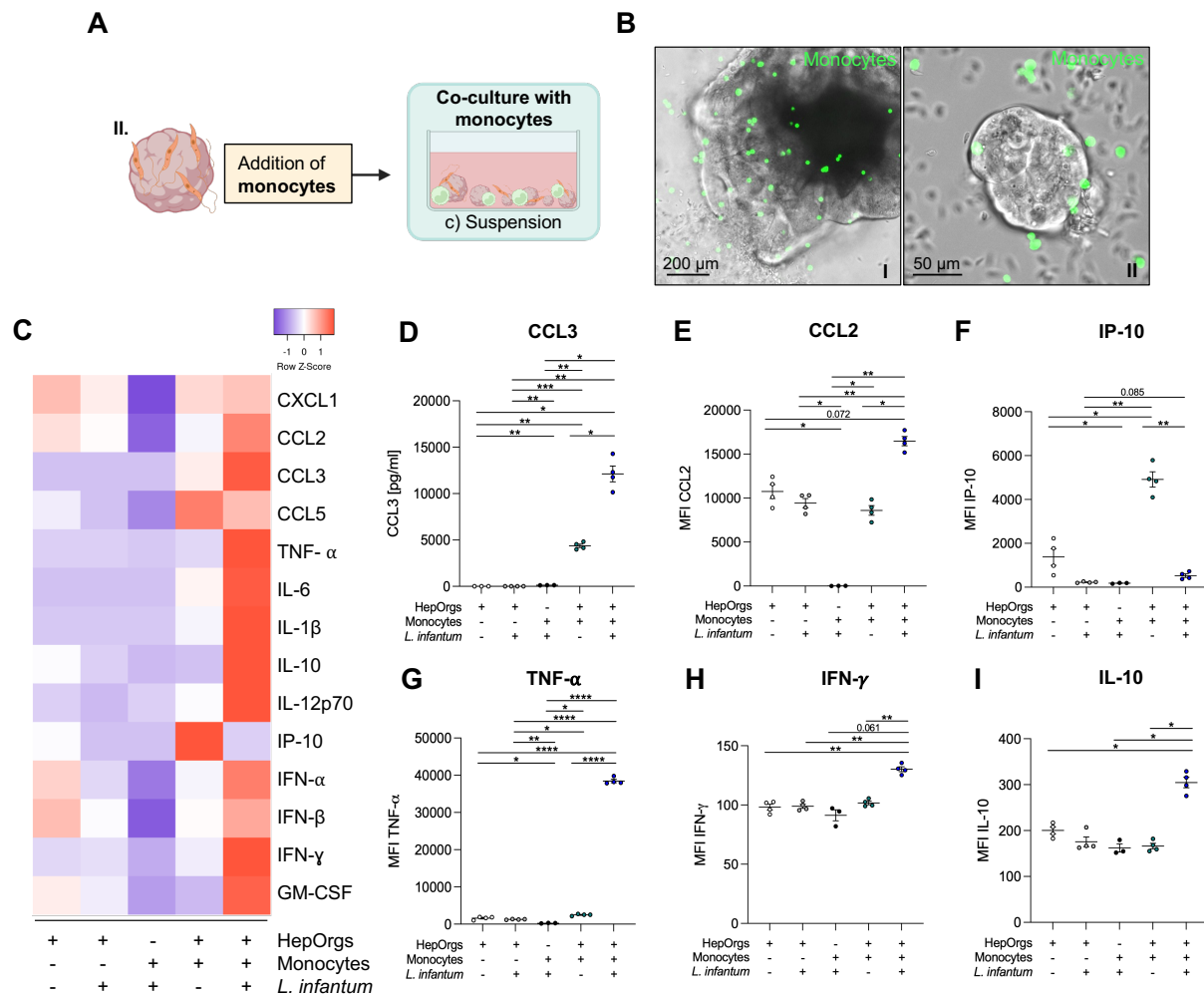


Figure 22: Co-culture of *L. infantum*-infected hepatocyte organoids with monocytes in suspension.

CMFDA stained monocytes were added to *L. infantum*-infected HepOrgs, taken up in liquid medium and co-cultivated in suspension for 24 h at a ratio of 1 to 3 (hepatocyte to monocytes). (A) Schematic representation of co-culture in suspension. (B) Phase contrast microscopy images of co-cultures of HepOrgs and monocytes after 24 h incubation, in different magnifications (I, II). CMFDA stained monocytes are depicted in green. Images were acquired using EVOS® FL Auto Fluorescence microscope. (C-I) Cytokines were detected in culture supernatants by ELISA (CCL3) and multiplex immunoassay (LEGENDplex™). The data was generated within a single experiment with $n = 3-4$ technical replicates. (C) Heatmap: the relative amounts of cytokines are given as row z-score of the indicated co-culture conditions. Purple indicates low levels of the cytokine, whereas red indicates high levels. (E-I) Graphs depict MFI or concentration (CCL3) of the identified cytokines. The data is presented as mean \pm SEM. P-values were calculated using one-way repeated measures ANOVA (* $p < 0.05$; ** $p < 0.01$; *** $p < 0.001$; **** $p < 0.0001$).

Overall, significant *L. infantum* infection-dependent differences were identified in the cytokine levels of HepOrgs co-cultured with monocytes, utilizing the suspension co-culture approach. Consequently, RNA extracted from this approach was subjected to quantitative RT-PCR analysis, to further investigate the expression of specific genes of interest at the transcript level.

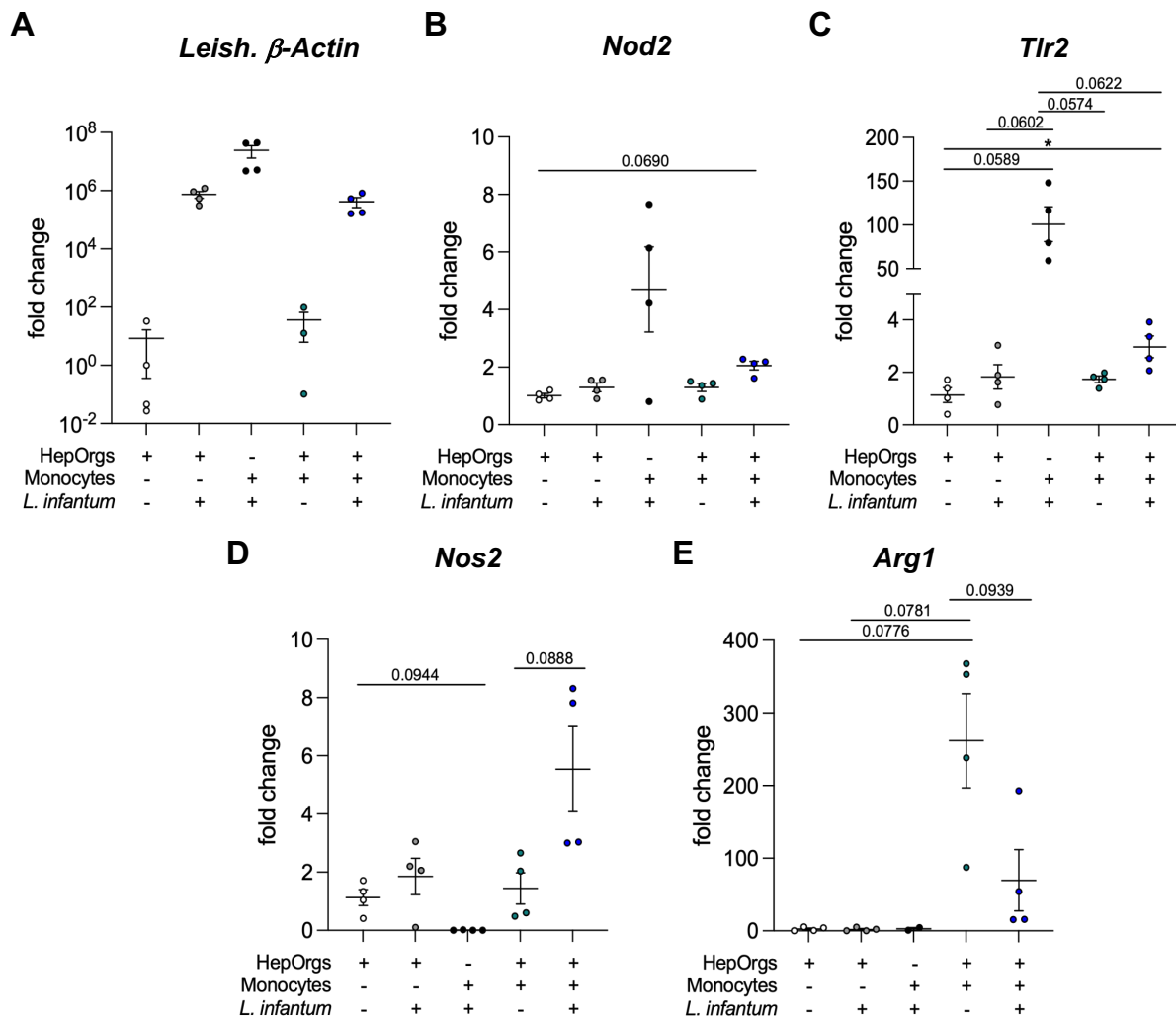


Figure 23: qPCR of genes of interest using suspension co-culture RNA samples.

CMFDA stained monocytes were added to *L. infantum*-infected HepOrgs, taken up in liquid medium and co-cultivated in suspension for 24 h at a ratio of 1 to 3 (hepatocyte to monocytes). RNA was isolated from the co-cultured cells. *Leishmania β -Actin* (A), *Nod2* (B), *Tlr2* (C), *Nos2* (D) and *Arg1* (E) transcripts were detected via RT-qPCR. Uninfected HepOrgs served as calibrators in the calculation of fold changes. *Rps9* was used as housekeeping gene. The data was generated within a single experiment with $n = 3-4$ technical replicates and is presented as mean \pm SEM. P-values were calculated using one-way repeated measures ANOVA (* $p < 0.05$).

Quantification of *Leishmania*-specific *β -Actin* enabled a distinct differentiation between uninfected and infected samples, with the presence of parasites detectable based on transcript levels of *β -Actin* (Figure 23 A). In addition, the expression levels of the PRRs *Tlr2* and *Nucleotide oligomerization domain 2 (Nod2)* (Figure 23 B+C) were quantified, as the expression of both is known to be influenced by *Leishmania* infection in monocytes or hepatocytes [127,128]. The expression of either receptor appeared to increase upon infection, observed in both HepOrgs and co-cultures of HepOrgs and monocytes. Notably, this tendency was more pronounced in *Tlr2* expression but could not be evaluated as statistically significant for either receptor. Overall, the expression of *Nod2* and *Tlr2* was higher in monocytes solely co-cultured with parasites, compared to the co-culture conditions also involving HepOrgs. Again, this trend was particularly prominent in *Tlr2* expression. Potential induction of iNOS expression was analyzed via *Nitric oxide synthase 2 (Nos2)* transcript levels. The expression exhibited a marked increase in co-cultures of HepOrgs and monocytes upon infection with *L.*

infantum, compared to respective uninfected controls and all other examined co-culture conditions (Figure 23 D). Finally, *arginase 1 (Arg1)* mRNA levels were quantified. A noticeable trend towards decreased transcript levels was observed in co-cultures of *L. infantum*-infected HepOrgs and monocytes compared to uninfected co-culture controls, while expression was considerably lower or non-existent in the other examined samples.

In summary, qPCR analysis revealed a trend towards infection-dependent increase of *Nod2*, *Tlr2* and *Nos2* transcripts in co-cultures of HepOrgs and monocytes. Conversely, *L. infantum* infection markedly decreased *Arg1* mRNA levels in corresponding co-cultures.

3.5 Co-culture of hepatocyte organoids with *L. infantum*-infected macrophages

In the preceding co-culture analysis, *L. infantum* infection was depicted through the exposure of HepOrgs to parasites followed by the introduction of uninfected monocytes. However, in the host not hepatocytes, but macrophages are the primary target cells for *Leishmania* parasites [79]. Thus, part III. of this project aimed to establish a model for co-culturing *L. infantum*-infected macrophages with uninfected HepOrgs. This way, the interactions of all three cell types should more accurately reflect hepatic *in vivo* dynamics during VL. For this purpose, two distinct co-culture approaches were employed and evaluated mainly based on their capacity to replicate previously assessed *in vivo* cytokine dynamics. In a first approach HepOrgs were dissociated into single cells, combined with *L. infantum*-infected macrophages and embedded into BME to form organoids, following previous protocols [121]. In parallel, HepOrgs were added into the growth medium of adherent infected macrophages and co-cultured in suspension (Figure 24 A).

To implement these co-culture techniques, initially a well-established protocol for the generation and infection of murine bone marrow-derived macrophages (BMDMs) was employed. Mouse bone marrow cells were isolated and differentiated into BMDMs for 10 days under the addition of M-CSF. Subsequently, these differentiated cells were subjected to infection with *L. infantum* parasites for 24 h. The resulting infected macrophages were then utilized for the above-mentioned co-cultures, while complementary approaches were employed to assess infection parameters. Quantification of infection was achieved through high content screening, which was performed following fixation and immunofluorescence staining of the infected macrophages (Figure 24 B).

Figure 24 C displays representative fluorescence images of *L. infantum*-infected macrophages, which served as input for quantifying infection parameters. Across the samples, the presence of parasites within the macrophages varied. Quantitative analysis revealed an average infection rate of 65 % in macrophages (Figure 24 D), with a median of 7.5 parasites per macrophage (Figure 24 E). As expected, these results were significantly different from uninfected controls.

In summary, macrophages were generated and subsequently infected with *L. infantum* parasites, followed by co-cultivation with HepOrgs. Quantitative analysis of infection parameters unveiled an average infection rate of 65 % with a median of 7.5 parasites per infected macrophage.

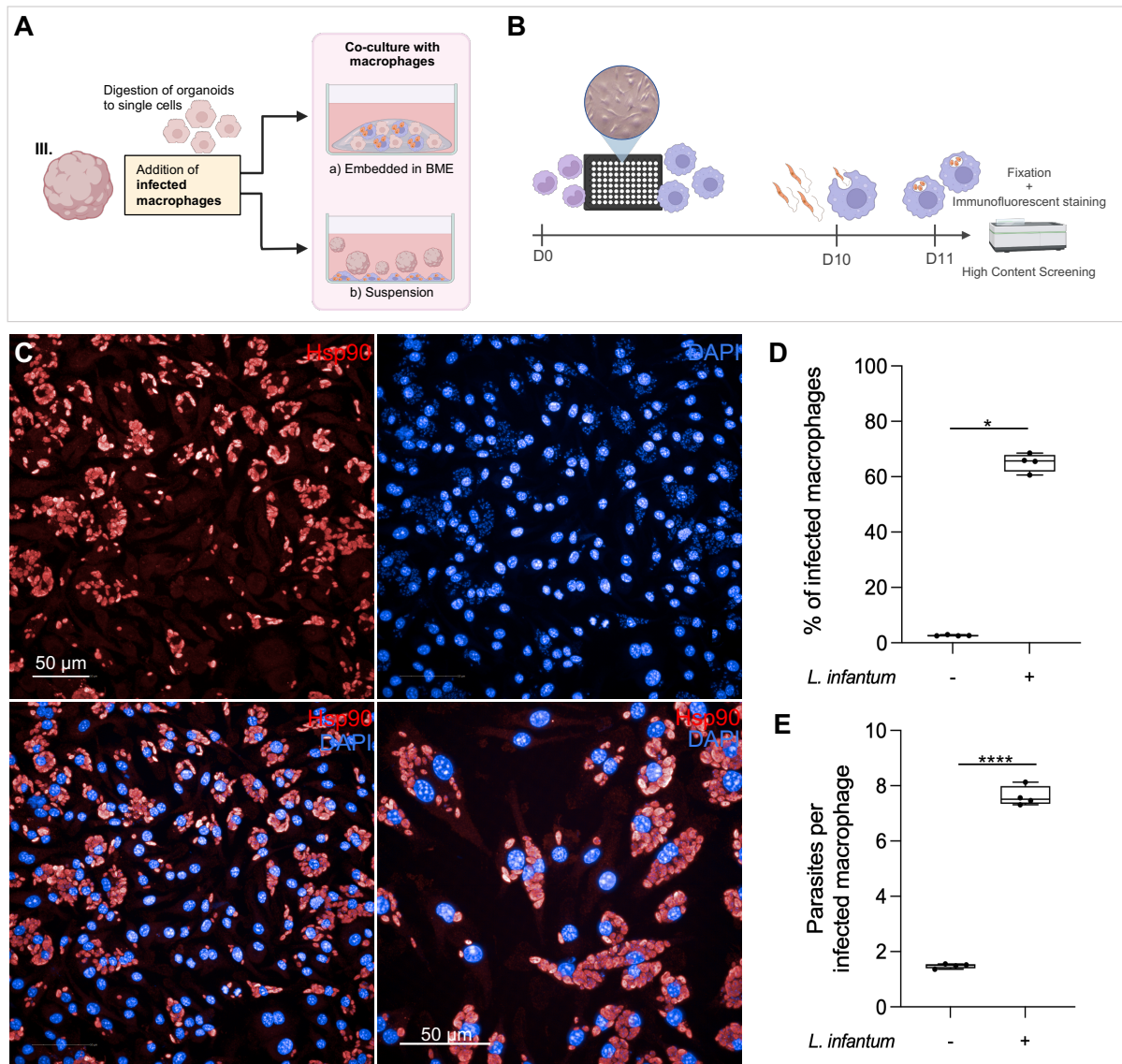


Figure 24: Co-culture setup of macrophages and hepatocyte organoids and evaluation of the infection of murine macrophages with *L. infantum* parasites.

(A) Schematic representation of the co-culture approaches of *L. infantum*-infected macrophages and HepOrgs. (B) Schematic depiction of the generation and infection of bone marrow derived macrophages (BMDMs): Cells were isolated from mouse bone marrow and differentiated into BMDMs for 10 days under the addition of M-CSF. BMDMs were infected with *L. infantum* metacyclic promastigotes at an MOI of 20:1 (20 parasites per macrophage) for 24 h, fixed and immunofluorescence stained for Hsp90 and DAPI. Immunofluorescence images were acquired by high content screening using the Opera Phenix™ system and analysed by Harmony 4.5 software from PerkinElmer. The output values were generated by applying a previously established algorithm. (C) Representative input images of *L. infantum*-infected BMDMs showing Hsp90 (red) and DAPI (blue) channels, plus overlay of Hsp90 and DAPI at different magnifications. (D, E) Quantification of the percentage of infected macrophages (D) and parasites per infected macrophage (E). The data is presented as boxplots of $n = 4$ technical replicates within a single experiment. P-values were generated using Unpaired Students t-test (* $p < 0.05$; **** $p < 0.0001$)

3.5.1 Co-culture of dissociated hepatocyte organoids and *L. infantum*-infected macrophages

In the initial macrophage co-culture strategy, single cell hepatocytes were embedded in BME along with infected macrophages. This experimental setup was chosen to discern whether macrophages were integrated into, or established direct contacts with, newly formed HepOrgs. Additionally, it was investigated whether the infection status of the macrophages influenced the interaction with HepOrgs and if the overall response to infection mirrored that observed *in vivo* during hepatic leishmaniasis. Therefore, organoids were dissociated into single cells, combined with *L. infantum*-infected macrophages and co-cultured for a duration of 8 days following embedding in BME. Medium was exchanged every 2 days, with supernatants collected for cytokine profiling. After 4 and 8 days of co-culture, the co-cultured BMDMs and HepOrgs were fixed and immunofluorescence-stained targeting Hsp90 and macrophage-specific F4/80 and subjected to confocal microscopy analysis. Additionally, cultures were processed for gDNA isolation to quantify *Leishmania* parasites via β -Actin qPCR. Control groups consisted of cultures lacking added macrophages, as well as those with the addition of uninfected macrophages (Figure 25 A).

The progression of the co-culture was monitored and recorded microscopically. Representative images depicting the three distinct conditions at days 4 and 8 after co-culture initiation are shown in Figure 25 B-D. When digested organoids were re-embedded in BME and cultured alone (Figure 25 B), organoids formed again within the first two days of culture. Shape and size of the organoids remained comparable to those of the original culture over the observed culture duration, along with the formation of CholOrgs. Upon addition of BMDMs to the digested organoids, reassembly of the latter appeared comparable to the controls lacking macrophages. However, macrophages were distinctly identified within the BME scaffold on the basis of their branched morphology. Notably, BMDMs were observed as individual cells dispersed within the BME, as well as accumulated in close proximity to newly forming organoids (Figure 25 B, C; Day 4). By day 8 of co-culture, macrophage morphology was less prominent and evidenced a more spherical appearance within the BME dome, although some cells at the bottom of the culture vessel retained characteristic branched morphology. Overall, no discernible morphological differences were observed upon microscopic evaluation of co-cultures comprising either uninfected or infected macrophages with HepOrgs.

Confocal microscopy was utilized to assess the expression of macrophage specific F4/80 and Hsp90, thereby facilitating the evaluation of macrophage and *L. infantum* survival in the co-culture system. As visualized in Figure 26 A-C, macrophages were identified through the expression of F4/80 after both 4 and 8 days of co-culture. Notably, macrophages were observed establishing direct contacts with HepOrgs, while also occurring as individual cells independent of HepOrgs (Figure 26 C). Interestingly, macrophages were found to be in close proximity to the outer layer of HepOrgs, although no evidence of their incorporation into the organoids was discerned. The detection of Hsp90 signal within infected macrophages after 4 days of co-culture, indicated the presence of parasites. However, the number of detected parasites was relatively low, especially when compared to HCS infection imaging. No parasites were detected outside of the macrophages after 4 days and their presence could not be demonstrated after 8 days of co-culture. Additionally, a significant reduction in β -Actin transcripts was shown by gDNA quantification after 8 days as compared to 4 days samples, suggesting a decrease in parasite load (Figure 26 E, * $p < 0.05$).

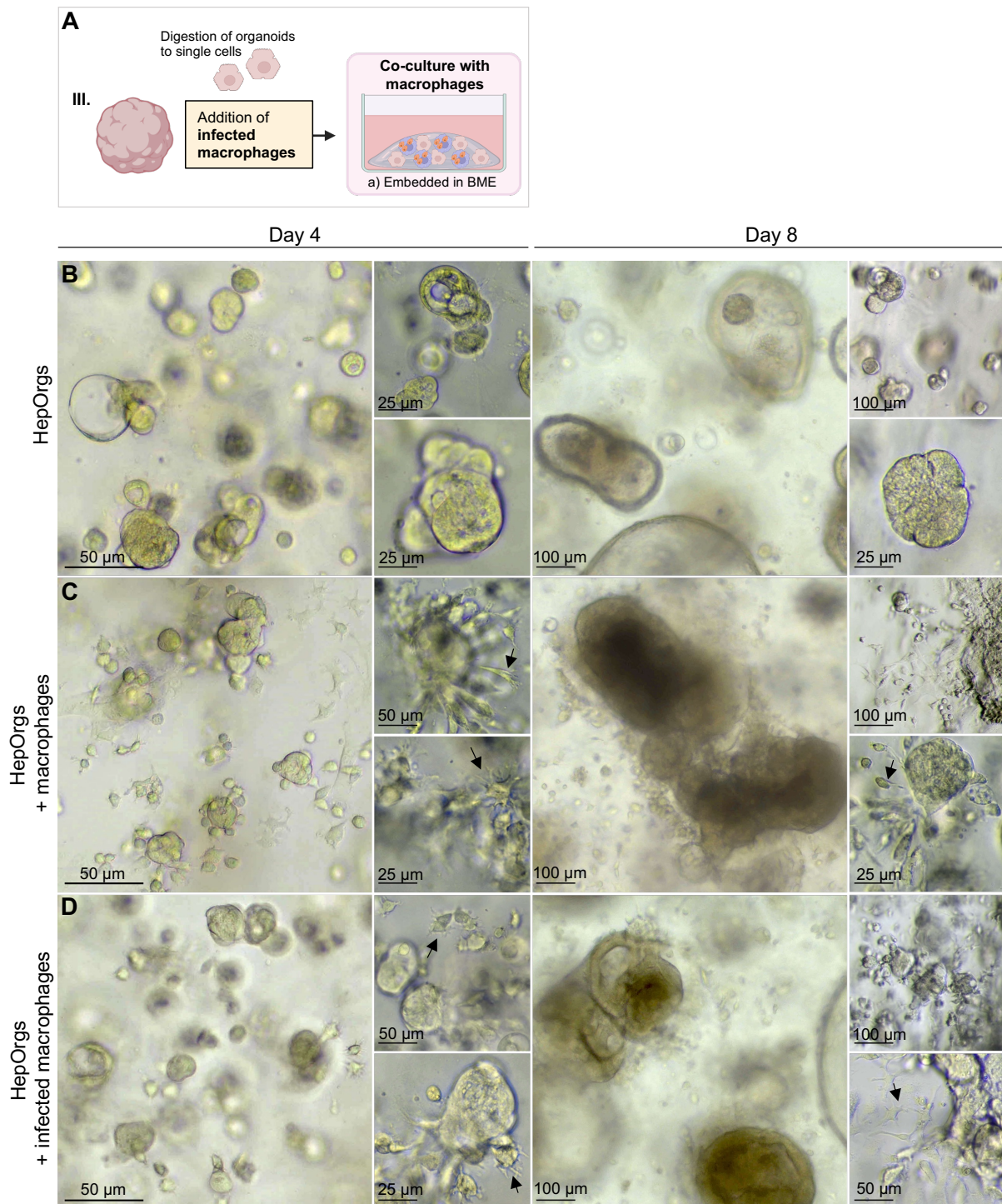


Figure 25: Microscopic monitoring of the co-cultivation of dissociated organoids and macrophages.

(A) Schematic representation of the co-culture of infected BMDMs with dissociated HepOrgs. (B-D) Dissociated HepOrgs were embedded in BME either individually (A) or in combination with uninfected (B) or *L. infantum*-infected (MOI 20:1) BMDMs (C) at a ratio of 2 to 1 (hepatocytes to BMDM). Shown are representative light microscopy images acquired after 4 and 8 days, at different magnifications. Arrows indicate branched macrophages. Images were acquired using Nikon ECLIPSE Ts2 Inverted Routine Microscope.

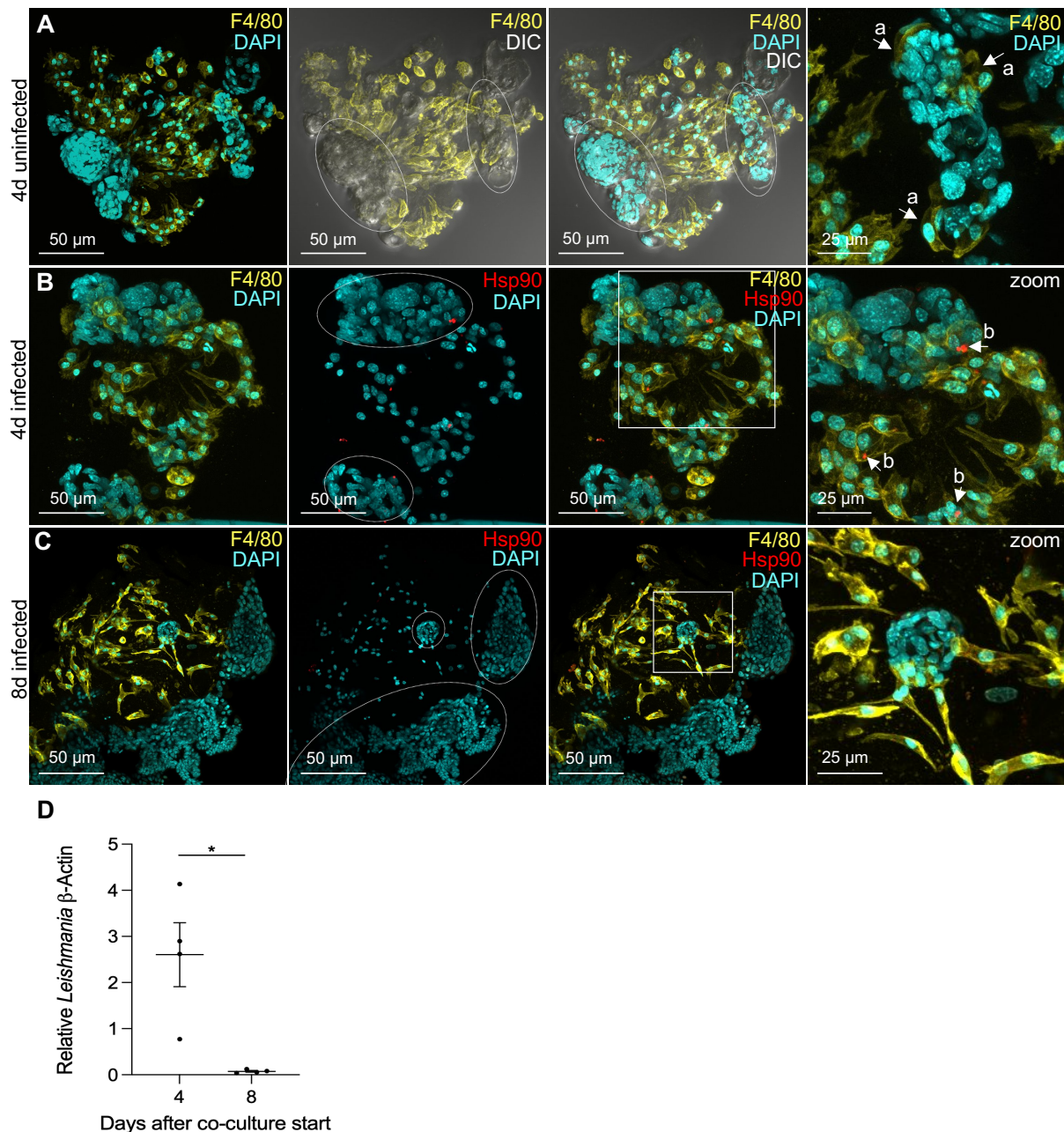


Figure 26: Immunofluorescence analysis of the co-culture comprising dissociated organoids and macrophages, and *Leishmania* β -Actin quantification.

HepOrgs and BMDMs were collected after 4 and 8 days of co-cultivation, fixed, immunofluorescence-stained or processed for gDNA isolation. (A-C) Confocal z-stack images of HepOrgs and BMDMs showing F4/80 (yellow, macrophages), Hsp90 (red, *Leishmania*) and DAPI (blue) channels as indicated overlays, plus overlay with DIC (A). HepOrgs are highlighted in dashed circles. Depicted are images of HepOrgs and uninfected (A) or infected BMDMs after 4 (B) and 8 days (C) of co-culture at different magnifications. Arrows indicate direct contacts of HepOrgs and BMDMs (a) and *L. infantum* parasites (b). (D) Quantification of the relative amount of *Leishmania* β -Actin gDNA via qPCR, after 4 and 8 days of co-cultivation. Depicted is the mean \pm SEM of n = 4 independent experiments. P-value was calculated using Paired Student's t-test (*p < 0.05).

Lastly, cytokine profiling was performed to analyse the infection-dependent interaction between macrophages and HepOrgs. Here, cytokines were measured in the co-culture supernatants taken every two days and are represented over time as well as area under the curve (AUC) (Figure 27). A multiplex assay focusing on cytokines associated with a response

against virus infection, precisely IFN- γ , CXCL1, TNF, CCL2, IL-12p70, CCL5, IL-1 β , IP-10, GM-CSF, IL-10, IFN- β , IFN- α , IL-6, as well as an ELISA for CCL3 detection were utilized. The depicted results exclusively represent data for CCL3, CCL2, IP-10, TNF, IFN- γ and IL-10.

CCL3 was only detected in co-culture supernatants following the addition of BMDMs. Notably, a prominent infection-dependent difference in cytokine concentration was observed after 2 and 4 days, whereas levels remained independent of BMDM infection status at later timepoints. Interestingly, CCL3 concentration appeared consistent in co-cultures of uninfected BMDMs and HepOrgs throughout the entire observation period. AUC quantification verified a tendency towards higher CCL3 levels following the addition of *L. infantum*-infected BMDMs compared to uninfected counterparts, although not statistically significant (Figure 27 A). In terms of CCL2 levels, representation over time as well as AUC quantification demonstrated a significant increase in CCL2 levels upon the inclusion of uninfected (* $p < 0.05$) or infected (** $p < 0.01$) BMDMs compared to solely cultured HepOrgs. While a trend towards higher CCL2 levels in supernatants of co-cultured infected BMDMs was identified, it was not strongly pronounced (Figure 27 B). IP-10 levels appeared higher in co-cultures of uninfected BMDMs with HepOrgs, compared to infected BMDMs after 2 and 4 days of culture, whereas levels were comparable after 6 and 8 days. Overall, expression was significantly elevated upon the addition of uninfected BMDMs compared to solely cultured HepOrgs (* $p < 0.05$), while a trend towards increased expression was identified when compared to infected BMDMs (Figure 27 C). TNF- α levels were significantly elevated upon the addition of uninfected BMDMs compared to solely cultured HepOrgs (* $p < 0.05$), while a trend towards increased expression was identified when compared to infected BMDMs (Figure 27 D). IFN- γ levels were significantly elevated upon the addition of uninfected BMDMs compared to solely cultured HepOrgs (* $p < 0.05$), while a trend towards increased expression was identified when compared to infected BMDMs (Figure 27 E). IL-10 levels were significantly elevated upon the addition of uninfected BMDMs compared to solely cultured HepOrgs (* $p < 0.05$), while a trend towards increased expression was identified when compared to infected BMDMs (Figure 27 F).

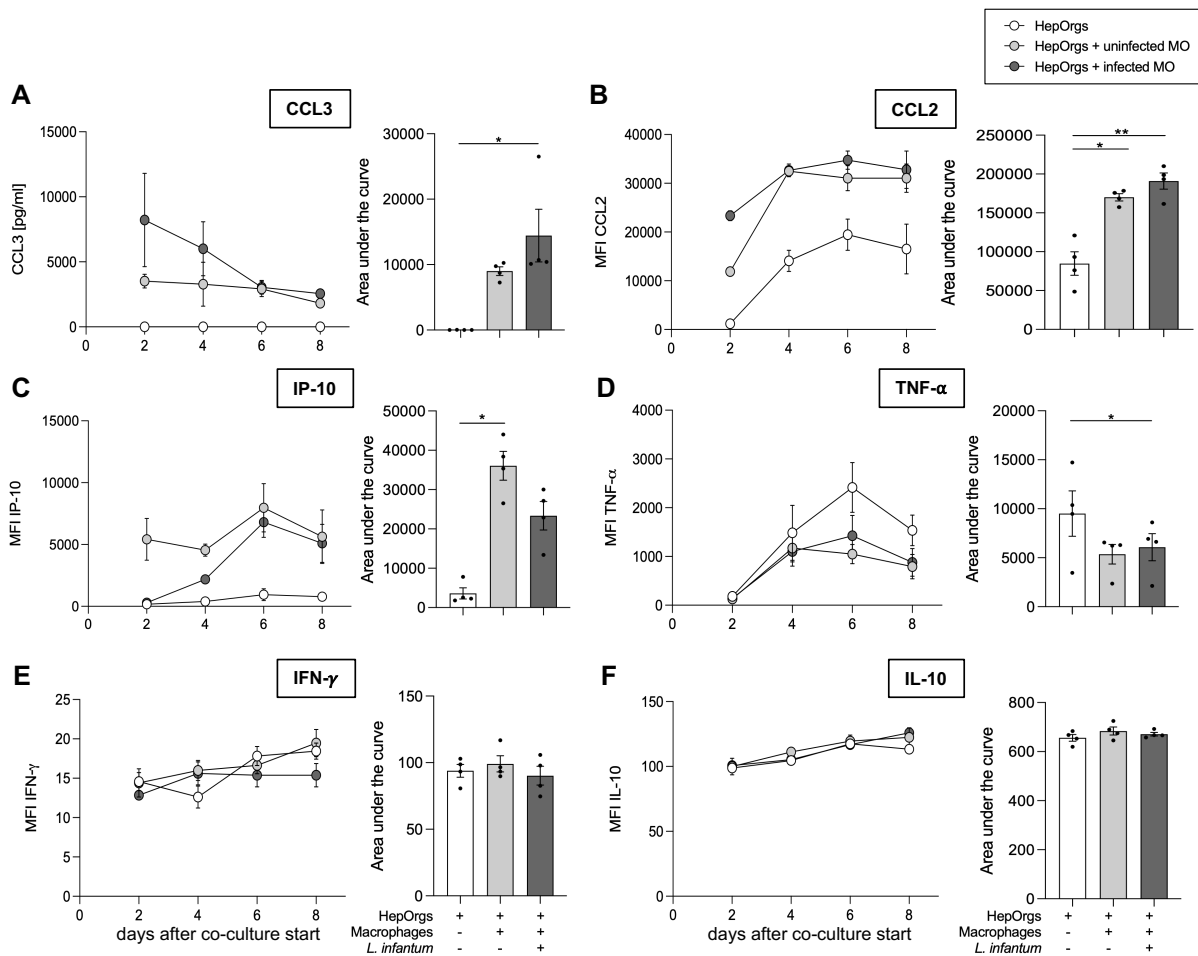


Figure 27: Assessment of cytokine levels in the culture supernatants of co-cultures comprising dissociated organoids and macrophages.

Dissociated HepOrgs and uninfected or infected (MOI 20:1) BMDMs were cultured for a total of 8 days at a ratio of 2 to 1 (hepatocytes to BMDM). Culture supernatants were collected every 2 days and replaced with fresh medium. Cytokines were detected by ELISA (CCL3) and multiplex immunoassay

(LEGENDplex™). Graphs show MFI or concentration (CCL3) of the indicated cytokines over the time course of the co-culture and as area under the curve. The data is presented as mean \pm SEM of $n = 4$ individual experiments. P-values were calculated using one-way repeated measures ANOVA (* $p < 0.05$; ** $p < 0.01$).

TNF levels evidenced a tendency towards higher levels in cultures comprising solely HepOrgs after 6 and 8 days, as opposed to co-cultures with uninfected or infected BMDMs. Notably, no substantial difference in TNF levels was observed between co-cultures of uninfected or infected BMDMs. AUC quantification confirmed a trend towards elevated TNF levels in solely cultured HepOrgs when compared to co-cultures with uninfected HepOrgs, as well as a significant difference when compared to infected BMDMs (Figure 27 D, * $p < 0.05$). Regarding both IFN- γ and IL-10, an increase in cytokine levels was observed over time across all culture conditions. However, analysis revealed no prominent differences between the various culture conditions either over time or summarized in AUC.

In summary, the co-cultivation of dissociated HepOrgs with both uninfected or *L. infantum*-infected BMDMs revealed the establishment of direct contacts between newly forming HepOrgs and BMDMs, as observed through microscopy. Furthermore, parasite presence was confirmed in co-cultures after 4 days but not after 8 days, as indicated by confocal microscopy and gDNA quantification. Lastly, cytokine profiling evidenced infection-dependent differences in cytokine levels. Specifically, a trend towards elevated levels following the addition of infected BMDMs was observed for CCL3 and CCL2, while IP-10 levels appeared lower compared to uninfected controls.

3.5.2 Co-culture of intact hepatocyte organoids with *L. infantum*-infected macrophages

The second macrophage co-culture approach was employed to assess the interaction between hepatocytes and BMDMs during macrophage infection, as well as to identify the differences in cytokine dynamics upon addition of HepOrgs to both uninfected and infected macrophages. Initially, bone marrow cells were harvested from mice, differentiated into BMDMs and subsequently infected with *L. infantum* parasites. HepOrgs, cultivated from four distinct individuals, were added to the adherent infected macrophages and maintained in suspension for 24 h. Comparative analysis included uninfected and infected BMDMs without HepOrgs, solely HepOrgs and HepOrg co-cultures with uninfected BMDMs as controls. To assess cytokine expression, the supernatants from these co-cultures were subjected to cytokine profiling through a multiplex immunoassay that targeted cytokines associated with M1 macrophages and an ELISA for the detection of CCL3 (Figure 28 A).

The application of the co-culture approach is illustrated in Figure 28 B, where representative microscopic images are depicted. In these images, branched macrophages are observed adhering to the bottom of the culture vessel, while HepOrgs are situated on top of them within the growth medium. Consequently, the lower regions of the organoids are in direct contact with the BMDMs (Figure 28 B, III). Notably, no discernible morphological differences in macrophages were observed following either *L. infantum* infection or introduction of HepOrgs (data not shown).

A distinct cytokine profile is evident from the heatmap shown in Figure 28 C. Specifically, in macrophage cultures without HepOrgs, heightened levels of IL-23, IL-18 and IL-12p70 were observed, with notable infection-dependent variations. Conversely, the cytokines CCL3, IL-6, TNF, IL-12p40 and IL-1 β exhibited markedly elevated levels in co-cultures including both

macrophages and HepOrgs. Interestingly, the levels of CXCL1 appeared consistent across all conditions including HepOrgs.

Overall, the cytokine assessment revealed considerable variability among the individuals analyzed, resulting in less definitive cytokine profiles. For CCL3, IL-6 and IL-1 β average cytokine levels appeared higher in co-cultures of BMDMs and HepOrgs, while a tendency towards an infection-dependent decrease was observed in co-cultures including infected BMDMs. Although the data variance appeared especially substantial in co-cultures of infected BMDMs and HepOrgs. Conversely, levels of TNF and IL-12p40 seemed higher in co-cultures of *L. infantum*-infected macrophages and HepOrgs compared to those with uninfected macrophages. However, these differences could not be evaluated as statistically significant, whereas cytokine levels were significantly lower in uninfected or infected macrophages, or HepOrgs cultured alone, when compared to co-cultures of uninfected BMDMs and HepOrgs. Notably, CXCL1 levels remained consistent among all conditions containing HepOrgs, while markedly reduced levels were observed in solely cultured macrophages, irrespective of *L. infantum* infection status.

In summary, co-cultivation of adherent macrophages along with HepOrgs resulted in a prominent elevation in some of the analyzed cytokines. CCL3, IL-6 and IL-1 β levels exhibited a tendency towards reduction, while TNF and IL-12p40 levels appeared higher in co-cultures with *L. infantum*-infected macrophages compared to those with uninfected macrophages. However, none of these infection-dependent observations was evaluated as statistically significant.

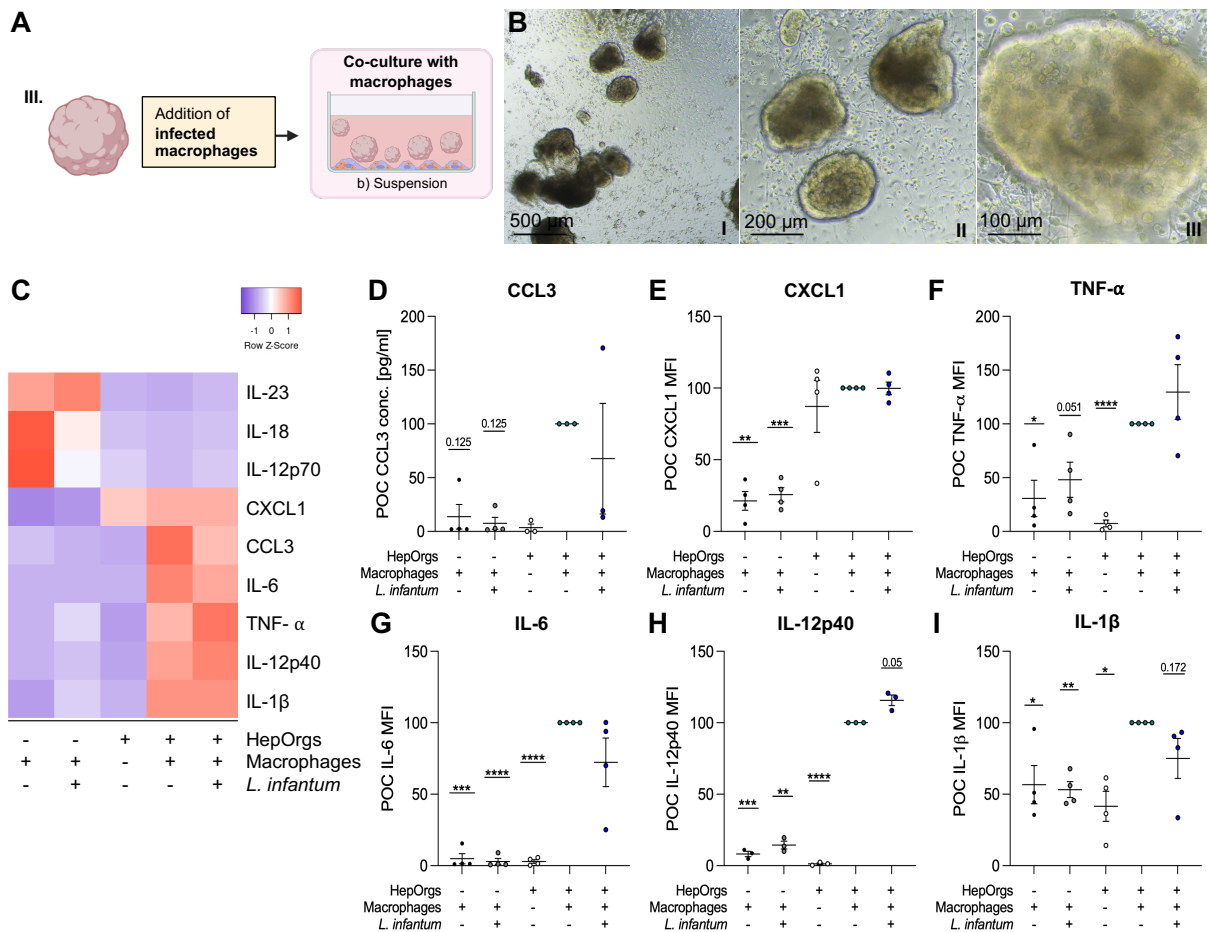


Figure 28: Co-culture of adherent macrophages with intact organoids.

BMDMs were infected with *L. infantum* metacyclic promastigotes at an MOI of 20:1 and incubated for 24 h. HepOrgs (cell count equivalent to 1×10^5 hepatocytes) were added in suspension, at a ratio of macrophages to hepatocyte of 3 to 1 and co-cultured for 24 h. (A) Schematic depiction of the applied co-culture methodology. (B) Representative light microscopy images of the co-culture at different magnifications. Images were acquired with a Nikon ECLIPSE Ts2 Inverted Routine Microscope. (C-I) The cytokine data was generated in $n = 3-4$ individual experiments. Cytokines were detected in culture supernatants by ELISA (CCL3) and multiplex immunoassay (LEGENDplex™). (C) Heatmap: the relative amounts of cytokines are given as row z-score of the indicated co-culture conditions. Purple indicates low levels of the cytokine, whereas red indicates high levels. (D-I) Graphs depict MFI or concentration (CCL3) of the detected cytokines. The data was normalized to the co-culture condition 'HepOrgs + Macrophages' per respective individual and is presented as mean \pm SEM. P-values were calculated using One sample t-test and refers to comparison with 'HepOrgs + Macrophages' (* $p < 0.05$; ** $p < 0.01$; *** $p < 0.001$; **** $p < 0.0001$).

3.6 Summary of the cytokine data obtained from the distinct co-culture approaches



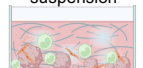



To offer a comprehensive overview of the results from the five distinct co-culture systems, Table 15 presents the infection-specific effects on key cytokines implicated in the immune response during hepatic VL. The trend of cytokine production following infection is depicted in comparison to the uninfected counterpart.

In comparison to experimental VL in murine models, the co-cultivation of *L. infantum*-infected HepOrgs with monocytes in suspension demonstrates the highest degree of correlation. Notably, this approach exhibits a significant infection-dependent elevation in cytokine levels, including CCL3, CCL2, TNF, IFN- γ and IL-10. In the very similar semi-suspension approach, comparable trends were observed for CCL3, CCL2, TNF and IFN- γ , albeit less pronounced. Upon co-cultivation of *L. infantum*-infected macrophages and dissociated HepOrgs embedded in BME, only an elevation in chemokines CCL3 and CCL2 aligns with findings from murine models, although without statistical significance. In contrast, the remaining two approaches involving co-cultures of *L. infantum*-infected HepOrgs with monocytes embedded in BME and *L. infantum*-infected macrophages with HepOrgs in suspension, fail to exhibit statistically significant trends corresponding to infection-specific effects on cytokine levels observed in the murine model.

Overall, the closest resemblance in cytokine dynamics to those observed in the animal model was found in the co-cultivation of infected HepOrgs with monocytes in suspension.

Table 15: Summary of co-culture cytokine data.

The arrows describe the increasing (up) or decreasing (down) effect of *L. infantum* infection on the indicated cytokine levels within the applied co-culture systems and in experimental mouse models, as compared to the uninfected control. P-values are specified as numbers (n.e. = no effect of infection; n.d. = not determined).

	Mouse model 	Monocytes in BME 	Monocytes in semi-suspension 	Monocytes in suspension 	Infected BMDMs in BME 	Infected BMDMs in suspension 
CCL3	↑	n.e.	↑ 0.0010	↑ 0.0191	↑ 0.2375	↓ 0.5112
CCL2	↑	n.e.	↑ 0.0511	↑ 0.0166	↑ 0.0007	n.d.
IP-10	↑	↓ 0.0379	↓ 0.0155	↓ 0.0065	↓ 0.0535	n.d.
TNF	↑	↓ 0.2875	↑ 0.0004	↑ <0.0001	n.e.	↑ 0.3285
IFN-γ	↑	n.e.	↑ 0.0232	↑ 0.0021	n.e.	n.d.
IL-10	↑	↓ 0.0521	n.e.	↑ 0.0149	n.e.	n.d.

4 Discussion

Leishmaniasis ranks among the top ten neglected tropical diseases, according to the WHO. It manifests in three distinct forms, with the visceral form displaying the most severe symptoms. The disease originates from arthropod-borne infections with protozoan parasites belonging to the *Leishmania* species [1–3]. Upon inoculation into the host, the parasites are phagocytosed primarily by macrophages in the skin. In the further course of visceral leishmaniasis manifestation, the parasites disseminate to visceral organs, including the spleen and liver [68–70]. Here, an effective immune response is characterized by T_H1-associated granuloma formation and parasite elimination [93]. However, there is some evidence suggesting that chemokine-mediated monocyte recruitment may contribute to disease progression and host susceptibility [96]. Although, the current literature lacks clarity regarding the role of monocyte recruitment in the progression of liver infection. Research into visceral leishmaniasis has revealed discrepancies between the infection course in humans and animal models. Although many processes observed in mice parallel those in humans, *Leishmania* liver infection in mice is self-resolving and asymptomatic, contrasting with the potentially lethal outcome in humans [29]. This discrepancy underscores the urgency for the development of novel research models, to study the underlying mechanisms of visceral leishmaniasis in humans.

Epithelial organoids have emerged as powerful tools to study tissue development and homeostasis, as well as disease mechanisms. In particular, 3D hepatocyte organoid culture has been shown to facilitate long-term cultivation and expansion of functional murine and human hepatocytes. Although these organoids only consist of a single cell type, the hepatocytes, they show a remarkable structural complexity [100,104]. However, HepOrgs lack components of vasculature and the immune system. To study the specific interactions of immune cells with epithelial organoids, such as HepOrgs, co-culture systems have to be developed [121].

In order to implement a novel model to study liver-specific immune responses during *Leishmania* infection, a co-culture system including HepOrgs, *L. infantum* parasites and monocytes / macrophages, the main target cells of the parasites, was established. A 3D murine and human hepatocyte organoid culture was initiated, following the protocols by Hu and colleagues [112]. Subsequently a protocol for infecting HepOrgs with *L. infantum* parasites was created and the underlying immunomodulatory responses of hepatocytes upon parasites exposure were evaluated by extensive cytokine and transcriptome analysis. Based on these findings, strategies for the co-cultivation of *L. infantum*-infected HepOrgs with monocytes, as well as for co-cultivating *L. infantum*-infected macrophages with HepOrgs were implemented. These innovative approaches enable the investigation of reciprocal interactions between hepatocytes and monocytes / macrophages during *Leishmania* infection, unraveling the complex dynamics of the immune response within the liver microenvironment.

4.1 Establishment of murine and human 3D hepatocyte organoids

The *in vitro* reproduction of the proliferative capacity of human hepatocytes, following partial hepatectomy (PHx) has posed a significant challenge for decades. However, through advances in the field of epithelial organoids, multiple scientists have successfully demonstrated proliferation of hepatocytes in 3D cell cultures. Hu, et al. published their protocol in 2018, demonstrating the long-term expansion of functional murine and human hepatocytes. Key to their approach was the administration of a specific combination of growth factors, such

as HGF and R-Spondin1 as well as the introduction of primary hepatocytes into an ECM-rich Hydrogel [112].

Using the specified protocol, a 3D culture of both murine and human hepatocytes was implemented. The growth of the murine HepOrgs was monitored and quantified during the initial culture phase (P0 – P2) (Figure 5). A significant increase in organoid diameter was observed during P0 and P1, with growth appearing to slow down upon reaching P2 and subsequent passages. Within these first 3 passages, HepOrgs reached a diameter of approximately 300 μm . According to the current literature, both murine and human HepOrgs can attain diameters of up to 400 μm during the initial culture phase and can be expanded for several months, although with a decreasing growth rate after 2–3 months [112]. This decline in growth rate in passages 2 and beyond may stem from reduced availability of nutrients and growth factors within the core of the HepOrgs. This underscores one of the major limitations of HepOrgs, the lack of vasculature and inadequate nutrient supply in the deeper tissue regions which may result in the formation of a necrotic core within the organoids. Regular passaging by mechanical fragmentation was employed to prevent necrotic core formation, rendering the organoid culture time-consuming and cost-intensive, particularly due to the high expense associated with ECM-rich hydrogels. In the framework of this study, HepOrgs were not cultured for longer than 2–3 months, whereby a reduction in growth was not observed. However, previous studies suggest an accelerated shortening of telomeres in liver organoids, paired with generally short telomeres in hepatocytes. This may explain why the expansion of HepOrgs is more restricted compared to other types of epithelial organoids [112,129,130].

Additionally, the emergence of cystic CholOrgs was observed in both human and murine HepOrg cultures. This observation has been documented in the available literature [112,131] and might be attributable to cholangiocyte contamination in the initial hepatocyte suspension. Furthermore, transdifferentiation of hepatocytes into cholangiocytes has been previously demonstrated *in vivo*, a process observed during bile duct regeneration following PHx or other forms of liver injury [132]. To avoid the spread of CholOrg contamination, manual removal of CholOrgs from the culture would be necessary [131]. However, this approach was not feasible within the scope of this study. Consequently, CholOrg contamination was tolerated, but should be considered when assessing the further results. Noteworthy, the morphology of the cultured HepOrgs closely resembled those depicted in available publications and presented as a grape-like dense cell cluster [131].

To assess the functional and structural characteristics of cultured murine and human HepOrgs, immunofluorescence staining was performed targeting albumin, ZO-1 and Ki67 (Figure 6 + Figure 7). Consistent with the literature, HepOrgs exhibited hepatocyte-specific albumin expression throughout the entire organoid structure, regardless of the duration of culture. Additionally, ZO-1 staining revealed the interconnectivity of hepatocytes, previously demonstrated by β -catenin staining. Here, the intricate structure of murine HepOrgs was further elucidated in a 3D context, presenting as a ‘bunch of grapes’ structure rather than a uniform spherical cell cluster. Ki67 expression was observed in both human and murine HepOrgs, confirming the proliferative capacity of the cultured organoids. Lastly, CYP3A4 expression was detected in murine HepOrgs. Notably, Hu *et al.* demonstrated in their publication, that HepOrgs expressed both albumin and CYP3A4 comparably to primary hepatocytes, thereby validating the functionality of hepatocytes in 3D HepOrgs [112].

4.2 Infection of hepatocyte organoids with *L. infantum* parasites

Alongside the spleen, the liver is the organ most profoundly impacted by visceral leishmaniasis. Although in contrast to the spleen, hepatic infection is in most cases self-containing, largely associated with T_H-dependent granuloma formation in experimental models of VL [88,92]. The exact immunological mechanisms that lead to the different outcomes of infection in the liver and spleen remain incompletely understood [87]. However, previous studies have predominantly focused on the immune cells involved, such as macrophages, monocytes, neutrophils, DCs and T-cells, while hepatocytes have been largely ignored. Given that hepatocytes constitute 70–85 % of the liver mass and are recognized for their pivotal role in immune homeostasis, they could substantially contribute to the immunological dynamics during visceral leishmaniasis in the liver [128]. Hence, a protocol for infecting murine and human HepOrgs with *L. infantum* parasites was established to investigate the immune responses mediated by hepatocytes upon *L. infantum* exposure. These responses were evaluated at both cytokine and transcriptomic level.

4.2.1 *L. infantum* parasites form direct contacts with HepOrgs following infection in suspension

In preparation for the following infection experiments, *L. infantum* parasites were initially cultured in the organoid-specific Hep medium, to assess its impact on parasite growth. As visualized in Figure 9 A, a prominent difference in parasite proliferation was detected after 48 h between cultivation in Hep medium and the conventional *Leishmania* medium M199+. This variance suggests a compromised reproductive potential upon culture in Hep medium. Consequently, for subsequent experiments, the infection period was limited to 24 h. It is noteworthy that all infection experiments were conducted with stationary phase parasites, thus further reproduction of parasites was not expected. However, a discernible adverse effect of the medium on the parasites was evident, raising the possibility that the choice of medium may have compromised parasite infectivity. A notable distinction between the two media compositions lies in the absence of serum in the organoid medium compared to the high serum content (20 % FBS) in the *Leishmania* medium. FBS supplementation is a common practice in *Leishmania* medium to promote proliferation and long-term culture of infective promastigotes [133].

To infect HepOrgs with *L. infantum* parasites, three distinct methods were tested to discern which facilitated direct interaction or potential infiltration of parasites into the HepOrgs (Figure 9 B-E). The promastigote parasites were either embedded in BME along with the HepOrgs (a), introduced into the supernatant of embedded HepOrgs (b) or cultured in suspension alongside the HepOrgs (c). Results indicated that parasite mobility was constrained by BME embedding and infiltration into BME droplets was only observed sporadically. Notably, direct contact between organoids and parasites was only demonstrated when both were co-cultured in suspension. During the *in vivo* infection, promastigote parasites are injected into the skin of the host, exposing them to the extracellular microenvironment and facilitating direct interactions with ECM components [134]. Promastigotes express metalloprotease gp63 on the surface of their plasma membrane, which aids the migration through the tissue from blood to target cell within the host [134,135]. Whereby the potential for parasite migration through the ECM-rich hydrogel could not be ruled out in advance. Nonetheless, significant differences in matrix composition and stiffness compared to the host's ECM might obstruct parasite migration. Elevated presence of Laminin I in the utilized BME, could lead to strong parasite adhesion to the matrix, hindering their movement, especially since promastigotes express a laminin binding protein (LBP) on their surface [134]. This correlation may provide insight into

the observed accumulation of parasites on the surface of BME droplets, when added to the supernatant of embedded HepOrgs. Consequently, both embedding approaches including parasites and HepOrgs, as well as HepOrgs alone, were not pursued further. In suspension, *L. infantum* parasites evidenced a prominent tropism towards HepOrgs, accumulating around them, suggesting direct interactions between both cell types. A similar phenomenon has been previously described in canine hepatocytes exposed to *L. infantum* parasites, where parasites exhibited a pronounced interaction with the cell membrane of hepatocytes [128]. Hence, this approach was considered suitable for further investigation of HepOrg infection. It is noteworthy that all described infection approaches have been previously applied in organoid infection studies with other pathogens, however infection of organoids embedded in ECM-rich hydrogels might be more applicable for modeling viral infections [136]. However, during suspension cultivation of the organoids, shedding of individual cells was noted, indicating potential compromise in organoid integrity in the absence of stabilizing scaffold. This could impact the responsiveness of individual cells and coordinated responses of the organoids as a whole.

4.2.2 *L. infantum* parasites infiltrate murine and human HepOrgs

To monitor potential infiltration of HepOrgs by parasites, fluorescent *L. infantum* transfectants were generated. A standard electroporation protocol was employed to introduce an mCherry expression facilitating vector, additionally conferring neomycin resistance, into the parasites. Despite selection under antibiotic pressure, only 30 % of the resulting parasites evidenced mCherry expression upon fluorescence microscopic evaluation (Figure 10). While this percentage may appear modest, similar efficiencies were reported in a previous study involving transfection of GFP constructs into *L. donovani* parasites [137]. When employing the transfected *L. infantum* parasites for infection experiments, it should be acknowledged that a significant proportion of the parasites may evade detection via fluorescence microscopy.

To evaluate the potential infiltration of HepOrgs by *L. infantum* parasites, mCherry transfectants were initially employed in the established infection protocol. Thus, transfectants were co-cultured in suspension with murine HepOrgs for 24 h. Subsequently, HepOrgs were immunofluorescence-stained targeting albumin and DAPI, followed by confocal microscopy analysis. As depicted in Figure 11 A-C, mCherry⁺ parasites were primarily localized at the outer edge of the HepOrgs, with some also observed within the organoids, albeit to a lesser extent, as evidenced by cross-sectional images at different z-levels. It should be considered that there could potentially be significantly more parasites surrounding and within the organoids that do not express mCherry and thus remain undetectable by fluorescence microscopy. Consequently, in a second approach, non-transfected *L. infantum* parasites were utilized in infection experiments with both murine and human HepOrgs, followed by immunofluorescence staining targeting Hsp90. Results for murine HepOrgs (Figure 11 D) reflected those obtained with mCherry-expressing transfectants, with the majority of parasites detected outside the HepOrgs, although some were also observed within the organoids. Here, the assumption was made that some parasites might have attached to remains of BME, instead of directly interacting with the hepatocyte membrane, hindering infiltration. The infection of human HepOrgs, depicted in Figure 13, appeared to exhibit a more pronounced infiltration by *L. infantum* parasites. However, due to high heterogeneity in HepOrg size and the associated number of parasites detected, quantification was not feasible. Moreover, quantification in relation to hepatocyte nuclei (stained with DAPI) count was challenging, due to hepatocyte polyploidy, implying that conclusions regarding the number of hepatocytes cannot be inferred solely from the count of cell nuclei [138]. From the acquired fluorescence microscopic images, it was inconclusive whether parasites within the HepOrgs had invaded hepatocytes or were

localized intercellularly. Nevertheless, previous findings have reported the presence of amastigote *L. donovani* parasites within hepatocytes in liver biopsies of VL patients, suggesting hepatocytes to be permissive to amastigote *Leishmania* parasites [139]. Additionally, primary hepatocytes from mice, rats, dogs and humans have been shown to be permissive to promastigote *Leishmania* parasites *in vitro*, albeit to a low degree [128,140]. Although parasites did not exhibit robust proliferation within hepatocytes, the possibility arises whether infected hepatocytes act as a parasite reservoir during latent infections [128]. Notably, in the indicated studies murine hepatocytes evidenced a higher infection rate compared to human hepatocytes, indicating that human hepatocytes may not inherently be more permissive to *Leishmania* infection, contrary to assumptions based on the more prominent infiltration of human HepOrgs. Based on the findings of the previous studies and the fluorescence microscopic images generated in this study, it is apparent that *L. infantum* parasites evidence a tropism towards both murine and human HepOrgs, establishing robust interactions primarily with the outer layer of hepatocytes within the HepOrgs. Moreover, there is evidence of partial invasion into the organoids, potentially even infiltration of individual hepatocytes. However, upon closer examination of the microscopic images, it can be assumed that only a fraction of the hepatocytes within the organoids are in direct contact with *L. infantum* parasites, whereby potential responses could also be limited to these hepatocytes.

4.2.3 Cytokine profiles of *L. infantum*-infected HepOrgs

To analyze the immunomodulatory effects of *L. infantum* exposure on murine HepOrgs and discern potential sex-specific differences in their response, cytokine levels were assessed in culture supernatants following infection. Utilizing a multiplex immunoassay, focusing on proinflammatory cytokines, GM-CSF, IL-1 β , IL-6, TNF and CCL2 were detected in culture supernatants (Figure 12 C). Interestingly, these cytokines evidenced higher levels in supernatants of female-derived HepOrgs, regardless of infection status. Noteworthy, considerable differences in cytokine levels were observed among supernatants of different individuals. Furthermore, IFN- γ was detected, with a tendency towards higher levels noted in supernatants of female-derived HepOrgs following *L. infantum* infection. The levels of the remaining analyzed cytokines, including IL-27, IL-23, IL12p70, IL-1 α , IL-10 and IFN- β , were similar to those of the negative control. This suggests that HepOrgs either did not secrete these cytokines or secreted them only to a minimal extent under the experimental conditions. Overall, no other infection-associated differences were discerned in the multiplex results. Consequently, the concentrations of the VL-associated cytokines IL-6, CCL2 and CXCL1 were further evaluated via ELISA (Figure 12 D-F), to quantify minor differences more accurately. Here, a decrease in IL-6 and CXCL1 levels was observed, while CCL2 levels remained unaffected by *L. infantum* exposure. Additionally, it was shown, that both CCL2 and CXCL1 concentrations were generally higher in supernatants of female-derived HepOrgs, whereas IL-6 concentration was higher in those of male-derived HepOrgs.

CXCL1 is known to be produced locally upon infection with *Leishmania* spp. and is associated with the recruitment of neutrophils and monocytes to the site of infection, an immune mechanism crucial for containing the infection. However, previous investigations involving *L. major* infections have revealed, that the parasites can directly degrade murine CXCL1 through specific metalloproteases, a potential way to evade host immune responses [141]. Although the expression of the corresponding metalloprotease has so far only been demonstrated for *L. major*, the current findings suggest that *L. infantum* may also employ CXCL1 degradation as a strategy for immune evasion. IL-6 decrease upon hepatocyte exposure to *L. infantum* was not confirmed by literature. Conversely, severity of visceral leishmaniasis in humans is associated

with elevated levels of IL-6 in the serum of patients, especially since systemic inflammation is a main driver of clinical manifestation of VL [142]. Additionally, Rodriguez *et al.* demonstrated an increase in IL-6 mRNA in canine hepatocytes following *L. infantum* exposure, although this was not assessed on protein level [128]. Therefore, post transcriptional events cannot be ruled out. Additionally, within this study, the gene expression of IL-6 receptor alpha (*Il6ra*) was significantly upregulated in HepOrgs subsequent to *L. infantum* exposure (refer to 4.2.4). Hence, a reassessment of IL-6 production by HepOrgs upon *L. infantum* infection, involving larger sample sizes, may be required.

Overall, no significant infection-related differences in the analyzed cytokine levels were detected. This could either indicate, that hepatocyte cytokine secretion is not prominently affected by infection or direct interaction with *L. infantum* parasites, or the ratio of hepatocytes in direct contact with *L. infantum* parasites was too low within HepOrg cell clusters to cause differences in cytokine concentrations at culture supernatant level.

Regarding sex-specific differences in cytokine levels, numerous studies have elucidated the influence of sex-specific hormones on the secretion of specific cytokines [56,143]. However, the generation of HepOrgs necessitates long-term *in vitro* cultivation (> 6 weeks) without the addition of exogenous hormones and under uniform conditions for both sexes. While the possibility of hepatocyte priming by hormones prior to isolation from mice cannot be disregarded, the influence of hormones within the applied experimental approach seems minimal. Consequently, epigenetic and genetic factors may underlie the observed differences in cytokine levels [144]. Nevertheless, the exact causes remain to be elucidated.

The cytokine response of human HepOrgs to *L. infantum* infection was additionally investigated. However, only organoids derived from a single male donor were employed. Therefore, further studies are needed to establish a comprehensive cytokine profile of human HepOrgs following exposure to *L. infantum*. The overall alterations in cytokine levels indicate that human HepOrgs may detect and respond to parasites. Notably, a significant decrease in IL-1 β and IFN- α was observed post-infection, while a trend towards decrease was additionally evident for IL-10, IFN- β , TNF, IL-8, IP-10 and CXCL1. A reduction in CXCL1 levels was previously observed in murine HepOrgs (Figure 12) and was attributed to direct degradation by *Leishmania* parasites, though this observation specifically excluded human CXCL1 [141]. Recent studies on human macrophages exposed to *L. infantum* parasites indicated an increase in CXCL1 expression on mRNA level, although this was not confirmed on protein level [Bea, A., unpublished observation]. Hence, further investigations on CXCL1 dynamics in humans during VL are required. Cytokine levels of TNF, IL-10 and IL-8 increased in supernatants of human macrophages upon *L. infantum* infection, while IL-1 β expression was unaffected by the infection [Bea, A., unpublished observation]. This contrasts with the reported reduction in these cytokine levels. Notably, specific previous data on the cytokine response of human hepatocytes after exposure to *Leishmania* parasites is lacking. Overall, the analyzed cytokines IL-10, IL-6, TNF and IL-8 are associated with a pathogenic response during VL in humans, while IFN- γ , TNF, IL-8 and IL-12 are linked to a protective response, indicating a dual role for certain cytokines [88]. Therefore, more comprehensive studies with larger sample sizes are imperative to delineate a robust cytokine response of human hepatocytes following *L. infantum* infection and to elucidate their participation in hepatic immune response during VL.

4.2.4 Transcriptome analysis of murine *L. infantum* infected HepOrgs

Following the cytokine analysis, a comprehensive investigation of the response of HepOrgs to *L. infantum* infection at the mRNA level was performed, employing RNA sequencing. To explore potential sex-specific differences in the HepOrg response, these were initially derived from both male and female mice. Subsequent to HepOrg infection with *L. infantum* parasites, the isolated RNA was subjected to NGS analysis.

Initial examination of the dataset obtained through PCA revealed substantial variations between individuals, irrespective of sex and infection status (Figure 15). However, no distinct clustering of samples was evident. Further analysis indicated minimal to no differential expression of genes in the specified comparisons between sex and infection status. Notably, the variance observed between HepOrgs derived from different individuals appeared to outweigh the variance attributed to infection, suggesting an overall low response of HepOrgs to *L. infantum* exposure after 24 h, consistent with the cytokine data. Previous work by Hu and colleagues conducted bulk mRNA sequencing on HepOrgs generated from various mice, demonstrating differences in gene expression profiles among HepOrgs, albeit intra-individual differences appeared less pronounced than in the present study [112]. Other studies employing organoids from diverse tissue sources have shown low batch-to-batch variation in gene expression profiles, although this was hypothesized to be influenced by concurrent handling of organoid cultures [145]. Within the scope of this study, ensuring identical treatment of HepOrg cultures throughout the entire culture period was not feasible. Notably, at the time of infection, the organoids had been cultivated for 5 to 6 weeks, thus being exposed to various factors over an extended period. These factors include differences in medium composition, batch-to-batch variability of BME, variability in passaging processes, variations in seeding density and organoid growth, as well as differences in the degree of CholOrg contamination, among others. Despite originating from mice with identical genetic backgrounds, these factors may contribute to the marked differences in gene expression profiles observed. However, the precise underlying causes remain elusive.

In a subset of data characterized by reduced variance between samples, differential expression analysis was conducted independently (Figure 16). This analysis identified a total of 23 upregulated and 25 downregulated genes, including all genes exhibiting significant regulation with a log-fold change (FC) > 0. Applying a more stringent FC criterion of > |1|, only 6 genes remain, indicating a substantially narrower scope compared to other transcriptome analyses [143,146]. This outcome underscores notable limitations inherent in the approach employed. Among the most prominent differentially expressed genes, some encoding for elements of the cytoskeleton were identified to be upregulated, namely *Acta1* and *Tubb3*. Previous studies have proposed a correlation between actin filaments and microtubules with the adhesion of *L. donovani* and *L. braziliensis* to macrophages [147,148]. The adhesion of *Leishmania* to host cells, as well as subsequent infection, was markedly reduced upon destruction of these cytoskeletal elements. Furthermore, evidence suggests that *Leishmania* infection can modulate the assembly of cytoskeleton, particularly with regard to actin filaments, to enhance phagocytosis [148]. Consequently, increased expression of these genes might facilitate increased uptake of parasites. However, it should be noted that the role of such mechanisms remains to be elucidated with regard to hepatocyte exposure to *Leishmania*. Moreover, to the best of my knowledge there is currently no available data regarding the specific upregulation of these genes in the context of leishmaniasis. Therefore, the underlying mechanisms remain unclear. Additionally, *Il6ra* and *S100a14* were shown to be upregulated in HepOrgs following *L. infantum* infection. Both fulfill functions in the regulation of inflammatory processes and are generally associated with the formation of proinflammatory responses in

the context of VL [142,149]. Aligning with the presented results an increase in S100a14 and IL-6 as a result of *Leishmania* infection was evident in prior studies on either protein or mRNA level [128,150]. However, cytokine studies conducted within this thesis did not demonstrate an infection-dependent elevation in IL-6 levels.

Based on the identified DEGs, KEGG pathway analysis was performed. It was shown that, GO biological process pathways were affected by *L. infantum* exposure of HepOrgs. Notably, pathways associated with inflammatory response and defense mechanisms were of particular interest in the context of infection. However, a nearly equal number of upregulated and downregulated genes were assigned to these pathways (see Supplementary data, Table S 5). Consequently, no conclusion can be drawn regarding a specific induction or inhibition of these pathways as a result of infection with *L. infantum*.

Furthermore, specific genes of interest beyond those significantly differentially expressed were investigated (Figure 17). Interestingly, a trend towards increased *Nod2* expression was evident, consistent with findings in canine hepatocytes following exposure to *L. infantum* [128]. This intracellular PRRs is thought to initiate protective and inflammatory mechanisms upon recognition of LPG and other *Leishmania*-derived molecules [128,151]. Similar mechanisms have been implicated for TLR2, although the previously cited study found no effect of *L. infantum* exposure on TLR2 expression in hepatocytes. In contrast, a significant decrease was observed within the present study, suggesting a potential immune-suppressive effect of *Leishmania* exposure. This notion was further supported by an infection-dependent increase in the expression of the anti-inflammatory cytokine IL-10 in canine hepatocytes early after parasite exposure [128]. While elevated cytokine levels of IL-10 were not detected 24 h post infection in this study, a significant increase in mRNA levels of the corresponding IL-10 receptor was observed. This could suggest a delayed upregulation, consistent with literature describing the induction of IL-10 receptor expression by various stimuli [152]. The expression of the functional markers albumin and CYP3A13 appeared unaffected by *L. infantum* infection, indicating no impairment of hepatocyte function.

Overall, the comprehensive transcriptome analysis revealed only a limited number of infection-specific differences in the gene expression of HepOrgs. Past investigations indicate that the response to infection with *L. infantum* parasites is very rapid but transient at the mRNA level in both human macrophages and canine hepatocytes [128]. Consequently, conducting an analysis 24 h post-infection may prove too delayed to capture the induced responses at the RNA level. This tendency may be especially notable in hepatocytes, which generally display a comparatively less pronounced response to infection compared to macrophages.

4.3 Co-culture of murine *L. infantum*-infected HepOrgs and monocytes

Aiming to replicate the interaction between murine hepatocytes and monocytes during *L. infantum* infection in the liver, three distinct methods were utilized to co-culture HepOrgs with monocytes. The cytokine profiles should be used to analyze which of the methods best reflect the murine *in vivo* cytokine dynamics. This approach aims to establish a model to analyze the underlying immune mechanisms during *L. infantum* infection in the human liver.

Among the cytokines analyzed, a specific focus was set on those that are primarily involved in hepatic immune processes during VL. As outlined in section 1.2.2.1 it is well known that upon parasite invasion into the liver the secretion of the chemokines CCL2, CCL3 and IP-10 is

induced [89]. Additionally, increased TNF and IFN- γ secretion was shown to be associated with an M1 polarization of macrophages, as well as granuloma formation, ultimately leading to elimination of parasites [88,92]. Conversely, IL-10 acts as an immunosuppressive factor during VL, as it promotes parasite survival through the inhibition of T_H1 immune responses. Increased IL-10 production is observed in early stages of VL in the liver, but not in later ones [88].

Interestingly, these cytokine dynamics were largely recapitulated in an infection-dependent manner across two of the three co-culture approaches investigated. In both semi-suspension (Figure 21) and suspension (Figure 22) co-cultures of monocytes and HepOrgs, a significant infection-dependent increase in CCL3, CCL2, TNF and IFN- γ levels was demonstrated. Moreover, in both approaches IP-10 levels were significantly lower in co-culture supernatants following prior infection of HepOrgs, while IL-10 levels showed a significant elevation exclusively in suspension co-cultures, subsequent to HepOrg infection. Although IP-10 (CXCL10) secretion has been demonstrated to be induced *in vivo* in the liver upon parasite invasion, it is plausible that free parasites in the employed co-culture systems might directly degrade IP-10 through metalloproteases, as discussed above with regard to CXCL1. Given the structural similarities within the C-X-C chemokine family, analogous mechanisms could lead to their degradation [153]. The elevated IL-10 production observed in early stages of VL aligns with the significantly heightened levels detected in suspension co-culture supernatants after *L. infantum* infection [88].

Notable, both approaches demonstrate a pronounced increase in the production of key cytokines, in particular CCL3 and TNF, when HepOrgs and monocytes are co-cultured. This augmentation is particularly striking for CCL3, which is not produced by either HepOrgs, with or without parasites, or monocytes cultured solely with parasites. Taken together, these findings suggest that the reciprocal interaction between monocytes and hepatocytes during *L. infantum* infection significantly induce immune responses that favor parasite elimination. Whether the interaction between monocytes and HepOrgs is based on direct cell-cell contacts or soluble factors remains elusive. However, the strong tendencies in the suspension co-culture point towards soluble factors, as direct contacts were primarily confined to two dimensions in this setting. This observation potentially elucidates why the infection is self-resolving in the murine liver, but persists in the spleen, providing insights into the involvement of hepatocytes in hepatic immune mechanisms during VL. Although, the intricacies of these mechanisms *in vivo* are certainly more complex and require further research.

The results of the co-culture conducted in BME (Figure 20) exhibited discernible discrepancies from those observed in the other two approaches. In this instance, the levels of the examined cytokines did not show an infection-dependent increase. This discrepancy suggests that the interaction among parasites, HepOrgs and monocytes may be impaired by embedding in BME. Furthermore, the extent to which embedding in BME influences cellular behavior of monocytes remains unclear [121]. Noteworthy, this approach was implemented using a substantially larger medium volume of 500 μ l, whereas suspension approaches were conducted in 200 μ l, while maintaining the same cell count. Consequently, trends in cytokine concentrations within this volume may be less pronounced, as overall concentrations were markedly lower, particularly in CCL3 concentrations. This may also be attributed to cytokines binding to BME scaffold structures, thereby diminishing their diffusion into the surrounding medium [154]. Since only the liquid medium was utilized for cytokine analysis, the cytokine reservoir within the BME was not accounted for. Altogether, this approach appears inadequate for reflecting the cytokine dynamics observed *in vivo*.

Analysis of the cytokine profiles revealed that the suspension co-culture approach most accurately reflected the infection-dependent *in vivo* dynamics of key cytokines. Consequently, RNA samples from this approach were selected for further investigation of gene expression at the mRNA level (Figure 23). Initially, *Leishmania*-specific β -Actin expression was assessed, allowing a clear distinction between uninfected and infected samples. Due to the intricate gene regulation in *Leishmania* [155], as well as variations in the quantities of murine cells across distinct co-culture conditions, direct comparison of parasite quantities was precluded. In addition, the expression of the PRRs *Tlr2* and *Nod2* was analyzed, as the expression of both is known to be influenced by *Leishmania* infection in monocytes or hepatocytes [127,128]. Consistent with prior findings, trends towards increased expression were observed upon *L. infantum* exposure in RNA samples obtained from both HepOrgs alone and HepOrgs co-cultured with monocytes. Although these trends appeared more pronounced in co-cultures of HepOrgs and monocytes, these did not reach statistical significance. Collecting RNA at earlier time points may yield more informative results, especially for hepatocytes already exposed to parasites for 48 h at this juncture [128]. Interestingly, expression levels of both receptors were highest in samples containing only monocytes and *L. infantum* parasites, suggesting that these receptors are potentially more highly expressed in monocytes compared to hepatocytes, which aligns with their functional role in the immune system. Finally, the expression of *Nos2* and *Arg1* was assessed, as both are closely linked to immune responses during VL. Although, while *Nos2* expression promotes the production of NO, thereby aiding in parasite elimination, *Arg1* expression is associated with parasite survival, driven by enhanced polyamine synthesis [82–84]. Consequently, the expression of these genes elicits opposing functions in immune reactions during VL. Consistent with this, contrasting trends were observed in the expression of both genes in co-cultures following *L. infantum* infection. While *Nos2* exhibited upregulation, *Arg1* expression appeared to decrease in an infection-dependent manner. This observation is consistent with the cytokine profile described above for this approach, wherein T_H1 cytokines were upregulated in co-cultures following *L. infantum* infection. Both the observed cytokine profile and the described effects on the expression of *Nos2* and *Arg1* collectively indicate a microenvironment conducive to parasite elimination through the production of NO.

Monocyte recruitment was evaluated using two of the three co-culture approaches employed, which were embedding in BME and semi-suspension. In the suspension approach, monocytes promptly adhered to the bottom of the culture vessel, thus confining their potential movement to two dimensions along the culture bottom. Given that the aim was to study recruitment to three-dimensional organoids, this appeared as an unsuitable limitation to this approach. Conversely, in the remaining two approaches, monocytes were observable in three dimensions during co-culture. Furthermore, both approaches indicated an increase in the number of monocytes proximal to the organoids following infection (Figure 20 C, Figure 21 C). However, it should be noted that the findings lack statistical significance due to considerable variance in the data sets. In the semi-suspension approach, this trend corresponds with elevated secretion of the chemokines CCL3 and CCL2, which are implicated in monocyte recruitment. Notably, CCL3 primarily facilitates recruitment into or within the tissue, whereas CCL2 promotes egress from the bone marrow [55]. Nonetheless, the recruitment results attained in this study remain inconclusive. In particular, due to the complexity of evaluating recruitment in three-dimensional approaches, resulting in substantial data variance. Moreover, time-lapse imaging (data not shown) did not capture any discernible immune cell movement, inconsistent with observations from other studies employing comparable experimental setups [119]. Given the potential detrimental role of monocyte recruitment in murine VL [96], successful modeling of this recruitment process could further elucidate these correlations. Of particular interest is the

potential conflicting impact of CCL3 [156] within the broader context of VL and its role in human infection. Hence, the employed methods should be revised, potentially addressing the medium requirements specific to monocytes and implementing distinct matrix dilutions.

In summary, the methods employed did not provide convincing evidence of monocyte recruitment. Nevertheless, it became evident that the introduction of an ECM-rich hydrogel might be indispensable for investigations within the context of recruitment to three-dimensional organoids.

4.4 Co-culture of hepatocyte organoids with *L. infantum*-infected macrophages

To model *Leishmania* infection in the liver more accurately, additional co-culture systems were implemented, focusing on the *L. infantum* infection of macrophages, the primary target cells of the parasites, prior to co-cultivation with uninfected HepOrgs [70]. Two distinct approaches were employed. Initially HepOrgs were dissociated into single cells and re-embedded into BME alongside infected macrophages. Whereas in the second approach intact HepOrgs were added in suspension to adherent infected macrophages. The primary focus of investigation in both approaches was the evaluation of the cytokine profiles, aiming to assess the representation of known immune dynamics within the liver.

Employing the initial co-culture approach (a), HepOrgs were digested into single cells and co-cultured with *L. infantum*-infected macrophages embedded in BME for a duration of 8 days. The progression of the co-culture as well as the interaction dynamics between newly forming HepOrgs and macrophages was assessed using both light and confocal microscopy. Interestingly, it was observed that macrophages appeared to establish direct contacts with HepOrgs, regardless of their infection status. This suggests that the applied co-culture approach was effective in supporting macrophage viability and enabling direct interaction with HepOrgs. Immunofluorescence staining targeting *L. infantum* parasites via Hsp90 (Figure 26 B, C) revealed the presence of parasites within the co-cultures after 4 days, however no parasites were detected after 8 days. This observation correlated with the quantification of *Leishmania*-specific β -Actin, which exhibited a significant decrease after 8 days compared to 4 days (Figure 26 D), indicating potential parasite clearance. However, while individual *L. infantum* parasites were detectable after 4 days of co-cultivation within F4/80-stained macrophages during confocal microscopy, the overall parasite burden appeared relatively low, compared to the initial infection parameters of the macrophage population (refer to Figure 24). Notably, prior studies on *L. infantum* infection in human macrophages [Bea, A., unpublished observation], demonstrated a substantial decline in infection rates and the number of parasites per infected cell within 76 h post-infection. This underscores a limitation inherent to *in vitro* macrophage infection, as the *in vivo* amplification of the parasites cannot be replicated [157,158]. Consequently, this suggests that earlier time points for microscopic evaluations may be more conducive to effective parasite detection. Although it should be noted that organoid re-growth might be less pronounced at earlier time points.

To characterize cytokine profiles, co-culture supernatants were collected at two-day intervals and subjected to cytokine measurements. Results for key cytokines were analyzed both over time and as area under the curve (AUC). Regarding the chemokines CCL3, CCL2 and IP-10 infection-dependent differences similar to those seen in the suspension approach of monocyte co-cultures were observed. Specifically, the total amounts (AUC) of CCL3 and CCL2 were

higher upon the addition of infected macrophages to HepOrgs, while IP-10 levels decreased compared to the addition of uninfected macrophages. These findings are consistent with the dynamics of these cytokines observed *in vivo*, as depicted in Figure 2, while the decrease in IP-10 was hypothesized to be due to direct degradation by *Leishmania* parasites [153]. Interestingly, both CCL3 and IP-10 levels displayed more prominent infection-dependent differences between added uninfected and infected macrophages after 2 and 4 days of co-culture, with levels converging at later time points. This observation aligns with the decrease in parasite burdens observed at later time points in both the present, as indicated by quantification of *Leishmania*-specific β -Actin and previous studies [Bea, A., unpublished observation]. Within the levels of the remaining cytokines TNF, IFN- γ and IL-10 no infection-dependent differences were observed, and there was also no significant difference compared to HepOrgs cultured alone. In future studies, increasing the ratio of both uninfected or infected macrophages to HepOrgs could enhance the prominence of differences resulting from the interaction of HepOrgs and macrophages. Notably, in monocyte co-culture, prominent infection-dependent results were in part achieved at a ratio of 1 to 3, hepatocyte to monocytes, whereas in this macrophage co-culture a ratio of 2 to 1, hepatocytes to macrophage was applied. Therefore, titrating the quantity of macrophages might be beneficial. Additionally, examining cytokine levels at earlier time points might be feasible, as the infection appears to be more pronounced then.

Based on HCS quantification, the infection rate among the employed macrophage population averaged 65 %, falling within the range of previously described murine macrophage infection rates. However, the median count of 7.5 parasites per infected macrophage was below prior observations [159], potentially leading to less pronounced infection-related effects. Overall, it should be noted that the utilization of easily accessible macrophage populations, derived from bone marrow as employed here, may not entirely reflect the tissue-specific heterogeneity inherent in macrophages. This discrepancy in macrophage origin might substantially influence the interactions between macrophages and tissue-specific epithelial cells, such as hepatocytes [160]. Employing a hepatic microenvironment during the differentiation of macrophages in future studies, akin to a method previously described for the differentiation of monocytes to DCs [161], might potentially reduce the tissue-specific limitations inherent in the applied co-culture systems.

In the second macrophage co-culture approach (b), macrophages were infected as described above and subsequently co-cultured with HepOrgs located above them in the culture medium. Co-culture supernatants were subjected to cytokine measurements (Figure 28 C-I). Interestingly, the cytokines CCL3, IL-6, TNF, IL-12p40 and IL-1 β exhibited markedly elevated levels in co-cultures of macrophages and HepOrgs, whereas these were scarcely detected in cultures containing either cell type alone. This suggests that reciprocal interactions between macrophages and HepOrgs might promote the production of these cytokines, aligning with findings from previous studies indicating activation of the respective cell types [162,163]. Conversely, CXCL1 levels remained consistent across all cultures containing HepOrgs. Prior investigations have demonstrated that hepatocytes can serve as the primary source of heightened serum CXCL1 levels in mice under pathological conditions [163], implying a substantial capacity for CXCL1 production in hepatocytes. In terms of infection-specific variations in cytokine levels, a discernible trend towards higher levels of IL-12p40 upon co-cultivation of *L. infantum*-infected macrophages with HepOrgs was observed in comparison to co-cultures with uninfected macrophages. Elevated IL-12 production during VL has been associated with the promotion of T_H1-specific immune responses, while concurrently suppressing T_H2 expansion [88], thereby contributing to parasite clearance.

Due to the pronounced variability in CCL3, IL-6 and TNF levels upon co-cultivation of *L. infantum*-infected macrophages with HepOrgs, further analysis of infection-specific differences was precluded. Compared to approach 'a', utilizing intact organoids poses the disadvantage of introducing inaccurate cell quantities, due to differences between cell counts in single-cell suspensions and the actual cell count in organoid suspensions. This discrepancy could lead to considerable variance in data sets sensitive to cell counts, such as cytokine levels. Additionally, enabling the formation of direct contacts between macrophages and HepOrgs exclusively at the lower regions of the organoids, was considered insufficient for establishing robust co-cultivation strategies. Subsequent investigations should be confined to approach 'a', whereby further improvements are also required, mainly including adaptation of the macrophage quantities and the time points for cytokine assessment.

Finally, as summarized in Table 15 it can be concluded that the co-cultivation of murine *L. infantum*-infected HepOrgs with monocytes in suspension, partially recapitulates cytokine dynamics, previously observed in experimental VL, *in vitro*. With further development, the methodologies outlined hold promise for diminishing reliance on animal experiments in VL research, aligning with the principles of the 3R concept (Replace, Reduce, Refine). Moreover, these techniques offer a platform for investigating human hepatic VL, thereby advancing the current understanding of host-pathogen interactions within the microenvironment of the human liver.

Supplementary data

Transcriptome analysis

Table S1: Differentially expressed genes between uninfected and infected female-derived HepOrgs (up-/downregulated in infected samples)

Gene ID	Sign	Base mean	log ₂ (fold change)	p-value	p-adjusted
Mcmbp	downregulated	237.355	-0.991	2.801E-11	4.547E-07
Acta1	upregulated	25.647	5.586	1.387E-05	1.123E-05
Rora	upregulated	246.867	0.751	2.297E-07	9.309E-04
Tubb3	upregulated	40.441	3.691	1.870E-07	9.309E-04
Gpx2	downregulated	484.884	-0.723	3.619E-07	1.173E-03
Rps13-ps2	downregulated	6.049	-5.714	4.060E-06	1.097E-02
Rrs1	downregulated	253.863	-0.681	7.807E-06	1.808E-02
Crybg3	downregulated	32.327	-1.634	8.984E-06	1.820E-02
Man2a1	downregulated	546.931	-0.683	1.093E-05	1.969E-02
Srrm2	upregulated	2995.914	0.362	2.203E-05	3.570E-02
NA	upregulated	8.690	6.320	2.806E-05	4.134E-02

Table S2: Differentially expressed genes between naive male- and female-derived HepOrgs (up-/downregulated in male-derived samples)

Gene ID	Sign	Base mean	log ₂ (fold change)	p-value	p-adjusted
Xist	downregulated	8046.391	-14.988	2.462E-51	5.047E-47
Eif2s3y	upregulated	210.957	11.323	1.836E-27	1.882E-23
Kdm5d	upregulated	164.270	10.980	4.276E-26	2.922E-22
Ddx3y	upregulated	176.136	11.077	6.532E-26	3.348E-22
Uty	upregulated	96.173	10.211	1.339E-22	5.492E-19
Kdm5c	downregulated	589.741	-0.711	3.519E-10	1.203E-06
NA	upregulated	6.051	6.214	1.160E-06	3.397E-03
Lym7	upregulated	24.573	1.784	5.070E-06	1.299E-02

Table S3: Differentially expressed genes between infected male- and female-derived HepOrgs (up-/downregulated in male-derived samples)

Gene ID	Sign	Base mean	log ₂ (fold change)	p-value	p-adjusted
Xist	downregulated	5453.7589	-15.229	2.558E-49	3.789E-45
Eif2s3y	upregulated	145.885	10.651	1.814E-24	1.343E-20
Ddx3y	upregulated	126.197	10.430	2.913E-23	1.438E-19
Kdm5d	upregulated	104.072	10.151	1.444E-22	5.348E-19
Uty	upregulated	61.851	9.389	6.397E-19	1.895E-15
Pcgf3	downregulated	357.884	-0.677	1.818E-07	4.487E-04
Erdr1	downregulated	27.118	-6.690	4.929E-06	1.043E-02
Wnk1	upregulated	1078.465	0.464	1.189E-05	2.202E-02
Npdc1	upregulated	330.093	0.459	2.212E-05	3.640E-02

Table S4: Differentially expressed genes between uninfected and infected HepOrgs (up-/downregulated in infected samples) - Data from sample subset

Gene ID	Sign	Base mean	log ₂ (fold change)	p-value	p-adjusted
Hmgn2	downregulated	1166.247	-0.342	1.857E-03	8.740E-03
PP1cc	downregulated	804.952	-0.293	1.294E-04	3.574E-02
Rab23	downregulated	101.458	-0.780	1.360E-04	3.639E-02
Hap1	upregulated	116.880	0.810	1.304E-04	3.574E-02
Gprc5b	downregulated	187.166	-0.702	9.790E-06	5.493E-03
Glis2	upregulated	272.497	0.550	7.739E-05	2.338E-02
Csf1	downregulated	1645.392	-0.414	1.303E-04	3.574E-02
Gdi1	upregulated	858,150	0.360	1.238E-05	6.342E-02
Itga2	downregulated	609.263	-0.486	1.004E-04	2.957E-02
Mmp7	downregulated	8563.340	-0.747	5.132E-10	1.209E-06
Plagl1	upregulated	172.395	0.716	2.275E-05	8.934E-03
Timp3	upregulated	1961.809	0.637	4.146E-05	1.576E-02
Dnmt3a	upregulated	306.334	0.612	6.665E-05	2.182E-02
Abcc3	upregulated	1102.720	0.437	1.092E-05	5.847E-03
Rida	downregulated	423.073	-0.638	3.661E-07	3.595E-04
Hdac7	upregulated	802.147	0.470	4.025E-09	7.904E-06
Parp3	upregulated	129.050	0.758	6.509E-05	2.182E-02
Tmem176a	downregulated	1976.676	-0.339	8.856E-06	5.218E-02

Man2a1	downregulated	524.152	-0.577	2.078E-06	1.530E-03
Ankrd1	upregulated	3619.832	0.280	1.515E-04	3.966E-02
Il6ra	upregulated	45.059	1.251	8.214E-06	5.094E-03
Sass6	downregulated	35.449	-1.368	6.479E-05	2.182E-02
Vcam1	downregulated	2859.188	-0.465	7.785E-07	7.057E-04
Fga	upregulated	1454.217	0.750	2.501E-12	1.473E-08
Prom1	downregulated	2657.042	-0.661	9.826E-11	2.895E-07
Scarb2	downregulated	698.318	-0.614	5.014E-05	1.846E-02
Tmem176b	downregulated	4185.208	-0.307	4.408E-06	2.886E-03
Acta1	upregulated	12.126	3.957	1.441E-06	1.132E-03
Arap1	downregulated	458.969	-0.441	1.931E-05	8.740E-03
Lss	upregulated	272.624	0.858	1.096E-06	9.221E-04
Plekhs1	downregulated	364.127	-1.258	5.620E-11	2.207E-07
Vnn1	upregulated	696.395	0.495	2.883E-06	1.998E-03
Tgm2	downregulated	1651.665	-0.651	6.953E-18	8.193E-14
Ppl	upregulated	1339.099	0.300	7.208E-05	2.295E-02
Car8	downregulated	289.791	-0.773	2.034E-05	8.740E-03
Plekha6	downregulated	804.032	-0.304	1.669E-04	4.275E-02
S100a14	upregulated	54.293	1.486	7.368E-08	1.085E-04
Gpx2	downregulated	497.164	-0.469	6.329E-05	2.182E-02
Paip2b	downregulated	154.113	-0.688	7.414E-05	2.299E-02
Stbd1	downregulated	314.515	-0.808	1.829E-08	3.079E-05
Mcmbp	downregulated	217.167	-0.781	1.612E-07	2.111E-04
Tmem245	upregulated	461.425	0.500	3.514E-07	3.595E-04
Tubb3	upregulated	25.586	2.446	3.040E-07	3.582E-04
Selenbp1	upregulated	1063.691	0.442	2.135E-05	8.740E-03
Klhdc7a	downregulated	358.795	-0.560	1.415E-05	6.949E-03
Ugt1a1	upregulated	663.391	0.628	1.744E-04	4.371E-02
NA	upregulated	2353.956	0.532	2.151E-05	8.740E-03

Table S5: Biological processes GO term enrichment analysis of all detected DEGs between uninfected and infected samples

GO Term	Associated DEGs
Neg. reg. of dendritic cell differentiation	Tmem176a, Tmem176b
Response to mechanical stimulus	Itga2, Mmp7, Ankrd1, Acta1, Ppl
Pos. reg. of neurogenesis	Ppp1cc, Hap1, Gdi1, Man2a1, Tgm2
Pos. reg. of cell projection organization	Hap1, Gprc5b, Gdi1, Itga2, Ankrd1, Scarb2, Arap1
Pos. reg. of cell adhesion	Csf1, Itga2, Vcam1, Fga, Vnn1, Tgm2
Mononuclear cell differentiation	Csf1, Hdac7, Tmem176a, Il6ra, Tmem176b, Vnn1
Inflammatory response	Gprc5b, Csf1, Itga2, Hdac7, Vcam1, Vnn1, Tgm2, Ugt1a1
Pos. reg. of cell differentiation	Ppp1cc, Hap1, Gprc5b, Csf1, Gdi1, Man2a1, Prom1, Vnn1, Tgm2
Reg. of cell differentiation	Ppp1cc, Hap1, Gprc5b, Csf1, Gdi1, Hdac7, Tmem176a, Man2a1, Prom1, Tmem176b, Vnn1, Tgm2
Generation of neurons	Ppp1cc, Hap1, Gprc5b, Gdi1, Dnmt3a, Man2a1, Ankrd1, Vcam1, Prom1, Scarb2, Tgm2, Tubb3
Neurogenesis	Ppp1cc, Hap1, Gprc5b, Csf1, Gdi1, Dnmt3a, Man2a1, Ankrd1, Vcam1, Prom1, Scarb2, Tgm2, Tubb3
Pos. reg. of multicellular organismal proc.	Ppp1cc, Hap1, Gprc5b, Csf1, Gdi1, Itga2, Man2a1, Il6ra, FgaVnn1, Tgm2
Defense response	Rab23, Gprc5b, Csf1, Itga2, Hdac7, Vcam1, Fga, Vnn1, Tgm2, S100a14, Ugt1a1

Harmony software setup

Table S6: HCS - Image analysis

	Channels	
Input Images	DAPI nuclear stain channel	HSP90 AlexaFluor 647

Table S7: HCS - Image Segmentation

Image Segmentation		
Find Nuclei (Detects nuclei in macrophages)	Channel ROI Method Common Threshold Area Split Facto Individual Threshold Contrast Output Population	DAPI None B -0.02 > 40 μm^2 16.9 0.14 > -0.71 Macrophages
Find Cytoplasm M1 (Detects macrophage cytoplasm and defines single macrophages)	Channel Nuclei Method Individual Threshold Output Population	Alexa 647 Macrophages A 0.06 Cytoplasm M1
Find Cytoplasm M2 (Detects macrophage cytoplasm and defines single macrophages)	Channel Nuclei Method Individual Threshold Output Population	Alexa 647 Macrophages A 0.06 Cytoplasm M2

Table S8: HCS - Definition of regions of interest

Definition of Regions of interest			
Calculate Intensity properties	Channel Population Region Method Mean Property Prefix	DAPI Macrophages Nucleus Standard Nucleus DAPI	Alexa 647 Macrophages Cell Standard Cell Alexa 647
Calculate Morphology properties	Population Region Method Mean Property Prefix	Macrophages Nucleus Standard (area/roundness) Nucleus	
Calculate Morphology properties for M1	Population Region Method Mean Property Prefix	Macrophages Cytoplasm Standard (area/roundness) M1 macrophages	
Calculate Morphology properties for M2	Population Region Method Mean Property Prefix	Macrophages Cytoplasm Standard (area/roundness) M2 macrophages	

Table S 9: HCS - Image segmentation

Image segmentation		
Find Spots (Detects intracellular spots within the region of interest in the Alexa 647 channel)	Channel	Alexa 647
	ROI	Macrophages
	ROI Region	Cell
	Method	B
	Detection Sensitivity	0.11
	Splitting Coefficient	0.844
	Calculate Spot Properties	
	Output Population	Spots

Table S10: HCS - Quantifying properties in regions

Quantifying Properties in Regions			
Calculate Morphology Properties (Quantification and calculation of properties of spots)	Input Population	Spots	
	Region	Spot	
	Method	Standard (area/roundness/width/length/ ratio width to length)	
	Output Property Prefix	Spots	
Calculate Intensity Properties	Region	Spot	Spot
	Method	Standard (mean/standard deviation/coefficient of variance/median)	Standard (mean)
	Output Property Prefix	Intensity Spot Alexa 647	Intensity Spot DAPI
Calculate Properties (Calculation of Properties)	Population	Spots	
	Method	By Formula	
	Formula	A/B	
	Variable A	Spot Alexa 647 mean	
	Variable B	Spot DAPI mean	
	Output Property	Alexa/DAPI intensity ratio	

Table S11: Identification of intracellular *L. infantum* parasites

Identification of intracellular <i>L. infantum</i> parasites		
Select Population I (Selection of parasites from false-positive spots)	Input Population	Spots
	Method Number of Classes	Linear Classifier 2
	Relative Spot Intensity	Spot Roundness
	Corrected Spot Intensity	Spot Width [μm]
	Uncorrected Spot Peak Intensity	Spot Length [μm]
	Spot Contrast	Spot Ratio Width to Length
	Spot Background Intensity	Spot Alexa 568 Mean
	Spot Area [px^2]	Spot DAPI Mean
	Region Intensity	ALEXA/DAPI intensity ratio
	Spot to Region Intensity	Intensity Surrounding Alexa 568 Mean
		Intensity Surrounding Alexa 568 Median
	Spot Area [μm^2]	

	Output Population A Output Population B	Likely Leishmania False-positive
	Population Method Likely Leishmania Output Population Population Method Spot Area [μm^2] ALEXA/DAPI intensity ratio Spot Area [μm^2] Corrected Spot Intensity	Spots Filter by Property > 0 Spots selected Spots selected Filter by Property > 4 > 0.3 < 35 > 100 (Stain-dependant) Boolean F1 and F2 and F3 and F4
	Operations	

Table S12: HCS - Relation of macrophages and parasites

Relation of macrophages and parasites		
Calculate Properties	Population Method Related Population Number of <i>Leishmania</i> Output Property Suffix	Macrophages By related population <i>Leishmania</i> Per Cell
	Population Method	Macrophages Filter by Property

Table S13: HCS - Identification of subpopulation II

Identification of subpopulations		
Select Population II	Number of Leishmania – per cell	>0
	Output Population Number of Leishmania – per cell	Infected macrophages >=2
	Output Population Number of Leishmania – per cell	Double Infected macrophages >0
	Output Population	Seriously infected macrophages

Table S 14: HCS - Readout values

Readout values		
Define Results	Method Population	List of outputs Macrophages – number of objects
	Population	Leishmania – number of objects
	Population	Infected macrophages – number of objects
	Population	Seriously infected macrophages – number of objects
	Population	M1 macrophages – number of objects
	Population	

		M2 macrophages – number of objects
	Method Formula Population Type Variable A – Number of Objects Variable B – Number of Objects Output name	Formula Output 1. a/b 2. to 4. $a/b*100$ Objects 1. Leishmania 2. Infected macrophages 3. Seriously infected macrophages 4. Double infected macrophages Macrophages 1. Leishmania per infected macrophage 2. % infected macrophages 3. % seriously infected macrophages 4. Double infected Macrophages

References

- [1] Leishmaniasis Worldwide and Global Estimates of Its Incidence | PLOS ONE n.d. <https://journals.plos.org/plosone/article?id=10.1371/journal.pone.0035671> (accessed March 14, 2024).
- [2] Leishmaniasis n.d. <https://www.who.int/news-room/fact-sheets/detail/leishmaniasis> (accessed March 14, 2024).
- [3] Steverding D. The history of leishmaniasis. *Parasites Vectors* 2017;10:82. <https://doi.org/10.1186/s13071-017-2028-5>.
- [4] Gramiccia M, Gradoni L. The current status of zoonotic leishmaniasis and approaches to disease control. *International Journal for Parasitology* 2005;35:1169–80. <https://doi.org/10.1016/j.ijpara.2005.07.001>.
- [5] Cox FEG, editor. *Modern parasitology: a textbook of parasitology*. 2nd ed. Oxford: Boston : Blackwell Scientific Publications; 1993.
- [6] Schmidt GD, Roberts LS, Roberts LS. *Foundations of parasitology*. Saint Louis, Miss: Mosby; 1977.
- [7] Vera-Izaguirre DS, Vega-Memije E, Quintanilla-Cedillo MR, Arenas R. Leishmaniasis. Revisión. *Dermatología Cosmética, Médica y Quirúrgica* 2006;4:252–60.
- [8] Seidelin H. Leishmaniasis and Babesiosis in Yucatan. *Annals of Tropical Medicine & Parasitology* 1912;6:295–300. <https://doi.org/10.1080/00034983.1912.11687069>.
- [9] Torres-Guerrero E, Quintanilla-Cedillo MR, Ruiz-Esmenjaud J, Arenas R. Leishmaniasis: a review. *F1000Res* 2017;6:750. <https://doi.org/10.12688/f1000research.11120.1>.
- [10] Reithinger R, Dujardin J-C, Louzir H, Pirmez C, Alexander B, Brooker S. Cutaneous leishmaniasis. *Lancet Infect Dis* 2007;7:581–96. [https://doi.org/10.1016/S1473-3099\(07\)70209-8](https://doi.org/10.1016/S1473-3099(07)70209-8).
- [11] Bravo F, Sanchez MR. New and re-emerging cutaneous infectious diseases in Latin America and other geographic areas. *Dermatol Clin* 2003;21:655–68, viii. [https://doi.org/10.1016/s0733-8635\(03\)00090-1](https://doi.org/10.1016/s0733-8635(03)00090-1).
- [12] CDC - DPDx - Leishmaniasis 2019. <https://www.cdc.gov/dpdx/leishmaniasis/index.html> (accessed March 15, 2024).
- [13] Organization PAHO. *Manual of procedures for leishmaniasis surveillance and control in the Americas*. 2019.
- [14] Harhay MO, Olliaro PL, Costa DL, Costa CHN. Urban parasitology: visceral leishmaniasis in Brazil. *Trends in Parasitology* 2011;27:403–9. <https://doi.org/10.1016/j.pt.2011.04.001>.
- [15] File:Leishmaniasis life cycle diagram en.svg - Wikipedia 2008. https://commons.wikimedia.org/wiki/File:Leishmaniasis_life_cycle_diagram_en.svg (accessed March 17, 2024).
- [16] Mondal D, Bern C, Ghosh D, Rashid M, Molina R, Chowdhury R, et al. Quantifying the Infectiousness of Post-Kala-Azar Dermal Leishmaniasis Toward Sand Flies. *Clinical Infectious Diseases* 2019;69:251–8. <https://doi.org/10.1093/cid/ciy891>.
- [17] Rutte EAL, Zijlstra EE, Vlas SJ de. Post-Kala-Azar Dermal Leishmaniasis as a Reservoir for Visceral Leishmaniasis Transmission. *Trends in Parasitology* 2019;35:590–2. <https://doi.org/10.1016/j.pt.2019.06.007>.
- [18] Faye B, Bañuls AL, Bucheton B, Dione MM, Bassanganam O, Hide M, et al. Canine visceral leishmaniasis caused by *Leishmania infantum* in Senegal: risk of emergence in humans? *Microbes and Infection* 2010;12:1219–25. <https://doi.org/10.1016/j.micinf.2010.09.003>.
- [19] Davidson R, Croft S. Visceral leishmaniasis in Africa. *Afr Health* 1992;14:18–9.
- [20] Mann S, Frasca K, Scherrer S, Henao-Martínez AF, Newman S, Ramanan P, et al. A Review of Leishmaniasis: Current Knowledge and Future Directions. *Curr Trop Med Rep* 2021;8:121–32. <https://doi.org/10.1007/s40475-021-00232-7>.
- [21] Bern C, Maguire JH, Alvar J. Complexities of Assessing the Disease Burden Attributable to Leishmaniasis. *PLOS Neglected Tropical Diseases* 2008;2:e313.

<https://doi.org/10.1371/journal.pntd.0000313>.

[22] While, C.; Resolution, W.; Sixtieth, W.; Health, A. A. Global Leishmaniasis Surveillance Le Point Sur La Situation Mondiale de La Leishmaniose 1998–2016. *Wkly Epidemiol Rec* 2018;530–40.

[23] Guerin PJ, Olliaro P, Sundar S, Boelaert M, Croft SL, Desjeux P, et al. Visceral leishmaniasis: current status of control, diagnosis, and treatment, and a proposed research and development agenda. *The Lancet Infectious Diseases* 2002;2:494–501. [https://doi.org/10.1016/S1473-3099\(02\)00347-X](https://doi.org/10.1016/S1473-3099(02)00347-X).

[24] Visceral leishmaniasis: what are the needs for diagnosis, treatment and control? | *Nature Reviews Microbiology* n.d. <https://www.nature.com/articles/nrmicro1748> (accessed March 17, 2024).

[25] Visceral leishmaniasis and HIV coinfection: WHO publishes new guideline with region-specific treatment recommendations n.d. <https://www.who.int/news/item/08-06-2022-visceral-leishmaniasis-and-hiv-coinfection-who-publishes-new-guideline-with-region-specific-treatment-recommendations> (accessed March 17, 2024).

[26] Jeronimo SMB, Duggal P, Braz RFS, Cheng C, Monteiro GRG, Nascimento ET, et al. An Emerging Peri-Urban Pattern of Infection with *Leishmania chagasi*, the Protozoan Causing Visceral Leishmaniasis in Northeast Brazil. *Scandinavian Journal of Infectious Diseases* 2004;36:443–9. <https://doi.org/10.1080/00365540410020451>.

[27] Rodríguez NE, Lima ID, Gaur Dixit U, Turcotte EA, Lockard RD, Batra-Sharma H, et al. Epidemiological and Experimental Evidence for Sex-Dependent Differences in the Outcome of *Leishmania infantum* Infection. *Am J Trop Med Hyg* 2018;98:142–5. <https://doi.org/10.4269/ajtmh.17-0563>.

[28] Sex Bias in Infectious Disease Epidemiology: Patterns and Processes | *PLOS ONE* n.d. <https://journals.plos.org/plosone/article?id=10.1371/journal.pone.0062390> (accessed March 17, 2024).

[29] Handman E. Leishmaniasis: Current Status of Vaccine Development. *Clinical Microbiology Reviews* 2001;14:229–43. <https://doi.org/10.1128/cmr.14.2.229-243.2001>.

[30] Loria-Cervera EN, Andrade-Narváez FJ. ANIMAL MODELS FOR THE STUDY OF LEISHMANIASIS IMMUNOLOGY. *Rev Inst Med Trop S Paulo* 2014;56:1–11. <https://doi.org/10.1590/S0036-46652014000100001>.

[31] Aronson N, Herwaldt BL, Libman M, Pearson R, Lopez-Velez R, Weina P, et al. Diagnosis and Treatment of Leishmaniasis: Clinical Practice Guidelines by the Infectious Diseases Society of America (IDSA) and the American Society of Tropical Medicine and Hygiene (ASTMH). *Clinical Infectious Diseases* 2016;63:e202–64. <https://doi.org/10.1093/cid/ciw670>.

[32] Aronson NE, Joya CA. Cutaneous Leishmaniasis: Updates in Diagnosis and Management. *Infectious Disease Clinics* 2019;33:101–17. <https://doi.org/10.1016/j.idc.2018.10.004>.

[33] Leishmaniasis WEC on the C of the, Organization WH. Control of the leishmaniasis: report of a meeting of the WHO Expert Committee on the Control of Leishmaniasis, Geneva, 22-26 March 2010. World Health Organization; 2010.

[34] Burza S, Croft SL, Boelaert M. Leishmaniasis. *Lancet* 2018;392:951–70. [https://doi.org/10.1016/S0140-6736\(18\)31204-2](https://doi.org/10.1016/S0140-6736(18)31204-2).

[35] Georgiadou SP, Makaritsis KP, Dalekos GN. Leishmaniasis revisited: Current aspects on epidemiology, diagnosis and treatment. *Journal of Translational Internal Medicine* 2015;3:43–50. <https://doi.org/10.1515/jtim-2015-0002>.

[36] Cañavate C, Herrero M, Nieto J, Cruz I, Chicharro C, Aparicio P, et al. Evaluation of Two rK39 Dipstick Tests, Direct Agglutination Test, and Indirect Fluorescent Antibody Test for Diagnosis of Visceral Leishmaniasis in a New Epidemic Site in Highland Ethiopia. *Am J Trop Med Hyg* 2011;84:102–6. <https://doi.org/10.4269/ajtmh.2011.10-0229>.

[37] Dietze R, Lemos EM, Guimarães Carvalho SF, Corey R. PERFORMANCE OF RECOMBINANT K39 ANTIGEN IN THE DIAGNOSIS OF BRAZILIAN VISCERAL LEISHMANIASIS. *The American Journal of Tropical Medicine and Hygiene* 2003;68:321–4. <https://doi.org/10.4269/ajtmh.2003.68.321>.

[38] Domingues Passero LF, Laurenti MD, Santos-Gomes G, Soares Campos BL, Sartorelli

- P, Lago JHG. *In Vivo* Antileishmanial Activity of Plant-Based Secondary Metabolites. In: Rai MK, Kon KV, editors. *Fighting Multidrug Resistance with Herbal Extracts, Essential Oils and Their Components*, San Diego: Academic Press; 2013, p. 95–107. <https://doi.org/10.1016/B978-0-12-398539-2.00007-0>.
- [39] Turvey SE, Broide DH. Innate immunity. *Journal of Allergy and Clinical Immunology* 2010;125:S24–32. <https://doi.org/10.1016/j.jaci.2009.07.016>.
- [40] Bonilla FA, Oettgen HC. Adaptive immunity. *Journal of Allergy and Clinical Immunology* 2010;125:S33–40. <https://doi.org/10.1016/j.jaci.2009.09.017>.
- [41] Murphy K, Weaver C. *Janeway's Immunobiology*. Garland Science; 2016.
- [42] Marshall JS, Warrington R, Watson W, Kim HL. An introduction to immunology and immunopathology. *Allergy Asthma Clin Immunol* 2018;14:49. <https://doi.org/10.1186/s13223-018-0278-1>.
- [43] Klein SL, Flanagan KL. Sex differences in immune responses. *Nat Rev Immunol* 2016;16:626–38. <https://doi.org/10.1038/nri.2016.90>.
- [44] Shepherd R, Cheung AS, Pang K, Saffery R, Novakovic B. Sexual Dimorphism in Innate Immunity: The Role of Sex Hormones and Epigenetics. *Front Immunol* 2021;11. <https://doi.org/10.3389/fimmu.2020.604000>.
- [45] Wilkinson NM, Chen H-C, Lechner MG, Su MA. Sex Differences in Immunity. *Annual Review of Immunology* 2022;40:75–94. <https://doi.org/10.1146/annurev-immunol-101320-125133>.
- [46] Ginhoux F, Jung S. Monocytes and macrophages: developmental pathways and tissue homeostasis. *Nat Rev Immunol* 2014;14:392–404. <https://doi.org/10.1038/nri3671>.
- [47] van Furth R, Sluiter W. Distribution of blood monocytes between a marginating and a circulating pool. *J Exp Med* 1986;163:474–9. <https://doi.org/10.1084/jem.163.2.474>.
- [48] Swirski FK, Nahrendorf M, Etzrodt M, Wildgruber M, Cortez-Retamozo V, Panizzi P, et al. Identification of Splenic Reservoir Monocytes and Their Deployment to Inflammatory Sites. *Science* 2009;325:612–6. <https://doi.org/10.1126/science.1175202>.
- [49] Ziegler-Heitbrock L, Hofer TP. Toward a Refined Definition of Monocyte Subsets. *Front Immunol* 2013;4. <https://doi.org/10.3389/fimmu.2013.00023>.
- [50] Serbina NV, Pamer EG. Monocyte emigration from bone marrow during bacterial infection requires signals mediated by chemokine receptor CCR2. *Nat Immunol* 2006;7:311–7. <https://doi.org/10.1038/ni1309>.
- [51] Auffray C, Fogg D, Garfa M, Elain G, Join-Lambert O, Kayal S, et al. Monitoring of Blood Vessels and Tissues by a Population of Monocytes with Patrolling Behavior. *Science* 2007;317:666–70. <https://doi.org/10.1126/science.1142883>.
- [52] Carlin LM, Stamatiades EG, Auffray C, Hanna RN, Glover L, Vizcay-Barrena G, et al. Nr4a1-Dependent Ly6Clow Monocytes Monitor Endothelial Cells and Orchestrate Their Disposal. *Cell* 2013;153:362–75. <https://doi.org/10.1016/j.cell.2013.03.010>.
- [53] Zimmermann HW, Trautwein C, Tacke F. Functional Role of Monocytes and Macrophages for the Inflammatory Response in Acute Liver Injury. *Front Physiol* 2012;3. <https://doi.org/10.3389/fphys.2012.00056>.
- [54] Wolf AA, Yáñez A, Barman PK, Goodridge HS. The Ontogeny of Monocyte Subsets. *Front Immunol* 2019;10. <https://doi.org/10.3389/fimmu.2019.01642>.
- [55] Shi C, Pamer EG. Monocyte recruitment during infection and inflammation. *Nat Rev Immunol* 2011;11:762–74. <https://doi.org/10.1038/nri3070>.
- [56] Sellau J, Groneberg M, Fehling H, Thye T, Hoenow S, Marggraff C, et al. Androgens predispose males to monocyte-mediated immunopathology by inducing the expression of leukocyte recruitment factor CXCL1. *Nat Commun* 2020;11:3459. <https://doi.org/10.1038/s41467-020-17260-y>.
- [57] Yam AO, Chtanova T. The Ins and Outs of Chemokine-Mediated Immune Cell Trafficking in Skin Cancer. *Front Immunol* 2019;10. <https://doi.org/10.3389/fimmu.2019.00386>.
- [58] Gautier EL, Shay T, Miller J, Greter M, Jakubzick C, Ivanov S, et al. Gene-expression profiles and transcriptional regulatory pathways that underlie the identity and diversity of mouse tissue macrophages. *Nat Immunol* 2012;13:1118–28. <https://doi.org/10.1038/ni.2419>.
- [59] Italiani P, Boraschi D. From Monocytes to M1/M2 Macrophages: Phenotypical vs. Functional Differentiation. *Front Immunol* 2014;5. <https://doi.org/10.3389/fimmu.2014.00514>.

- [60] Yona S, Kim K-W, Wolf Y, Mildner A, Varol D, Breker M, et al. Fate Mapping Reveals Origins and Dynamics of Monocytes and Tissue Macrophages under Homeostasis. *Immunity* 2013;38:79–91. <https://doi.org/10.1016/j.immuni.2012.12.001>.
- [61] Yunna C, Mengru H, Lei W, Weidong C. Macrophage M1/M2 polarization. *European Journal of Pharmacology* 2020;877:173090. <https://doi.org/10.1016/j.ejphar.2020.173090>.
- [62] Shapouri-Moghaddam A, Mohammadian S, Vazini H, Taghadosi M, Esmaeili S-A, Mardani F, et al. Macrophage plasticity, polarization, and function in health and disease. *Journal of Cellular Physiology* 2018;233:6425–40. <https://doi.org/10.1002/jcp.26429>.
- [63] Sica A, Mantovani A. Macrophage plasticity and polarization: in vivo veritas. *J Clin Invest* 2012;122:787–95. <https://doi.org/10.1172/JCI59643>.
- [64] Mantovani A, Biswas SK, Galdiero MR, Sica A, Locati M. Macrophage plasticity and polarization in tissue repair and remodelling. *The Journal of Pathology* 2013;229:176–85. <https://doi.org/10.1002/path.4133>.
- [65] Wang C, Ma C, Gong L, Guo Y, Fu K, Zhang Y, et al. Macrophage Polarization and Its Role in Liver Disease. *Front Immunol* 2021;12. <https://doi.org/10.3389/fimmu.2021.803037>.
- [66] Kaye P, Scott P. Leishmaniasis: complexity at the host–pathogen interface. *Nat Rev Microbiol* 2011;9:604–15. <https://doi.org/10.1038/nrmicro2608>.
- [67] Kaye PM. The Immunology of Visceral Leishmaniasis: Current Status. In: Farrell JP, editor. *Leishmania*, vol. 4, Boston, MA: Springer US; 2002, p. 137–50. https://doi.org/10.1007/978-1-4615-0955-4_10.
- [68] Von Stebut E. Cutaneous Leishmania infection: progress in pathogenesis research and experimental therapy. *Experimental Dermatology* 2007;16:340–6. <https://doi.org/10.1111/j.1600-0625.2007.00554.x>.
- [69] Filho AAP, Nascimento AA de S, Saab NAA, Fugiwara RT, D'Ávila Pessoa GC, Koerich LB, et al. Evasion of the complement system by *Leishmania* through the uptake of factor H, a complement regulatory protein. *Acta Tropica* 2021;224:106152. <https://doi.org/10.1016/j.actatropica.2021.106152>.
- [70] Costa-da-Silva AC, Nascimento D de O, Ferreira JRM, Guimarães-Pinto K, Freire-de-Lima L, Morrot A, et al. Immune Responses in Leishmaniasis: An Overview. *Tropical Medicine and Infectious Disease* 2022;7:54. <https://doi.org/10.3390/tropicalmed7040054>.
- [71] Regli IB, Passelli K, Hurrell BP, Tacchini-Cottier F. Survival Mechanisms Used by Some *Leishmania* Species to Escape Neutrophil Killing. *Front Immunol* 2017;8. <https://doi.org/10.3389/fimmu.2017.01558>.
- [72] Rochael NC, Guimarães-Costa AB, Nascimento MTC, DeSouza-Vieira TS, Oliveira MP, Garcia e Souza LF, et al. Classical ROS-dependent and early/rapid ROS-independent release of Neutrophil Extracellular Traps triggered by *Leishmania* parasites. *Sci Rep* 2015;5:18302. <https://doi.org/10.1038/srep18302>.
- [73] Moradin N, Descoteaux A. *Leishmania* promastigotes: building a safe niche within macrophages. *Front Cell Inf Microbiol* 2012;2. <https://doi.org/10.3389/fcimb.2012.00121>.
- [74] Laufs H, Müller K, Fleischer J, Reiling N, Jahnke N, Jensenius JC, et al. Intracellular Survival of *Leishmania major* in Neutrophil Granulocytes after Uptake in the Absence of Heat-Labile Serum Factors. *Infect Immun* 2002;70:826–35. <https://doi.org/10.1128/IAI.70.2.826-835.2002>.
- [75] Laskay T, Van Zandbergen G, Solbach W. Neutrophil granulocytes – Trojan horses for *Leishmania major* and other intracellular microbes? *Trends in Microbiology* 2003;11:210–4. [https://doi.org/10.1016/S0966-842X\(03\)00075-1](https://doi.org/10.1016/S0966-842X(03)00075-1).
- [76] Charmoy M, Hurrell BP, Romano A, Lee SH, Ribeiro-Gomes F, Riteau N, et al. The Nlrp3 inflammasome, IL-1 β , and neutrophil recruitment are required for susceptibility to a nonhealing strain of *Leishmania major* in C57BL/6 mice. *Eur J Immunol* 2016;46:897–911. <https://doi.org/10.1002/eji.201546015>.
- [77] Van Zandbergen G, Klinger M, Mueller A, Dannenberg S, Gebert A, Solbach W, et al. Cutting Edge: Neutrophil Granulocyte Serves as a Vector for *Leishmania* Entry into Macrophages. *The Journal of Immunology* 2004;173:6521–5. <https://doi.org/10.4049/jimmunol.173.11.6521>.
- [78] Aga E, Katschinski DM, Van Zandbergen G, Laufs H, Hansen B, Müller K, et al. Inhibition of the Spontaneous Apoptosis of Neutrophil Granulocytes by the Intracellular

- Parasite *Leishmania major*. The Journal of Immunology 2002;169:898–905. <https://doi.org/10.4049/jimmunol.169.2.898>.
- [79] Peters NC, Egen JG, Secundino N, Debrabant A, Kimblin N, Kamhawi S, et al. In Vivo Imaging Reveals an Essential Role for Neutrophils in Leishmaniasis Transmitted by Sand Flies. Science 2008;321:970–4. <https://doi.org/10.1126/science.1159194>.
- [80] Vinet AF, Fukuda M, Turco SJ, Descoteaux A. The *Leishmania donovani* Lipophosphoglycan Excludes the Vesicular Proton-ATPase from Phagosomes by Impairing the Recruitment of Synaptotagmin V. PLOS Pathogens 2009;5:e1000628. <https://doi.org/10.1371/journal.ppat.1000628>.
- [81] Ndjamen B, Kang B-H, Hatsuzawa K, Kima PE. *Leishmania* parasitophorous vacuoles interact continuously with the host cell's endoplasmic reticulum; parasitophorous vacuoles are hybrid compartments: *Leishmania* PVs and ER interact continuously. Cellular Microbiology 2010;12:1480–94. <https://doi.org/10.1111/j.1462-5822.2010.01483.x>.
- [82] von Stebut E, Tenzer S. Cutaneous leishmaniasis: Distinct functions of dendritic cells and macrophages in the interaction of the host immune system with *Leishmania major*. International Journal of Medical Microbiology 2018;308:206–14. <https://doi.org/10.1016/j.ijmm.2017.11.002>.
- [83] Feijó D, Tibúrcio R, Ampuero M, Brodskyn C, Tavares N. Dendritic Cells and *Leishmania* Infection: Adding Layers of Complexity to a Complex Disease. Journal of Immunology Research 2016;2016:e3967436. <https://doi.org/10.1155/2016/3967436>.
- [84] Elmahallawy EK, Alkhaldi AAM, Saleh AA. Host immune response against leishmaniasis and parasite persistence strategies: A review and assessment of recent research. Biomedicine & Pharmacotherapy 2021;139:111671. <https://doi.org/10.1016/j.biopha.2021.111671>.
- [85] Paraguai de Souza E, Paula Esteves Pereira A, Machado FCS, Melo MF, Souto-Padrón T, Palatnik M, et al. Occurrence of *Leishmania donovani* parasitemia in plasma of infected hamsters. Acta Tropica 2001;80:69–75. [https://doi.org/10.1016/S0001-706X\(01\)00150-4](https://doi.org/10.1016/S0001-706X(01)00150-4).
- [86] Zhang W-W, Mendez S, Ghosh A, Myler P, Ivens A, Clos J, et al. Comparison of the A2 Gene Locus in *Leishmania donovani* and *Leishmania major* and Its Control over Cutaneous Infection*. Journal of Biological Chemistry 2003;278:35508–15. <https://doi.org/10.1074/jbc.M305030200>.
- [87] Stanley AC, Engwerda CR. Balancing immunity and pathology in visceral leishmaniasis. Immunol Cell Biol 2007;85:138–47. <https://doi.org/10.1038/sj.icb7100011>.
- [88] Samant M, Sahu U, Pandey SC, Khare P. Role of Cytokines in Experimental and Human Visceral Leishmaniasis. Front Cell Infect Microbiol 2021;11. <https://doi.org/10.3389/fcimb.2021.624009>.
- [89] Gupta G, Bhattacharjee S, Bhattacharyya S, Bhattacharya P, Adhikari A, Mukherjee A, et al. CXC Chemokine-Mediated Protection against Visceral Leishmaniasis: Involvement of the Proinflammatory Response. The Journal of Infectious Diseases 2009;200:1300–10. <https://doi.org/10.1086/605895>.
- [90] Cotterell SE, Engwerda CR, Kaye PM. *Leishmania donovani* infection initiates T cell-independent chemokine responses, which are subsequently amplified in a T cell-dependent manner. Eur J Immunol 1999;29:203–14. [https://doi.org/10.1002/\(SICI\)1521-4141\(199901\)29:01<203::AID-IMMU203>3.0.CO;2-B](https://doi.org/10.1002/(SICI)1521-4141(199901)29:01<203::AID-IMMU203>3.0.CO;2-B).
- [91] Svensson M, Zubairi S, Maroof A, Kazi F, Taniguchi M, Kaye PM. Invariant NKT cells are essential for the regulation of hepatic CXCL10 gene expression during *Leishmania donovani* infection. Infect Immun 2005;73:7541–7. <https://doi.org/10.1128/IAI.73.11.7541-7547.2005>.
- [92] Wilson ME, Jeronimo SMB, Pearson RD. Immunopathogenesis of infection with the visceralizing *Leishmania* species. Microb Pathog 2005;38:147–60. <https://doi.org/10.1016/j.micpath.2004.11.002>.
- [93] Alexander J, Brombacher F. T Helper1/T Helper2 Cells and Resistance/Susceptibility to *Leishmania* Infection: Is This Paradigm Still Relevant? Front Immunol 2012;3. <https://doi.org/10.3389/fimmu.2012.00080>.
- [94] *Leishmania* Hijacks Myeloid Cells for Immune Escape - PubMed n.d.

- <https://pubmed.ncbi.nlm.nih.gov/29867798/> (accessed April 22, 2024).
- [95] Sato N, Kuziel WA, Melby PC, Reddick RL, KostECKI V, Zhao W, et al. Defects in the Generation of IFN- γ Are Overcome to Control Infection with *Leishmania donovani* in CC Chemokine Receptor (CCR) 5-, Macrophage Inflammatory Protein-1 α -, or CCR2-Deficient Mice. *The Journal of Immunology* 1999;163:5519–25. <https://doi.org/10.4049/jimmunol.163.10.5519>.
- [96] Terrazas C, Varikuti S, Oghumu S, Steinkamp HM, Ardic N, Kimble J, et al. Ly6Chi inflammatory monocytes promote susceptibility to *Leishmania donovani* infection. *Sci Rep* 2017;7:14693. <https://doi.org/10.1038/s41598-017-14935-3>.
- [97] Dey R, Majumder N, Majumdar SB, Bhattacharjee S, Banerjee S, Roy S, et al. Induction of Host Protective Th1 Immune Response by Chemokines in *Leishmania donovani*-infected BALB/c Mice. *Scandinavian Journal of Immunology* 2007;66:671–83. <https://doi.org/10.1111/j.1365-3083.2007.02025.x>.
- [98] Oghumu S, Lezama-Dávila CM, Isaac-Márquez AP, Satoskar AR. Role of chemokines in regulation of immunity against leishmaniasis. *Experimental Parasitology* 2010;126:389–96. <https://doi.org/10.1016/j.exppara.2010.02.010>.
- [99] Prior N, Inacio P, Huch M. Liver organoids: from basic research to therapeutic applications. *Gut* 2019;68:2228–37. <https://doi.org/10.1136/gutjnl-2019-319256>.
- [100] Marsee A, Roos FJM, Verstegen MMA, Gehart H, De Koning E, Lemaigre F, et al. Building consensus on definition and nomenclature of hepatic, pancreatic, and biliary organoids. *Cell Stem Cell* 2021;28:816–32. <https://doi.org/10.1016/j.stem.2021.04.005>.
- [101] Simian M, Bissell MJ. Organoids: A historical perspective of thinking in three dimensions. *Journal of Cell Biology* 2016;216:31–40. <https://doi.org/10.1083/jcb.201610056>.
- [102] Method of the Year 2017: Organoids. *Nat Methods* 2018;15:1–1. <https://doi.org/10.1038/nmeth.4575>.
- [103] Baker BM, Chen CS. Deconstructing the third dimension: how 3D culture microenvironments alter cellular cues. *J Cell Sci* 2012;125:3015–24. <https://doi.org/10.1242/jcs.079509>.
- [104] Hu H, Gehart H, Artegiani B, López-Iglesias C, Dekkers F, Basak O, et al. Long-Term Expansion of Functional Mouse and Human Hepatocytes as 3D Organoids. *Cell* 2018;175:1591-1606.e19. <https://doi.org/10.1016/j.cell.2018.11.013>.
- [105] Huch M, Gehart H, van Boxtel R, Hamer K, Blokzijl F, Verstegen MMA, et al. Long-term culture of genome-stable bipotent stem cells from adult human liver. *Cell* 2015;160:299–312. <https://doi.org/10.1016/j.cell.2014.11.050>.
- [106] Wu F, Wu D, Ren Y, Huang Y, Feng B, Zhao N, et al. Generation of hepatobiliary organoids from human induced pluripotent stem cells. *J Hepatol* 2019;70:1145–58. <https://doi.org/10.1016/j.jhep.2018.12.028>.
- [107] Takebe T, Enomura M, Yoshizawa E, Kimura M, Koike H, Ueno Y, et al. Vascularized and Complex Organ Buds from Diverse Tissues via Mesenchymal Cell-Driven Condensation. *Cell Stem Cell* 2015;16:556–65. <https://doi.org/10.1016/j.stem.2015.03.004>.
- [108] Koike H, Iwasawa K, Ouchi R, Maezawa M, Giesbrecht K, Saiki N, et al. Modelling human hepato-biliary-pancreatic organogenesis from the foregut-midgut boundary. *Nature* 2019;574:112–6. <https://doi.org/10.1038/s41586-019-1598-0>.
- [109] Kim J, Koo B-K, Knoblich JA. Human organoids: model systems for human biology and medicine. *Nat Rev Mol Cell Biol* 2020;21:571–84. <https://doi.org/10.1038/s41580-020-0259-3>.
- [110] Duncan AW, Dorrell C, Grompe M. Stem Cells and Liver Regeneration. *Gastroenterology* 2009;137:466–81. <https://doi.org/10.1053/j.gastro.2009.05.044>.
- [111] Shan J, Schwartz RE, Ross NT, Logan DJ, Thomas D, Duncan SA, et al. Identification of small molecules for human hepatocyte expansion and iPS differentiation. *Nat Chem Biol* 2013;9:514–20. <https://doi.org/10.1038/nchembio.1270>.
- [112] Hu H, Gehart H, Artegiani B, López-Iglesias C, Dekkers F, Basak O, et al. Long-Term Expansion of Functional Mouse and Human Hepatocytes as 3D Organoids. *Cell* 2018;175:1591-1606.e19. <https://doi.org/10.1016/j.cell.2018.11.013>.
- [113] Nguyen R, Da Won Bae S, Qiao L, George J. Developing liver organoids from induced pluripotent stem cells (iPSCs): An alternative source of organoid generation for liver cancer research. *Cancer Letters* 2021;508:13–7. <https://doi.org/10.1016/j.canlet.2021.03.017>.

- [114] Mun SJ, Ryu J-S, Lee M-O, Son YS, Oh SJ, Cho H-S, et al. Generation of expandable human pluripotent stem cell-derived hepatocyte-like liver organoids. *J Hepatol* 2019;71:970–85. <https://doi.org/10.1016/j.jhep.2019.06.030>.
- [115] Takebe T, Zhang R-R, Koike H, Kimura M, Yoshizawa E, Enomura M, et al. Generation of a vascularized and functional human liver from an iPSC-derived organ bud transplant. *Nat Protoc* 2014;9:396–409. <https://doi.org/10.1038/nprot.2014.020>.
- [116] Kobayashi T, Naik S, Nagao K. Choreographing Immunity in the Skin Epithelial Barrier. *Immunity* 2019;50:552–65. <https://doi.org/10.1016/j.immuni.2019.02.023>.
- [117] McNamara HA, Cockburn IA. The three Rs: Recruitment, Retention and Residence of leukocytes in the liver. *Clin Transl Immunology* 2016;5:e123. <https://doi.org/10.1038/cti.2016.84>.
- [118] Gerbe F, Sidot E, Smyth DJ, Ohmoto M, Matsumoto I, Dardalhon V, et al. Intestinal epithelial tuft cells initiate type 2 mucosal immunity to helminth parasites. *Nature* 2016;529:226–30. <https://doi.org/10.1038/nature16527>.
- [119] Sachs N, Papaspyropoulos A, Zomer-van Ommen DD, Heo I, Böttinger L, Klay D, et al. Long-term expanding human airway organoids for disease modeling. *The EMBO Journal* 2019;38:e100300. <https://doi.org/10.15252/embj.2018100300>.
- [120] Holokai L, Chakrabarti J, Broda T, Chang J, Hawkins JA, Sundaram N, et al. Increased Programmed Death-Ligand 1 is an Early Epithelial Cell Response to *Helicobacter pylori* Infection. *PLoS Pathog* 2019;15:e1007468. <https://doi.org/10.1371/journal.ppat.1007468>.
- [121] Bar-Ephraim YE, Kretzschmar K, Clevers H. Organoids in immunological research. *Nat Rev Immunol* 2020;20:279–93. <https://doi.org/10.1038/s41577-019-0248-y>.
- [122] Biton M, Haber AL, Rogel N, Burgin G, Beyaz S, Schnell A, et al. T Helper Cell Cytokines Modulate Intestinal Stem Cell Renewal and Differentiation. *Cell* 2018;175:1307–1320.e22. <https://doi.org/10.1016/j.cell.2018.10.008>.
- [123] Lo Piparo, Marko. Establishing co-cultures of murine liver organoids and *L. infantum* infected macrophages 2023.
- [124] iGenomes n.d. https://emea.support.illumina.com/sequencing/sequencing_software/igenome.html (accessed April 16, 2024).
- [125] Pfaffl MW. A new mathematical model for relative quantification in real-time RT-PCR. *Nucleic Acids Res* 2001;29:e45. <https://doi.org/10.1093/nar/29.9.e45>.
- [126] Solcà MS, Andrade BB, Abbehusen MMC, Teixeira CR, Khouri R, Valenzuela JG, et al. Circulating Biomarkers of Immune Activation, Oxidative Stress and Inflammation Characterize Severe Canine Visceral Leishmaniasis. *Sci Rep* 2016;6:32619. <https://doi.org/10.1038/srep32619>.
- [127] Viana AG, Magalhães LMD, Giunchetti RC, Dutra WO, Gollob KJ. Infection of Human Monocytes with *Leishmania infantum* Strains Induces a Downmodulated Response when Compared with Infection with *Leishmania braziliensis*. *Front Immunol* 2018;8. <https://doi.org/10.3389/fimmu.2017.01896>.
- [128] Rodrigues A, Alexandre-Pires G, Valério-Bolas A, Santos-Mateus D, Rafael-Fernandes M, Pereira MA, et al. Dog hepatocytes are key effector cells in the liver innate immune response to *Leishmania infantum*. *Parasitology* 2019;146:753–64. <https://doi.org/10.1017/S0031182018002068>.
- [129] Aini W, Miyagawa-Hayashino A, Ozeki M, Adeeb S, Hirata M, Tamaki K, et al. Accelerated telomere reduction and hepatocyte senescence in tolerated human liver allografts. *Transpl Immunol* 2014;31:55–9. <https://doi.org/10.1016/j.trim.2014.06.008>.
- [130] Verma S, Tachtatzis P, Penrhyn-Lowe S, Scarpini C, Jurk D, Von Zglinicki T, et al. Sustained telomere length in hepatocytes and cholangiocytes with increasing age in normal liver. *Hepatology* 2012;56:1510–20. <https://doi.org/10.1002/hep.25787>.
- [131] Hendriks D, Artegiani B, Hu H, Chuva de Sousa Lopes S, Clevers H. Establishment of human fetal hepatocyte organoids and CRISPR–Cas9-based gene knockin and knockout in organoid cultures from human liver. *Nat Protoc* 2021;16:182–217. <https://doi.org/10.1038/s41596-020-00411-2>.
- [132] Sekiya S, Suzuki A. Hepatocytes, rather than cholangiocytes, can be the major source of primitive ductules in the chronically injured mouse liver. *Am J Pathol* 2014;184:1468–78.

<https://doi.org/10.1016/j.ajpath.2014.01.005>.

[133] Habibzadeh S, Doroud D, Taheri T, Seyed N, Rafati S. Leishmania Parasite: the Impact of New Serum-Free Medium as an Alternative for Fetal Bovine Serum. *Iran Biomed J* 2021;25:349–58. <https://doi.org/10.52547/ibj.25.5.349>.

[134] Ghosh A, Bandyopadhyay K, Kole L, Das PK. Isolation of a laminin-binding protein from the protozoan parasite *Leishmania donovani* that may mediate cell adhesion. *Biochem J* 1999;337:551–8.

[135] McGwire BS, Chang K-P, Engman DM. Migration through the Extracellular Matrix by the Parasitic Protozoan *Leishmania* Is Enhanced by Surface Metalloprotease gp63. *Infect Immun* 2003;71:1008–10. <https://doi.org/10.1128/IAI.71.2.1008-1010.2003>.

[136] Dutta D, Clevers H. Organoid culture systems to study host–pathogen interactions. *Current Opinion in Immunology* 2017;48:15–22. <https://doi.org/10.1016/j.coi.2017.07.012>.

[137] Robinson KA, Beverley SM. Improvements in transfection efficiency and tests of RNA interference (RNAi) approaches in the protozoan parasite *Leishmania*. *Molecular and Biochemical Parasitology* 2003;128:217–28. [https://doi.org/10.1016/S0166-6851\(03\)00079-3](https://doi.org/10.1016/S0166-6851(03)00079-3).

[138] Duncan AW, Taylor MH, Hickey RD, Hanlon Newell AE, Lenzi ML, Olson SB, et al. The ploidy conveyor of mature hepatocytes as a source of genetic variation. *Nature* 2010;467:707–10. <https://doi.org/10.1038/nature09414>.

[139] Duarte MIS, Mariano ON, Corbett CEP. Liver parenchymal cell parasitism in human visceral leishmaniasis. *Vichows Archiv A Pathol Anat* 1989;415:1–6. <https://doi.org/10.1007/BF00718599>.

[140] Gangneux J-P, Lemenand O, Reinhard Y, Guiguen C, Guguen-Guillouzo C, Gripon P. In vitro and ex vivo permissivity of hepatocytes for *Leishmania donovani*. *J Eukaryot Microbiol* 2005;52:489–91. <https://doi.org/10.1111/j.1550-7408.2005.00055.x>.

[141] Yorek MS, Poudel B, Mazgaeen L, Pope RM, Wilson ME, Gurung P. *Leishmania major* degrades murine CXCL1 – An immune evasion strategy. *PLoS Negl Trop Dis* 2019;13:e0007533. <https://doi.org/10.1371/journal.pntd.0007533>.

[142] Santos PL dos, Oliveira FA de, Santos MLB, Cunha LCS, Lino MTB, Oliveira MFS de, et al. The Severity of Visceral Leishmaniasis Correlates with Elevated Levels of Serum IL-6, IL-27 and sCD14. *PLOS Neglected Tropical Diseases* 2016;10:e0004375. <https://doi.org/10.1371/journal.pntd.0004375>.

[143] Er-Lukowiak M, Hänzelmann S, Rothe M, Moamenpour DT, Hausmann F, Khatri R, et al. Testosterone affects type I/type II interferon response of neutrophils during hepatic amebiasis. *Front Immunol* 2023;14. <https://doi.org/10.3389/fimmu.2023.1279245>.

[144] Chlamydas S, Markouli M, Strepkos D, Piperi C. Epigenetic mechanisms regulate sex-specific bias in disease manifestations. *J Mol Med (Berl)* 2022;100:1111–23. <https://doi.org/10.1007/s00109-022-02227-x>.

[145] Frontiers | Congruence of Transcription Programs in Adult Stem Cell-Derived Jejunum Organoids and Original Tissue During Long-Term Culture n.d. <https://www.frontiersin.org/articles/10.3389/fcell.2020.00375/full> (accessed April 9, 2024).

[146] Hoenow S, Yan K, Noll J, Groneberg M, Casar C, Lory NC, et al. The Properties of Proinflammatory Ly6Chi Monocytes Are Differentially Shaped by Parasitic and Bacterial Liver Infections. *Cells* 2022;11:2539. <https://doi.org/10.3390/cells11162539>.

[147] Azevedo E, Oliveira LT, Castro Lima AK, Terra R, Dutra PML, Salerno VP. Interactions between *Leishmania braziliensis* and Macrophages Are Dependent on the Cytoskeleton and Myosin Va. *J Parasitol Res* 2012;2012:275436. <https://doi.org/10.1155/2012/275436>.

[148] Bamra T, Shafi T, Das S, Kumar M, Das P. *Leishmania donovani* mevalonate kinase regulates host actin for inducing phagocytosis. *Biochimie* 2024;220:31–8. <https://doi.org/10.1016/j.biochi.2023.12.003>.

[149] Ambartsumian N, Klingelhöfer J, Grigorian M. The Multifaceted S100A4 Protein in Cancer and Inflammation. *Methods Mol Biol* 2019;1929:339–65. https://doi.org/10.1007/978-1-4939-9030-6_22.

[150] Jaiswal P, Ghosh M, Patra G, Saha B, Mukhopadhyay S. Clinical Proteomics Profiling for Biomarker Identification Among Patients Suffering With Indian Post Kala Azar Dermal Leishmaniasis. *Front Cell Infect Microbiol* 2020;10. <https://doi.org/10.3389/fcimb.2020.00251>.

[151] Becker I, Salaiza N, Aguirre M, Delgado J, Carrillo-Carrasco N, Kobeh LG, et al.

- Leishmania* lipophosphoglycan (LPG) activates NK cells through toll-like receptor-2. *Molecular and Biochemical Parasitology* 2003;130:65–74. [https://doi.org/10.1016/S0166-6851\(03\)00160-9](https://doi.org/10.1016/S0166-6851(03)00160-9).
- [152] Moore KW, Malefyt R de W, Coffman RL, O'Garra A. Interleukin-10 and the Interleukin-10 Receptor. *Annual Review of Immunology* 2001;19:683–765. <https://doi.org/10.1146/annurev.immunol.19.1.683>.
- [153] Antonia AL, Barnes AB, Martin AT, Wang L, Ko DC. Variation in *Leishmania* chemokine suppression driven by diversification of the GP63 virulence factor. *PLoS Negl Trop Dis* 2021;15:e0009224. <https://doi.org/10.1371/journal.pntd.0009224>.
- [154] Akashi T, Minami J, Ishige Y, Eishi Y, Takizawa T, Koike M, et al. Basement Membrane Matrix Modifies Cytokine Interactions between Lung Cancer Cells and Fibroblasts. *Pathobiology* 2005;72:250–9. <https://doi.org/10.1159/000089419>.
- [155] Grünebast J, Clos J. *Leishmania*: Responding to environmental signals and challenges without regulated transcription. *Computational and Structural Biotechnology Journal* 2020;18:4016–23. <https://doi.org/10.1016/j.csbj.2020.11.058>.
- [156] Kumar R, Bhatia M, Pai K. Role of Chemokines in the Pathogenesis of Visceral Leishmaniasis. *Current Medicinal Chemistry* 2022;29:5441–61. <https://doi.org/10.2174/0929867329666220509171244>.
- [157] Vanaerschot M, Maes I, Ouakad M, Aduai V, Maes L, Doncker SD, et al. Linking In Vitro and In Vivo Survival of Clinical *Leishmania donovani* Strains. *PLOS ONE* 2010;5:e12211. <https://doi.org/10.1371/journal.pone.0012211>.
- [158] Gupta S, Nishi. Visceral leishmaniasis: Experimental models for drug discovery. *Indian Journal of Medical Research* 2011;133:27.
- [159] Fehling H, Niss H, Bea A, Kottmayr N, Brinker C, Hoenow S, et al. High Content Analysis of Macrophage-Targeting EhPIb-Compounds against Cutaneous and Visceral *Leishmania* Species. *Microorganisms* 2021;9:422. <https://doi.org/10.3390/microorganisms9020422>.
- [160] Gorgani NN, Ma Y, Clark HF. Gene signatures reflect the marked heterogeneity of tissue-resident macrophages. *Immunol Cell Biol* 2008;86:246–54. <https://doi.org/10.1038/sj.icb.7100131>.
- [161] Donaghy L, Cabillic F, Corlu A, Rostan O, Toutirais O, Guguen-Guillouzo C, et al. Immunostimulatory Properties of Dendritic Cells after *Leishmania donovani* Infection Using an In Vitro Model of Liver Microenvironment. *PLOS Neglected Tropical Diseases* 2010;4:e703. <https://doi.org/10.1371/journal.pntd.0000703>.
- [162] Li H, Zhou Y, Wang H, Zhang M, Qiu P, Zhang M, et al. Crosstalk Between Liver Macrophages and Surrounding Cells in Nonalcoholic Steatohepatitis. *Front Immunol* 2020;11. <https://doi.org/10.3389/fimmu.2020.01169>.
- [163] Su L, Li N, Tang H, Lou Z, Chong X, Zhang C, et al. Kupffer cell-derived TNF- α promotes hepatocytes to produce CXCL1 and mobilize neutrophils in response to necrotic cells. *Cell Death Dis* 2018;9:1–12. <https://doi.org/10.1038/s41419-018-0377-4>.

Acknowledgements

First and foremost, I extend my sincere gratitude to Prof. Dr. Hanna Lotter for giving me the opportunity to pursue my doctoral thesis within her research group. Throughout this period, I have learned a lot and am very grateful for the support provided during the course of this project, as well as the experiences gained. Additionally, I would like to thank Prof. Dr. Tim Gilberger for taking on the role as an evaluator of this thesis.

I am grateful for Dr. Tobias Spielmann and Dr. Lara Linnemann for their dedication to co-supervising my project.

I would also like to express my special thanks to the current and former members of the Molecular Infection Immunology research group. This time would not have been the same without each and every one of you. In particular, I would like to thank Dr. Helena Fehling and Dr. Marco Er-Lukowiak for their support and guidance with regard to experimental problems. Our joint discussions and reflections on my experimental approaches have consistently opened up new perspectives and supported the progress of this work. I would also like to thank Claudia Klossi Marggraff for her constant support, both experimentally and emotionally. Her efforts in organizing game nights and Hedi visits provided much needed and welcome diversion. Working, gaming and dancing with you all has been a joy. A special thanks goes to my fellow doctoral colleagues Charlotte Hansen, (Dr.) Annika Bea, Dr. Barbara Honecker, Stefanie Tewes und Nils Groth for the great time we spent together in and around the institute. I couldn't have asked for better colleagues. I am deeply grateful for the opportunity to share this journey with you and I am certain that I could not have accomplished this without your support. I also want to acknowledge Marko Lo Piparo, for his contributions to this project as part of his master's thesis. Furthermore, I would like to thank all former students, especially Valentin Bärreiter, David Moamenpour, Fabian Roggatz and Anastasia Langanz, whose time in the lab brought a lot of joy, making my PhD at the BNI so special.

Moreover, I wish to thank my dearest PhD girls Charlotte Hansen, (Dr.) Annika Bea, Dr. Barbara Honecker, Stefanie Tewes, Juliett Anders and Pilar Martinez, who have become close friends to me in the last three years. Meeting you all through our work at the BNI has been a true blessing and I look forward to our continued gatherings for Mamma Mia evenings, Margarita nights or breakfast dates even beyond our time at the institute.

In addition to the people at the institute, I would like to express my gratitude to my family. I owe immense thanks to my parents, Monika and Dirk, who have consistently supported me in all my endeavors and enabled me to move to Hamburg, which soon led to this PhD position. While I might not express it often enough, I am eternally grateful for everything you have done to me. Furthermore, I would like to express my appreciation to my siblings Philipp, Oliver, Jessica and also KC. Your unwavering support and reliability are invaluable to me and I am fortunate to have each of you in my life.

Finally, I would like to thank my friends who have offered me emotional support throughout my PhD journey and therefore helped me tremendously to reach this point, either by listening to my work-related issues or by helping me to take my mind off things. Your support has been immensely meaningful to me. Here, I would like to specifically address Theresa, Philine and Flo.